République algérienne démocratique et populaire
Ministre de l'enseignement supérieur et la recherche scientifique.
Universite´ Mohamed khider de Biskra
Laboratoire de l'INFormatique Intelligente LINFI

THESE

Pour l'obtention des diplôme de :

Doctorat en Informatique de l'Universite´ de Biskra.
Spécialité: Intelligence Artificielle.

Brain Tumor Growth Modelling

Par: KAMLI ADEL.

Soutenue le **12 december 2021** devant le jury compose de :

Pr. Okba KAZAR	Univ MK de Biskra	Président.
Pr.Rachida SAOULI .	Univ MK de Biskra	Directrice de la thèse.
Pr Khaled REZEG	Univ MK de Biskra	Examinateur.
Pr Mohamed Ben mohamed	Univ Mentouri Constentine	Examinateur.
HDR. Hadj BATATIA	Univ Paul.S Toulouse	Examinateur.

Année universitaire 2020/2021

ABSTRACT

Prediction methods of Glioblastoma tumors growth constitute a hard task due to the lack of medical data, which is mostly related to the patients' privacy, the cost of collecting a large medical dataset, and the availability of related notations by experts. In this thesis, we study and propose a Synthetic Medical Image Generator (SMIG) with the purpose of generating synthetic data based on Generative Adversarial Network in order to provide anonymized data. In addition, to predict the Glioblastoma multiform (GBM) tumor growth we developed a Tumor Growth Predictor (TGP) based on End to End Convolution Neural Network architecture that allows training on a public dataset from The Cancer Imaging Archive (TCIA), combined with the generated synthetic data. We also highlighted the impact of implicating a synthetic data generated using SMIG as a data augmentation tool. Despite small data size provided by TCIA dataset, the obtained results demonstrate valuable tumor growth prediction accuracy.

Resume

Les méthodes de prédiction de la croissance des tumeurs du glioblastome constituent une tâche difficile en raison du manque de données médicales, qui est principalement lié à la vie privée des patients, au coût de la collecte d'un grand ensemble de données médicales et à la disponibilité de notations connexes par des experts.

Dans cette thèse, nous étudions et proposons un générateur d'images médicales synthétiques (SMIG) dans le but de générer des données synthétiques basées sur un réseau adversarial génératif afin de fournir des données anonymes. De plus, afin de prédire la croissance de la tumeur du glioblastome multiforme (GBM) nous avons développé un prédicteur de croissance tumorale (TGP) basé sur une architecture de réseau neuronal à convolution de bout en bout qui permet l'entraînement sur un ensemble de données publiques provenant de The Cancer Imaging Archive (TCIA), combiné aux données synthétiques générées. Nous avons également souligné l'impact de l'implication des données synthétiques générées à l'aide de SMIG comme outil d'augmentation des données. Malgré la petite taille des données fournies par le jeu de

données TCIA, les résultats obtenus démontrent une grande précision dans la prédiction de la croissance tumorale.

ملخص

تشكل طرق التنبؤ بنمو الاورام الدبقية مهمة صعبة بسبب نقص البيانات الطبية، والتي ترتبط في الغالب بخصوصية المرضى، وتكلفة جمع مجموعة بيانات طبية كبيرة، وتوافر الملاحظات ذات الصلة من قبل الخبراء.

في هذه الأطروحة، ندرس ونقترح فكرة توليد صور طبية اصطناعية عن طريق اقتراح فكرة خوارزمية ذكية لتوليد صور طبية (SMIG) ، وهذا بغرض إنشاء بيانات مزيفة بناءً على شبكة التوليدية من أجل توفير صور طبية تستعمل للأبحاث حيث لا تحمل بيانات خصوصية للمرضى.

بالإضافة إلى ذلك، للتنبؤ بنمو الورم الدبقية متعدد الأشكال (GBM) عملنا على تطوير برنامج لتوقع نمو حجم الورم (TGP) استنادًا إلى بنية الشبكة العصبية والتي تسمح بالتدريب على مجموعة بيانات مفتوحة المصدر و متاحة للاستخدام من أرشيف تصوير السرطان (TCIA) ، اضافة إلى الصور الطبية الاصطناعية التي قمنا بإنشائها.

لقد أبرزنا أيضًا تأثير أثر استخدام البيانات الصور الطبية الاصطناعية (المزيفة) التي تم إنشاؤها باستخدام SMIG كأداة لزيادة بيانات تدريب برامج التعلم العميق (Deep Learning)

على الرغم من صغر حجم البيانات التي قدمتها مجموعة بيانات TCIA ، فإن النتائج التي تم الحصول عليها تظهر دقة تنبؤ قيمة لنمو الورم.

Keywords: *Tumor growth prediction, Generative Adversarial Network, Glioblastoma multiform, convolution neural network, Literature*.

إهداء

في جميع مراحل الحياة يوجد أناس يستحقون منا الشكر و الامتنان

إلى صاحب السيرة العطرة والفكر المستنير، فلقد كان له الفضل الأول في بلوغي التعليم العالي (والدي الحبيب فضيل) أطال الله في عمره ورزقه الصحة والعافية.

إلى من وضعتني على طريق الحياة وجعلتني ربط الجأش، وراعتني حتى صرت كبيراً (أمي الغالية خديجة) ادامها الله فوق رؤوسنا.

إلى إخوتي، من كان لهم بالغ الأثر في كثير من العقبات والصعاب، إلى جميع أساتذتي الكرام، ممن لم يتوانوا في مد يد العون لي.

حبا وكرامة أهدي إليكم بحثي.

ACKNOWLEDGEMENT

With immense pleasure and deep sense of gratitude, I wish to express my sincere thanks to my supervisor **Pr. Rachida SAOULI** , Biskra University, without her motivation and continuous encouragement, this research would not have been successfully completed.

I am grateful to the Chancellor of Smart Computer Sciences Laboratory **Pr. Okba kazar** , Department of Computer Sciences, University of Biskra, Algeria, for motivating me to carry out research in the LinFi Laboratery and also for providing me with infrastructural facilities and many other resources needed for my research.

I express my sincere thanks to **Dr. Hadj BATATIA** , University of Toulouse, IRIT/INP-ENSEEIHT Toulouse, France for his kind words of support and encouragement. I like to acknowledge the support rendered by **my colleagues** in several ways throughout my research work.

I wish to extend my thanks to the jury members: **Pr. Mohammed ben mohamed** and **Pr. Rezeg Khaled** for thier in deepth work and thier feedbacks, that what helps me to improve my work.

My profound sense of gratitude to **my parents** for all the sacrifices they made during my research and also providing me with moral support and encouragement whenever required.

Last but not the least, I would like to thank my friend **Mostefa Bennaceur** for his constant encouragement and moral support along with patience and understanding.

Date: 30/04/2021 **Kamli Adel**

TABLE OF CONTENTS

ABSTRACT i
ACKNOWLEDGEMENT iii
LIST OF FIGURES vii
LIST OF TABLES xii
LIST OF TERMS AND ABBREVIATIONS xii

List of Terms and Abbreviations **1**

1 Medical background **6**
1.1 Glioblastoma 6
1.2 GBM Investigations level 14
1.2.1 In Vivo: 14
1.2.2 In Vitro 14
1.2.3 In Silico 14
1.3 Medical Imaging 15
1.3.1 MRI imaging techniques 16
1.3.2 MRI Types 18
1.3.3 Challenge in medical images: 19
1.4 Dataset (ADNI, BraTS, TCIA) 21
1.4.1 The Cancer Imaging Archive (TCIA) 21
1.4.2 Alzheimer's Disease Neuroimaging Initiative ADNI: 22
1.4.3 Brain Tumor Segmentation BraTS 23
1.5 Conclusion 23

2 Tumor growth modeling **24**
2.1 Introduction 24
2.2 The math of GBM growth 24

2.2.1 Microscopic models 25
2.2.2 Macroscopic models 27
2.2.3 Overview of mathematical modeling approaches 31
2.3 Genetic of Brain Tumor 32
2.3.1 State of the art for Genetic investigation: 33
2.4 Proposed MLP for genetic profile prediction: 37
2.4.1 Materiel and methods: 38
2.4.2 Data preparation 39
2.4.3 Model Conception and Implementation : 39
2.4.4 Our model classification results : 41
2.5 Discussion and Conclusion 42

3 Brain Tumor Growth Predictor 44

3.1 Motivation and objectives 45
3.2 Background theory: machine learning 46
3.2.1 Machine learning for health care 48
3.3 Brain tumor growth prediction pipeline 48
3.3.1 MRI image quality limitations 49
3.3.2 Skull stripping 50
3.3.3 Registration and resizing 52
3.3.4 Normalization and standardization 53
3.3.5 Filtering and denoising 55
3.4 TGP model conception and architecture 56
3.4.1 Training parameters 58
3.4.2 Implementation and working environment 59
3.5 TGP Experimental results 59
3.5.1 Evaluating TGP performance 61
3.6 Discussion and Conclusion 63

4 Synthetic Medical Image Generator 65

4.1 Introduction 65
4.2 Motivation and objectives 66
4.3 Background Theory : Generative adversarial networks (GANs) 66
4.3.1 Generative adversarial networks: Model conception 66

4.3.2 Generative adversarial networks: Training strategy 67
4.3.3 Game theory 68
4.4 State of the art: GANs in Medical investigation 69
4.4.1 Synthetic medical image generations: 70
4.4.2 Medical image quality enhancing. 71
4.5 Synthetic Medical Image generator (SMIG) pipeline 71
4.5.1 SMIG Model Training 74
4.5.2 SMIG model Results 75
4.5.3 model limitation and future work 76
4.5.4 Conclusion 77

5 Synthetic MRI images to predict GBM growth 78

5.1 Introduction 78
5.1.1 Problem statement 78
5.1.2 Objectives and motivation 78
5.2 Related work 79
5.3 SMIG data based on TCIA dataset 80
5.4 Tumor Growth Prediction Based on SMIG data 81
5.5 Evaluating strategy 83
5.5.1 Combination result validation 84
5.6 Experimental results 86
5.7 Discussion 88
5.8 Conclusion 89

REFERENCES 92

LIST OF PUBLICATIONS 105

LIST OF FIGURES

1.1 Representative image show a large portion of tumor cells (GBM tumor lesion) 7

1.2 A CT scan shows the rapid growing and infiltrative development of GBM tumor [Janelidze et al. (2009)] 11

1.3 Illustration of old women tumor using non-contrast MR T2 weighted image 12

1.4 An illustration of the four types of MRI images for the GBM patients . 19

1.5 illustration of the MRI provided by TCIA dataset, that contains T1(pre- and post-contrast agent), FLAIR, T2, and binary tumor masks (generated using T1 images) 22

1.6 Illustration of an example of ADNI dataset images 22

1.7 Illustration of Brain Tumor Segmentation BraTS images 23

2.1 Illustration of microscopic tumor tissue representation where each cell is considered independently, in the left a microscopic image for real tumor Fox et al. (2011), in the right is a schematic representation. 26

2.2 Illustration of Al Mahmud et al. (2014) obtained results. The authors demonstrate the relation between the increase tumor invasion and the creation of cell resistance to the drugs. 28

2.3 Swanson Simulation of tumour invasion of a high-grade glioma in the superior cerebral hemisphere. the left side is the tumor area by the standard threshold of detection. Where the sensitive threshold of detection shown in the right side Swanson et al. (2000). 30

2.4 Timeline of major mathematical models of brain tumor growth. 32

2.5 Zhou et al. (2017) model to predict survival rate and molecular profile . 33

2.6 Li et al. (2017) model diagram for IDH status prediction for low-grade glioma patients 34

2.7 Li et al. (2017) flowchart to recognize the tumor regions in the MR images to extract the deep filters 35
2.8 Flowchart and implementation info for the Zeynettin model Akkus et al. (2017) 35
2.9 Chon Lao et al. (2017) used a radiomic feature-based imaging signatures to predict survival 36
2.10 Yiming Li et al. (2018) machine learning flowchart to predict molecular information TP53 based on the radiomic features 37
2.11 Patients' clinical data (age, sex, tumor grade, . . .) 38
2.12 Patient's VASARI features extracted by an expert based on medical images includes : (Tumor location, Side of Tumor, Lesion Size . . .) 39
2.13 Patient's features used for the model training : 38 features (VASSARI + clinical) in green color and IDH1 status in blue. Separate Dataset into two division (training and testing) green and yellow 40
2.14 Multilayer perceptron architecture (MLP). the green/yellow indicate the input feature for training and testing, the blue is the prediction output (binary classification of IDH status) 41
2.15 Illustration of our classification results, we showed 7 result cases obtained using different training hyper-parameters. All result are based on BRATS 2017 dataset 41
3.1 A representation overview of the relationship and the field of artificial intelligence in general Holzinger (2016*b*) 47
3.2 a representation overview of the relationship and the field of artificial intelligence in general Holzinger (2016*b*) 48
3.3 Illustrate the workflow for TGP model,As input TGP take MRI image(four channels), the result is a model that capable to predict the tumor volume in late-stage (tumor area after 90days). 49
3.4 illustration of skull stripping for patient's images using the BET-FSL tool, the original image in the $1^{s}t$ row, and images result after skull stripping are shown in the $2^{n}d$ image row 51

3.5 Brain-suit skull stripping steps: (1) Filtration using anisotropic diffusion filter (2) Edge detection (based on Marr- Hildreth algorithm) (3) Finding the brain (based on a series of mathematical morphological operators (4) extracting the brain by applying a mask. 52

3.6 Visualization results of skull stripping obtained by Brain Surface Extractor (BSE) of brain suit package, the original image is in the 1st row, the 2nd row shows the process of BES (detect the brain boundaries) and the 3rd row shows the brain surface 53

3.7 An example of registration of the raw image with size (260*320*24) to the reference image with size (256*256*23) 54

3.8 Normalization- standardization result. 54

3.9 Illustration of the resulted images after applying different filter: (a) the original input image (b), (c) and (d) the result of filtering average, median and wiener respectively 55

3.10 Diagram illustrates the outline that is used in our work starting with preprocessing (normalization, standardization and registration), then skull stripping (based on BET and BES and the combination of them). The result of each skull stripping method pass by three steps: the first, slices selection (selecting 10 slices where tumor appear), the last step is patches extraction to prepare data as input for CNN model. 57

3.11 A schematic representation of the principal idea of convolution autoencoder, where its start by compressing the input image to a small piece called feature map (convolution part). The compression uses MaxPolling layers (in red color). The second part is responsible of reproduce the original image size based on the feature maps (de-convolution part). The decompression based on Up-samplling layers (green color) . 58

3.12 Our TGP model conception inspired by convolution auto-encodeur 58

3.13 An example of the TGP model prediction results compared to the segmentation provided by TCIA expert. We illustrate two GBM patient scans (T1, T2, FLAIR and T1C). The two last columns represent the binary lesion mask provided by the expert and TGP prediction. 60

3.14 An example of the validation result which shows True Positive, False Positive, True Negative, and False Negative, that are indicated by colors in the order of green, black, red, gray and represent the number of pixels in each class. 61
3.15 A schema representation for the Cross-validation testing procedure that used to evaluate TGP performance 62
3.16 Evaluating TGP model and measuring the impact of pre-processing on TGP performance 62
4.1 The illustration of GANs workflow Goodfellow et al. (2016). 67
4.2 Illustration of training GAN for (a) MRI-to-brain segmentation; (b) label-to-MRI synthesis Shin et al. (2018). 72
4.3 Workflow of getting synthetic images with variation. On BRATS data set, MRI-to-label image translation GAN is applied to T1-weighted images to get brain atlas. It is then merged with the tumor label given in the BRATS data set, possibly with alterations (shift tumor location; enlarge; shrink). The merged labels (with possibly alterations) are then used as an input to label to- MRI GAN, to generate synthetic multi-parametric MRI with brain tumor Shin et al. (2018). 73
4.4 Illustration of our proposed Synthetic Medical Image Generator (SMIG) training workflow, (A) SMIG trained to generate abnormal brain based on a healthy brain from ADNI dataset and tumor volume provided by TCIA, (B) SMIG trained to change the tumor location Kamli et al. (2020) 74
4.5 An example of SMIG synthetic generated image compared to the original patient images from the BraTS dataset. 75
4.6 An example of the application of SMIG model on a single patient images from the BraTS dataset compared to the traditional data augmentation techniques 76
5.1 Illustration of an example of synthetic image generated using SMIG model based on TCIA dataset 80
5.2 Preprocessing steps applied to prepare the input images for TGP model . 82

5.3 diagram illustrate the outline that used in our work starting with pre-processing (normalization, strandarisation and registration) then skull stripping (based on BET and BES and the combination), the result of each skull stripping method pass by three steps: the first, slices selection (select 10 slices where tumor appear), the second is data augmentation based on traditional technique beside GAN, the last step was patches extraction to prepare data as input for CNN model. 83

5.4 Patch extraction diagram from the input image size(256*256*23) high*width*slices to data augmentation the patch extraction to get image size (128*128*4) where 128*128 is high*width and four is the channel number(T1 pre,T1 post, T2, and Flair). 84

5.5 An example of the validation result which True Positive, False Positive, True Negative, False Negative, that are indicated by colors in the order of green, black, red, gray and represent the number of pixels in each class in the binary lesion mask on the compared images. 85

5.6 Recall, Precision, and Dice metric evaluation of the performance of our TGP models trained on 05 datasets with different ratios of synthetic/original images. We observe that 80% ratio of synthetic data gen- erated by SMIG and 20% from TCIA data have a greater effect on model accuracy 76.8%, 80.2%, 82.1% 87

5.7 Comparison of the state-of-the-art methods for the issue of tumor prediction with our proposed TGP model (which is noted by adding #..... 89

LIST OF TABLES

1.1 The reported statistics for the median age diagnosis for Glioblastoma (GBM) patients.....8
1.2 World Health Organization Classification of Tumors of the Central Nervous System (GBM classification according to IDH mutation).....9
2.1 Details data used in Yiming Li et al. (2018) model.....36
2.2 The molecular information guided decision-making World Health Organisation 2020 38
2.3 Overview of state-of-the-art mathematical modelling approaches for brain tumor growth modelling.....43
3.1 Table illustrates TGP model result and the impact of different pre-processing tools on TGP performance. 63
5.1 Table illustrates Recall, Precision, and Dice metric evaluation of the performance of our **TGP** models trained on 04 datasets with different ratios of synthetic/original images. 87

List of Terms and Abbreviations

GBM Glioblastoma Multiform tumors

LGG Low Grade Glioma

GGG High Grade Glioma

MRI Magnetic Resonance Imaging

ML Machine Learning

GANs Generative Adversarial Networks

ADNI Alzheimer's Disease Neuroimaging Initiative

BraTS multimodal BRAin Tumor Segmentation challenge

TCIA The Cancer Imaging Archive

TGP Tumor Growth Predictor

SMIG Synthetic Medical Images Generator

FLAIR T2-weighted FLuid-Attenuated Inversion Recovery

T1C T1-weighted Contrast-enhanced

T1 T1-weighted

T2 T2-weighted

WHO World Health Organization

GPU Graphics Processing Unit

NMR Nuclear Magnetic Resonance

General Introduction

Introduction

Nowadays, Brain tumor detection has become a very active area of research, which is still at the level of experiments. Glioblastoma multiforme (GBM) is one of the most fast-growing gliomas and heterogeneous brain tumors with a high potential for lethality. These tumors could be detected using magnetic resonance imaging (MRI), which helps neurosurgery to identify and predict the treatment plan by analyzing patients' images and biomarkers [Tamimi and Juweid (2017)]. However, there seems to be no cure in the case of many patients, particularly higher-grade tumors.

Cancer research has gone beyond the walls of medical institutions and biology labs. The investigations encompass research in mathematical models and Machine Learning ML algorithms as well. These techniques may provide an opportunity for novel clinical insights and discoveries.

In brain tumor research, ML aims to simulate human cognitive capacity in analyzing and comprehension of the complex tumor growth criteria. In the literature, ML are proposed to extract useful information from medical data, in which it plays a very important role in brain tumor diagnosis, segmentation, and growth prediction. These models are mainly focused to work on the image-based diagnosis and image analysis to improve treatment and helps in therapy decisions.

For tumor detection, Google's DeepMind [Powles and Hodson (2017)] develop an algorithm that can detect cancerous and abnormal conditions in healthy tissues. DeepMind helps to speed up the segmentation process, thereby improves the accuracy and effectiveness of radiotherapy planning.

Moreover, for radiotherapy effect prediction, Microsoft conducts various research in computer vision and machine learning. InnerEye [Oktay et al. (2020)] perform automatic and quantitative three-dimensional radiographic images. This technique provides an accurate image that is effectively used as a measuring device. Furthermore, getting an efficient segmentation of brain tumors is a research-active area where many works [Pereira et al. (2015), Havaei et al. (2017), Akil et al. (2020), Naceur et al. (2019)] propose a GBM segmentation model that based on Convolutional Neural Networks (CNNs) [LeCun et al. (1998)].

Thesis Motivation and Objectives

The main aims of this thesis are to develop a supporting decision-making tool for brain tumor growth prediction, which can predict GBM tumor growth based on automatic medical image analysis. In the literature, Swanson team [Swanson et al. (2000, 2003, 2008), Jackson et al. (2015), Randall et al. (2018)] has the major contributions in using mathematical modeling for GBM tumor growth. However, the major challenge in mathematical modeling is the parameters needed to accurately predict the tumor growth [Swanson et al. (2008)]. In the other hand, to the best of our knowledge, fewer investigations are based on machine learning for GBM growth, [Morris et al. (2006), Elazab et al. (2020)].

Due to the lack of sufficient training data and the complexity of GBM tumor behavior, brain tumor prediction is still a challenging task and a lot of efforts remain to be done for improving the prediction accuracy.

We focus our interests on machine learning investigation in brain tumor growth prediction. However, providing sufficient study data is a challenging task, the data medical data privacy and the lack of publicly available datasets. Generative Adversarial Networks (GANs) prepare a future seeing to generate a synthetic medical image, also, GANs provide data anonymizing and guarantee a free public dataset.

GANs are known as the combination of two types of networks; the first network is the generative model [Oord et al. (2016)] which study the spatial distribution from different features in the image. The second network is a Discriminator [Beyerlein (1997)], which classifies the two input images according to their characteristics and appearance differences. GANs could be trained to learn and use the internal representations in unlabeled data, and aim produces new content based on the extracted features.

In the literature, wide broad potential applications of GANs including:

- New image generation [Wang and Gupta (2016)].
- Text-to-image synthesis [Xu et al. (2018)].
- Face aging [Antipov et al. (2017)].
- Complete the missing parts of images [Li et al. (2019)].

The common uses of GANs in the medical field are for synthetic image generation and data anonymization, [Frid-Adar et al. (2018)] combines a GAN model with CNN architecture in order to develop a liver lesion classification network. The authors proved a positive effect by using GAN in improving the classification rate on a liver lesion classification. Furthermore, [Iqbal and Ali (2018)] proposed a GAN-based framework as

data augmentation with the aim to enhance the retinal vessel image segmentation. For GAN in brain research, [Han et al. (2018)] proposed to generate multi-sequence brain MR images. Han model increases the diagnostic reliability and the results are approved by physician [Geman et al. (2015)]. Moreover, [Shin et al. (2018)] proposed to generate synthetic multi-series abnormal brain MRIs. Shin model is based on two publicly available datasets (ADNI, BRATS), and the aim is to provide training data as well as an effective tool for medical images anonymizing.
In addition, [Bowles et al. (2018)] show the impact of using the generated image in the brain tumor segmentation accuracy.
GBM treatment planning, follow-up need an accurate prediction result and keep a challenging task. We are motivated by the huge evolution in machine learning algorithms and image analysis, that may use to consider information from different medical images. In the next section, we cite a list of our contributions to deal with this situation.

Contributions

This thesis has three main contributions:

1. Tumor Growth Predictor TGP model [Kamli et al. (2020)] is proposed to predict the tumor growth based on multi-modal MRI images and motivated by:
    - The lack of investigations on GBM volume growth prediction using deep-learning.
    - The short survival rate of GBM patients and the complexity of the prediction task.
    - TGP is a Fully automatic brain tumor prediction method.
    - Otherwise, compared to the majority of the prediction mathematical model, the TGP model didn’t require any patient’s supplementary data (based only on images).
2. To overcome the issue of data privacy, imbalanced data, and the lack of sufficient training data, we propose Synthetic Medical Image Generator (SMIG) [Kamli et al. (2020)]. SMIG is considered as data augmentation and an anonymizing technique.
3. The two previously mentioned models have been combined to show a proof of concept for a general framework to predict brain tumor growth based on multi-model images. This concept integrates information from different MRI image modalities, which are usually available for each single brain tumor patient.

4. We reviewed the impact of using various preprocessing steps on the accuracy of tumor growth prediction.

Thesis Outline

Including this general introduction, our thesis is divided into 6 chapters:

- In chapter 1, we provide the medical background and information about Glioblastoma multiforme (GBM) and brain tumor imaging, before citing the public dataset used in this work and their provided sample details.
- In chapter 2, the state of the art in tumor growth modeling and the mathematical viewpoint of GMB growth, the studies in the microscopic and macroscopic levels are briefly discussed and reviewed. Besides, we provide an overview of GBM tumor growth investigation based on artificial intelligence for treatment planning and genetic profile prediction in order to study treatment efficacity.
- In chapter 3, our TGP model as the first contribution is detailed. TGP aims to predict the volume changing and tumor growth based on multi-modal images. Besides, we studied the pre-processing tools used in literature and their impact on the model pre- diction accuracy; include the important methods for separating the brain from the skull, resizing, and registration, and finely image denoising.
- Chapter 4 deals with our SMIG model as the second contribution. The objective and motivation and the math behind the generative adversarial model also detailed, the used methods and the contribution compared to related work also provided. The results and examples of generative images are demonstrated as well
- Chapter 5, We combined the two previous approaches, and aimed to demonstrate that using SMIG data improve GBM prediction performance.
- Finally, the general conclusion that include all our results and future improvements work are summarized before the current status is critically assessed and potential future, as well as new developments, are discussed and detailed.

CHAPTER 1

Medical background

1.1 Glioblastoma

As neurosurgery and neuro-oncology have evolved, so has the classification system for central nervous system tumors, and Glioblastoma multiforme has been chosen as the most common type of malignant brain tumor in adults and represents approximately 27% of all primary brain tumors and 80% of malignant primary brain tumors in the United States Ostrom et al. (2018). Glioblastoma multiforme (GBM) is a fast-growing glioma that develops from star-shaped glial cells (astrocytes and oligodendrocytes) that support the health of the nerve cells within the brain. Figure 1.1 shows a representative image for a large portion of tumor cells (GBM tumor lesion). GBM brain tumors are heterogeneous brain tumors with a high risk of being lethal. Generally, it is the most aggressive malignant primary brain tumor with an incidence rate of 32 people per million in the USA, where 64 years is the average age of GBM patients Tamimi and Juweid (2017). The overall incidence and histological types of intracranial tumors vary with age. In general, there is a small peak before the age of 10, and it rises steadily from the age of 15. The Central Brain Tumor Registry of the United States (CBTRUS) data indicate that the incidence of intracranial tumors tends to flatten or even decrease after the age of 75, but this finding may be due to insufficient assessment of the elderly patients with neurologic disability. Low-grade gliomas, such as astrocytomas, are more common in the young, and high-grade tumors, such as glioblastoma, are more common in the elderly. Medulloblastomas and germ cell tumors of the pineal region are tumors of childhood. Study in the period 1973–1991 report only 208 glioblastomas under age 20, compared to 3 479 over age 65. Conversely, pilocytic astrocytomas, a low-grade tumor, were more common under age 20 (n = 252) than over age 65 (n = 7). There were 578 medulloblastomas under age 20 and only 3 over age 65. Pineal region tumors numbered 25 under age 20 and only 1 over age 65.26 The lifetime risk of a GBM malignancy is 0.67% for men and 0.52% for women.Buckner et al. (2007).

A population study in Japan compared the incidence of intracranial tumors under 70 years of age. Between 1989 and 1995, 1354 new primary intracranial tumors were diag-

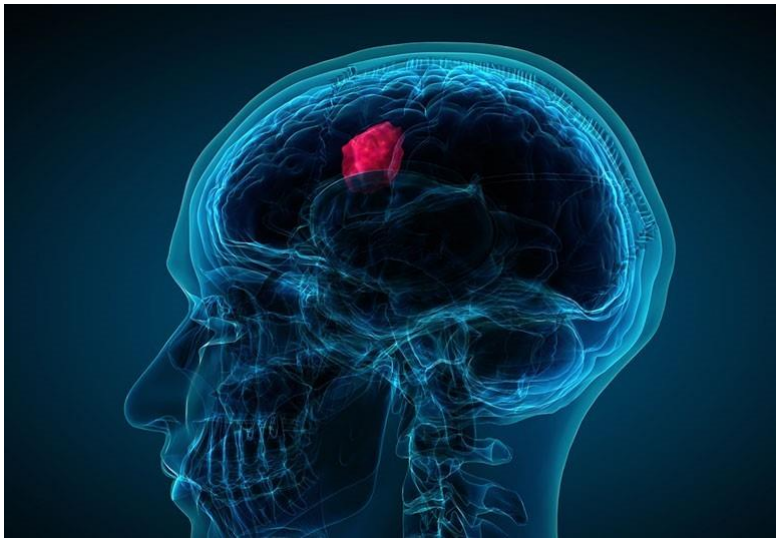

Fig. 1.1 Representative image show a large portion of tumor cells (GBM tumor lesion)

nosed in Kumamoto City, Japan. The total age-adjusted incidence rate for people over 70 years of age was 18.1/105, compared with 8.7/105 for younger people. CBTRUS data shows that with age, the incidence of all intracranial tumors is increasing. The age group with the highest incidence is 75-84 years old. Glioblastoma peaks between 65 and 74 years of age, and decreases slightly after 75 years of age. The incidence of meningioma also increases with age and does not decrease after the age of 75 (See Table 1). The reported incidence of brain tumors also varies by geographic location. The incidence of primary brain tumors reported in the least developed countries is higher than that of less developed countries. According to reports, the age-adjusted incidence rate in Scandinavia is 31.4 per million, which is much higher than the 21.7 for blacks and 26.4 for whites in the United States. In the United States, Canada, Western Europe, and Australia, this ratio is similar and higher than in Eastern Europe.Buckner et al. (2007) The lowest incidence rates in developed countries are Japan, India, and Singapore. Although the overall incidence in Asia is lower, certain tumors are more common. For example, germ cell tumors are more common in Japanese boys than in any other population in the world. The migration rate of the immigrant population is usually higher than that of the immigrants from the adopting country, and the rate of immigrants who stay in the country of origin is higher, which shows that environmental factors are important. It is not yet clear how the geographic differences between countries are affected by diagnostic facilities and autopsy rates. Buckner et al. (2007)

These tumors could be detected using magnetic resonance imaging (MRI) which creates an image of soft tissue that could be used after that to detect and measure the tumor's size. The study of GBM growth behavior is a very challenging task due to tumor malignancy and short survival times Smoll et al. (2013), thus, the processing of MRI

	Age at diagnosis (years)							
Histology	0-19	20-34	35-44	45-54	55-64	65-74	75-84	+85
Total tumors	3.69	5.67	9.50	15.78	24.92	36.45	39.81	31.55
Glioblastoma	0.17	0.41	1.21	3.81	8.16	11.34	11.22	5.41
Mcningioma	0.10	0.64	1.13	4.35	6.60	11.50	14.70	14.30
Lymphoma	0.01	0.26	0.47	0.41	0.65	1.09	1.22	0.47

Table 1.1 The reported statistics for the median age diagnosis for Glioblastoma (GBM) patients

images has vital importance for the diagnosis and evaluation of progressive disease during the treatment of GBM patients, generating MR-derived growth pattern models for GBM is an active research field in neuro-oncology.GBM is often referred to as a grade IV astrocytoma. These are the most invasive type of glial tumors, rapidly growing and commonly spreading into nearby brain tissue. Lima et al. (2012). GBMs can arise in the brain "de novo" or evolve from lower-grade astrocytomas or oligodendrogliomas. In adults, GBM occurs most often in the cerebral hemispheres, especially in the frontal and temporal lobes of the brain. GBM is a devastating brain cancer that typically results in death in the first 15 months after diagnosisBrem and Abdullah (2016). The development of neurosurgery and neuropathology served as the first necessary steps in understanding glioblastoma and the early detection of glioblastoma through biomarkers and response to therapy promises to inform future clinical trials and accelerate the pace of discovery to continuously increase survival. Glioblastoma has one of the poorest survival rates of any malignant brain tumor and contributes disproportionately to cancer mortality and morbidity. Median survival after diagnosis with glioblastoma is approximately 12 months, and this survival period increases to approximately 14 months when patients are treated with current standard therapy, which consists of maximal safe surgical resection followed by concurrent radiation and temozolomideDeAngelis (2001). The new 2016 WHO Classification of Tumors of the Central Nervous System was a paradigm shift: some of the tumors were defined also by their genetic composition as well as their cell morphology. The landscape of molecular and genetic profiling of glioblastoma is continuously expanding, and, as these phenomena are increasingly well described, therapeutic targets with biological underpinnings may more accurately be tailored to care and treatment in the clinical realm. The grading of gliomas changed importantly and glioblastoma was now mainly classified according to the molecular and genetic pathways, and especially on the status of isocitrate dehydrogenase (IDH) mutation: IDH-wildtype or IDH-mutant (see table 1.2)Louis et al. (2016).

GBM is lethal cancer and without treatment, patients diagnosed with this disease survive nine months. With the best therapeutics science has to offer, including surgical resection, radiation therapy, and temozolomide, patients survive only five more months. Brain tumors are difficult to detect early because the brain is covered by the skull and

	IDH-wildtype glioblastoma	IDH-mutant glioblastoma
Synonym	Primary glioblastoma	Secondary glioblastoma
Precursor lesion	Identified de novo	Diffuse/Anaplastic astrocytoma
Proportion of glioblastomas	-90%	-10%
Median age at diagnosis	-62 years	-44 years
Male:Female ratio	1.42:1	1 051
Median length of clinical history at diagnosis	4 months	15 months
Median overall survival		
Surgery + radiotherapy	9.9 months	24 months
Surgery + radiotherapy + chemotherapy	15 months	31 months
Location	Supratentorial	Preferentially frontal
Necrosis	Extensive	Limited
TERT promoter mutations	72%	26%
TP53 mutations	27%	81%
ATRX mutations	Exceptional	71%
EGFR amplification	35%	Exceptional
PTEN mutations	24%	Exceptional

Table 1.2 World Health Organization Classification of Tumors of the Central Nervous System (GBM classification according to IDH mutation)

the brain tumors do not show very specific clinical symptoms. Generally, three different categories of brain tumor symptoms can be distinguished Buckner et al. (2007) : 1. Increased cranial pressure can lead to headache, vomiting, and altered states of consciousness. 1. Cognitive and behavioral impairment, personality, or emotional changes can be attributed to brain dysfunction. 3. Symptoms of irritation like absences, fatigue, or seizures can be observed. However, all these symptoms are not just for brain tumors. Therefore, diagnosis usually starts with asking the patient's medical history and symptoms. If a brain tumor is suspected, imaging plays a central role. Currently, different methods of magnetic resonance imaging (MRI) are the latest technology for the non-invasive diagnosis of brain tumors DeAngelis (2001). However, despite the crucial role of imaging, a definitive diagnosis can only be confirmed by histological examination of tumor tissue samples, which have been obtained by biopsy or surgery. Once the tumor is diagnosed, treatment options range from surgery to radiotherapy or chemotherapy Buckner et al. (2007). Combination therapy is also possible. The purpose of surgery is to completely remove the tumor while preserving nerve function. In radiotherapy, the goal is to selectively kill tumor cells by splitting several irradiations while preserving healthy tissue in the brain. Chemotherapy can be used in combination with other therapies, but for many patients with brain tumors, it can only provide moderate benefits Buckner et al. (2007). All treatment options require imaging for treatment planning and treatment monitoring. Before and during treatment, it is important to distinguish the different tumor compartments based on the image and to outline important healthy brain structures. Each tumor compartment exhibits different biological processes and should therefore be considered separately. GBM are brain tumors derived from a single glial cell. Some brain tumors are benign, which means they will not recur after treatment (surgical removal and radiotherapy). But most tumors are malignant and even continue

to grow and spread after treatment, and ultimately lead to patient death. In general, malignant tumors outpace the growth of surrounding normal tissue as cancer cells divide and multiply more rapidly. A cell becomes cancerous after it undergoes some mutation (a chromosomal or genetic change) that increases the mitotic division in this cell or a decrease in a protein that suppresses cell division Hoang-Xuan et al. (2005). Eventually, cells that have undergone these genetic mutations become immune to inhibitory growth signals from their surrounding normal cells. As mutations in malignant cells accumulate while these cells divide, tumors become even more invasive to normal tissue and threaten the patient's life. The speed and degree of invasion of malignant tumor growth are described in terms of tumor grades. Four distinct glioma grades are ranging from low-grade brain neoplasms (astrocytomas originating from an astrocyte glial cell) and intermediate (anaplastic astrocytoma) to aggressive grade-four gliomas. Tumors in general and high-grade gliomas, in particular, are still recurrent, despite extensive clinical efforts and more sophisticated treatment methods. Tumor recurrence can be due to several factors, including cancer tissue resistance to therapy or the presence of occult malignant cells not destroyed by formal therapy Morris (2005). Although the visible tumor mass may have been removed or irradiated. The occult cells continue to diffuse in healthy brain regions outside The tumor boundary and form other small masses of cancer cells while the visible tumor may have been removed. With MR imaging, such small masses can remain undetected as they exist around the visible tumor in small concentrations. For example, even though surgical treatment eliminates the visible tumor mass, the tumor will likely grow again from the diffuse cells and tendrils that have invaded the healthy tissue around the border of the original tumor. The malignant cells fight for nutrients in more violent tumors that develop into a considerably large mass, creating a necrotic region at the heart of the tumor as the cells at the center are dead. However, cancer cells begin to proliferate at the periphery of the tumor border, adding to the slower-growing malignant mass and typically secreting chemicals that make the tumor expand into blood vessels supplying it with nutrients (this phenomenon is known as angiogenesis) Morris (2005). Malignant cells take advantage of nutrients and normal cell resources, share materials with normal cells, overwhelm them with waste products, and are in many ways able to threaten their survivalMorris (2005). Treatment for GBM is typically successful in extending the life of the patient by some years or months. But the treatment, in particular with radiotherapy, can become more effective and may even grant the cure to many patients if the treatment volume is specified in a way that would help eradicate the diffuse cancer cells and tendrils by applying a high radiation dose; therefore reducing the possibility of recurrence while minimizing the amount of healthy tissue compromised.

At the moment of diagnosis, GBMs are often large due to rapid and infiltrative

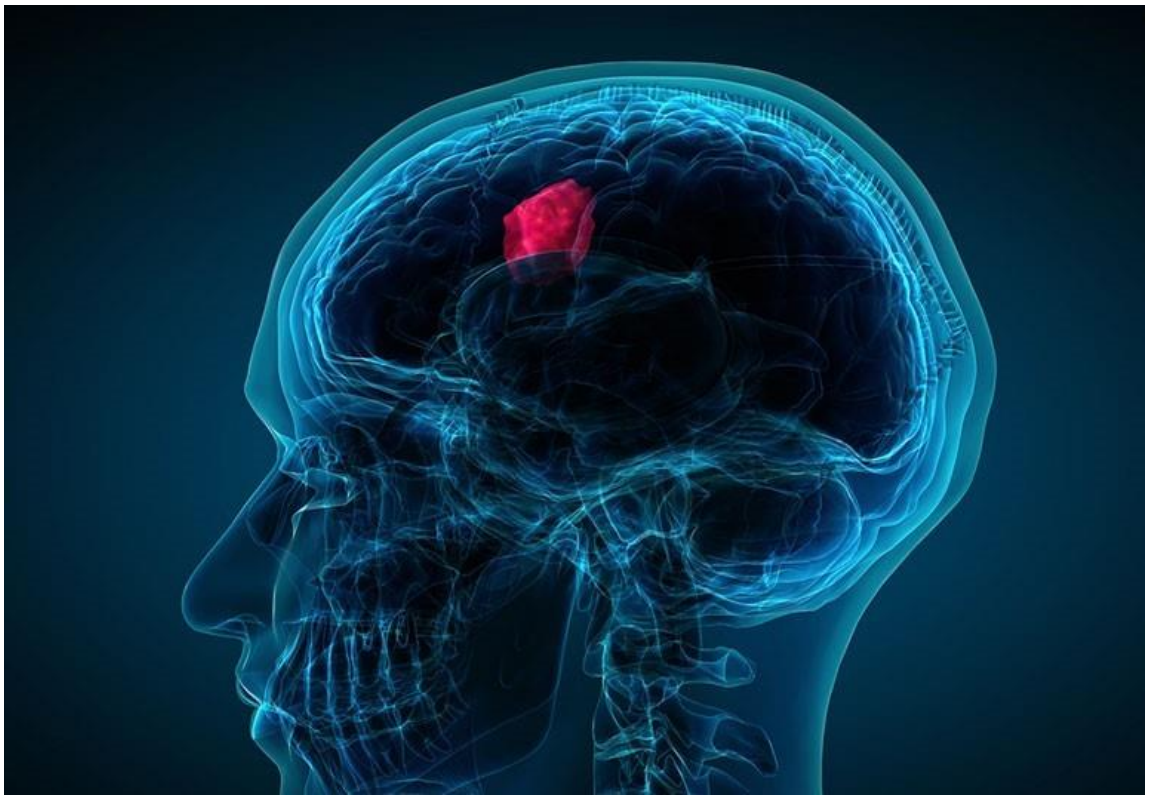

Fig. 1.2 A CT scan shows the rapid growing and infiltrative development of GBM tumor [Janelidze et al. (2009)]

development. The normal treatment of GBM consists of surgery, radiotherapy, and chemotherapy. It can not be fully resected by surgery due to the infiltrative nature of the tumor, but full surgical resection is desirable to reduce the symptoms caused by increased intracranial pressure and to provide tissue for histologic diagnosis. However, surgical resection may not always be necessary, depending on the location of the tumor. Figure 1.2 shows the rapid growing cancers and often outgrow their blood supply so the center ofthe tumor is literally dead cells or necrotic. Advances in brain tumor surgery, such as intraoperative magnetic resonance imaging, brain mapping, and fluorescence-guided surgery, have improved the extent of resection, but it is not clear whether this affects patient survival. GBM treated eventually recur, generally within 2 cm of the original location, with a median progression period of 6.9 months after radiation treatment and a median progression time of 6.9 months after radiation treatment and temozolomide Janelidze et al. (2009). Traditional therapy resistance is primarily due to many reasons including The first, inadequate drug delivery due to blood-brain barrier and high intratumoral pressure, The second reason, is genome instability leading to single-therapy resistant cell clonal populations, Thirdly, invasive tumor cells, And the fourth reason is stem-like cells with separate resistance mechanisms from the rest of the tumor cells, and lastly, the properties of DNA repair. Infiltrating tumor cells

also form microsatellites located at a distance from the bulk of the contrast-enhancing tumor, thereby preventing therapy with surgical resection and radiation. Further on, it has been shown that migration and cell proliferation are mutually exclusive, suggesting that migrating tumor cells do not proliferate Svensson (2015).

Any brain tumor is inherently serious and life-threatening because of its invasive and infiltrative character in the limited space of the intracranial cavity. However, brain tumors (even malignant ones) are not invariably fatal, especially lipomas which are inherently benign. Brain tumors or intracranial neoplasms can be cancerous (malignant) or non-cancerous (benign); however, the definitions of malignant or benign neoplasms differ from those commonly used in other types of cancerous or non-cancerous neoplasms in the body. Its threat level depends on the combination of factors like the type of tumor, its location, its size, and its state of development. Because the brain is well protected by the skull, the early detection of a brain tumor occurs only when diagnostic tools are directed at the intracranial cavity. Usually, detection occurs in advanced stages when the presence of the tumor has caused unexplained symptoms. FIGURE 1.3 Moore et al. (1996) depicts an aging woman's inability to be diagnosed with a brain tumor. A lady in her 70s presented with a new-onset headache. In this elderly patient, a non-contrast MR T2 weighted (left image) scan showed a right temporal lobe lesion (arrow), which was interpreted as ischemic vascular disease. The headaches went away, but then she started having mood changes, confusion, and fatigue, a contrast-enhanced MR scan (right image) revealed that the previously tiny lesion had grown into a massive glioblastoma (arrow).

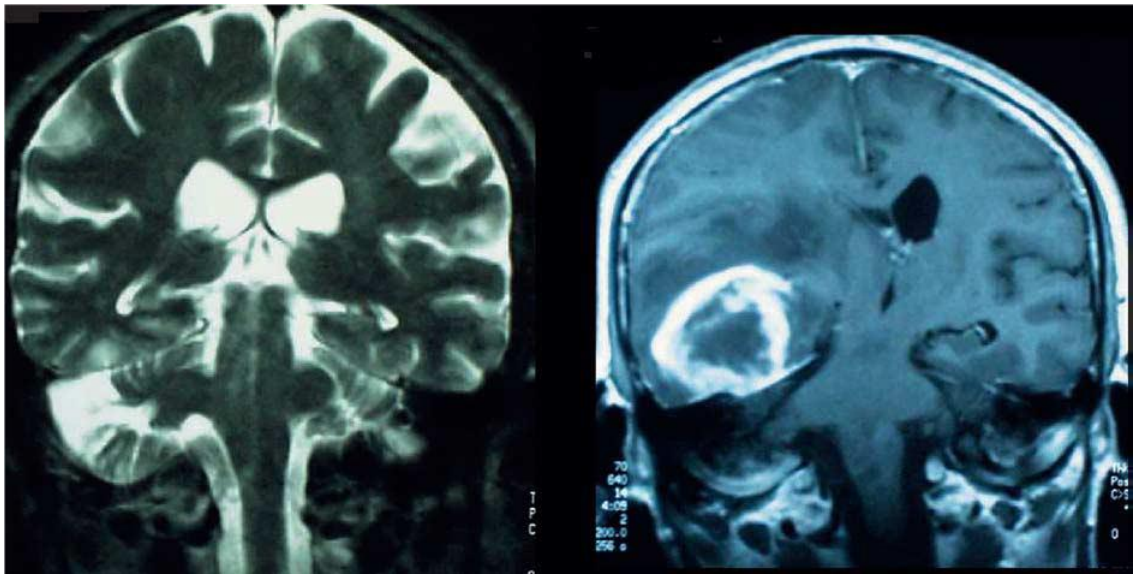

Fig. 1.3 Illustration of old women tumor using non-contrast MR T2 weighted image

The tumor's origin determines symptoms, surgical resectability, and, as a result,

prognosis. Tumors in the non-dominant frontal lobe, for example, are often asymptomatic before they reach a large scale, can also be entirely resected, and have a higher prognosis than tumors in extremely symptomatic but surgically unavailable regions like the brainstem or basal ganglia. Tumors that arise outside of the brain, such as meningiomas and pituitary tumors, have a higher prognosis than tumors that arise within the brain's parenchyma. The patient's age is a significant prognostic factor. Surgery Black (2000) is the most important single modality in the treatment of intracranial tumors, treatment planning techniques permits the design of treatment plans which match how should this patient get the treatment for his brain tumor, according to many features related to tumor grade, patient age, sex, and health general state.Moore et al. (1996) Surgery establishes the diagnosis and often relieves neurologic symptoms but whether it prolongs survival is controversial. 43 Older patients (> 40 years) with tumors >3 cm and with mass effect do appear to benefit from resection. Surgery seems to improve both quality and duration of life in children with astrocytomas, both low- and highgrade44 and we believe that it also does so in adults. However, surgery does not cure (pilocytic astrocytoma is an exception); surgery conventionally has been followed by radiotherapy Moore et al. (1996). Radiotherapy RT Walker et al. (1979) is curative; for some, it significantly prolongs longevity or at the very least slows progression. Radiation techniques have evolved, allowing greater exposures to the tumor while sparing normal brain, As with surgery, recent developments in radiation therapy have made that treatment modality both more effective for some tumors and less toxic to the brain Many health institutions have focused their efforts on cancer research leading to numerous advances in cancer treatment. But there seems to be no cure in the case of many patients; in particular, those affected with higher-grade tumors. Because of this, cancer research has gone beyond the walls of medical institutions and biology labs to encompass research in mathematical and computational sciences as well. Chemotherapeutic Vuorinen et al. (2003) drugs have been shown to be ineffective in the management of the majority of brain tumors. Cerebral germinomas, medulloblastomas, central nervous system lymphomas, and some oligodendrogliomas are anomalies. Chemotherapy's role in the treatment of astrocytomas is debatable, but most experts agree it plays a minor role in increasing recovery in certain patients. For meningiomas, acoustic neuromas, and most pituitary adenomas, no adequate chemotherapeutic agents have been created. Chemotherapy is thought to work in the same way with all cancers. The diagnosis of GBM can be done by clinical imaging techniques, with MRI being the most common technique. When viewed with traditional imaging techniques, GBM often appears as ring-enhancing lesions with non-specific boundaries: due to very high cell invasiveness, Glioma Growth Modeling unlike solid tumors, GBM does not form a solid and compact mass with cells dispersed around the lesion Duffau (2017*b*).

1.2 GBM Investigations level

From literature brain tumor investigation, we distinguish three portmanteaux models Andre´ et al. (2004*a*)

1.2.1 In Vivo:

Experimentation in vivo (Latin for ”inside the living”) refers to using a whole, living organism rather than a partial or dead organism. Animal studies and clinical trials are two forms of in vivo research. Because it is best suited for monitoring the overall effects of an experiment on a living subject, in vivo testing is often used over in vitro testing. While there are several reasons to think that in vivo studies have the potential to provide definitive insights into the nature of medicine and disease, there are many ways in which these findings can be inaccurate. A treatment, for example, may provide a short-term benefit but cause long-term harm.

1.2.2 In Vitro

This method allows to carry out a biological procedure in a controlled environment outside of a living organism usually in test tubes or on Petri dishes. The process of conducting a given procedure in a controlled environment outside of a living organism is referred to as in vitro (Latin for inside the glass). Many cellular biology experiments are carried out outside of organisms or cells. One of the most serious shortcomings of in vitro experiments is their inability to reproduce the exact cellular conditions of an organism, especially a microbe. In fact, the investigation in vitro level are much faster than in vivo experiment but did not replace it completely and may lead to results that do not correspond to the circumstances occurring around a living organism.

1.2.3 In Silico

The term ”in silico” refers to work done on a computer or through computer simulation. The word in silico was first used in public in 1989 in a workshop to describe biological experiments conducted entirely on a computer. Although in silico studies are still a relatively new avenue of investigation, they are increasingly being used in studies that predict how drugs interact with the body and pathogens. In a 2009 study, for example, software emulations were used to predict how certain already-on-the-market drugs would treat multidrug-resistant and widely drug-resistant. In GBM investigation Mathematic model and computer simulation models may provide testing proceeds on virtual patients, to study and simulate how the tumor would look like in the late stage, also how treatment will react with GBM growth and innovation. Such a model had no risk of harm or threat to the safety and it’s the most used in GBM investigation.

1.3 Medical Imaging

Diagnosis of tumors is centered on the examination of biopsy tissue samples collected. Biopsies are highly invasive and risky. Biopsy morbidity is estimated at 1.4 to 3.5 %, with a death rate of 0.2 to 0.8 %, and is rarely done on infirm or elderly patients, or in patients with very slow-growing tumors. Noninvasive imaging methods like MRI Dale et al. (2015*a*), Computed Tomography (CT) Buzug (2011), and Positron Emission Tomography (PET) Bailey et al. (2005) can diagnose a brain tumor, without surgery. MRI provides soft-tissue contrast with high-resolution information and is an approach for the anatomical assessment of brain tumors.

The method despite its familiarity in clinical practice fails on metabolic change detections. Proton is a sensitive nucleus and is a prominent option for medical applications. MRI has become a major aid in the clinical diagnosis of brain tumors. The technique assesses tumor extents, anatomical location, and morphology and has a high spatial resolution. Stacked images of the whole brain are used for tumor localization. MRI with different contrasts allows assessing the integrity of the blood-brain barrier. Brain tumors often result in an interruption of the blood-brain barrier and contrast agent discharges out of the vasculature into the brain or tumor tissue, thereby giving rise to abnormal enhancement. MRI is a helpful mechanism for brain tumor diagnosis and treatment.

- Magnetic resonance imagingDale et al. (2015*a*) : MRI is the most used device that provides pictures of various planes. The MRI provides clear images of tumors as it detects signals emitted from normal and abnormal tissues (more details in next section).

- Computed Tomography scanBuzug (2011) (formerly known as computed axial tomography): CT combines upgraded x-ray and computer technology that can showcase a combination of soft tissue, bone, and blood vessels. CT images allow to determine certain types of tumors and also help in detecting swelling, bleeding, and bone. Usually, iodine is the contrast agent made use of during a CT scan.

- Positron emission tomographyBailey et al. (2005) : PET scan gives a picture of the brains function, rather than its structure, by calculating the rate at which a tumor takes in glucose (a sugar). The patient is injected with deoxyglucose that has been labeled with radioactive markers. The PET scan identifies the brain activity and sends this data obtained to a computer, which forms a live image. Pathologists use PET scans to view the difference between scar tissue and recurring tumor cells.

- Tumor tissue biopsyVuorinen et al. (2003) : A sample of tissue is extracted from

the tumor-affected area and a microscopic study is made by a surgical procedure called a biopsy. Biopsy provides information about the abnormal cells present in the tumor and is used to find the type and grade of a tumor, which diagnose accurately. A craniotomy is an open biopsy, for which a small piece of skull is removed for the extraction of the tumor part. After the tumor is resected (completely removed) or debulked (partially removed), the bone is again fixed. The surgeon drills a small hole into the skull and passes a narrow hollow needle into the tumor to remove a sample. A closed biopsy called stereotactic or needle biopsy is performed when the tumor is in a difficult part of the brain. The tissue is analyzed under a microscope for a detailed report.

1.3.1 MRI imaging techniques

Functional brain imaging can be strictly or more broadly defined. It considers it broadly to include the full range of techniques by which physiological changes accompanying brain activity are defined. Different techniques are sensitive to different types of changes. Dale et al. (2015*b*)

Magnetic resonance (MR) is based upon the interaction between an applied magnetic field and a nucleus that possesses spin. Nuclear spin or, more precisely, nuclear spin angular momentum, is one of several intrinsic properties of an atom and its value depends on the precise atomic composition. Every element in the Periodic Table except argon and cerium has at least one naturally occurring isotope that possesses spin. Thus, in principle, nearly every element can be examined using MR, and the basic ideas of resonance absorption and relaxation are common to all of these elements. The precise details will vary from nucleus to nucleus and from system to system. Poldrack et al. (2011)

The concept of Nuclear magnetic resonance (NMR) imaging used in present-day MRI systems was proposed by Paul Lauterbur as early as 1973. MRI exploits the presence of the vast amount of hydrogen (protons) in a human body as the water content in a human body is said to be about 80 % Poldrack et al. (2011). When protons in the tissues of the body, aligned in a static magnetic field (B0), are subjected to resonant RF excitation, they absorb energy. Proton relaxes back and emits a resonant signal which is a characteristic of the tissue. The signal is picked up by a receiver located inside the magnet bore and is used to construct the image using Fourier transform. Since the NMR signal frequency is proportional to the magnetic field the whole tissue can be mapped by assigning different values of the proton frequency to different proton locations in the sample using a well-computed field gradient. All MRIs use proton NMR for mapping proton density which is different in different types of tissues. The images show contrast which helps in identifying those tissues and the changes occurring in a sample tissue.

MRI turns out to be an ideal technique for soft tissue regions of the body such as the brain, eyes, and soft tissue part of the head. Since bones have a low density of protons they appear as dark regions. Poldrack et al. (2011).

The focus on magnetic resonance-based techniques arises from the extraordinary flexibility and range of potential applications for magnetic resonance methods, as well as the safety and widespread availability of MRI scanners. In contrast to many of the in vitro methods used to define brain function, methods used in vivo generally are concerned not with the behaviors of single neurons but with the activities of large populations of neurons. This nonetheless is highly informative, as single neurons do not work independently, but function in large aggregates (consider, for example, the vertical integration of neurons in columns in the primary sensory cortex). Despite the small sizes of individual neurons, useful information concerning brain function therefore can be obtained using methods that have an in-plane spatial resolution of even 3 mm or greater. Information transfer in the brain along axons occurs by electrical conduction. Information is transferred between neurons by the release of neurotransmitter molecules at synapses and their subsequent interactions with specific receptors on target neurons. These neurotransmitter–receptor interactions then lead to changes in membrane current flow which change the post-synaptic neuronal membrane potential (and the accompanying extracellular electrical field) and after depolarization frequency. Dale et al. (2015*b*).

Brain tumor therapy is highly dependent on diagnosis, which must be as close as possible at the early stages of the disease. Since the asymptomatic period can last for a long period (months or ages), this is crucial to diagnose the disease before local expansion or metastatic invasion. Every indication should motivate every person to ask for medical assistance, since the recognition of a symptom (e.g. persistent headaches, cough, swelling, or hardening of the breast) may be the first step for early diagnosis of malignant neoplasia. Diagnosis is critical for identifying the type and the characteristics of a tumor. Misdiagnosis can often lead to an erroneous prognosis and treatment. Poldrack et al. (2011)

MRI is particularly useful for examining the brain and spinal cord, considered the best technique to detect tumors in these locations. The energy from the radio waves is absorbed and then released in a pattern linked to the tissue and certain diseases. Special computer software translates the pattern into a very detailed image which can be represented in 3 dimensions. In most cases, the patient receives a contrast agent, called gadolinium (Gd), by intravenous injection before scanning to obtain clearer images. Dale et al. (2015*b*).

In general, MR measurements are made on collections of similar spins rather than on an individual spin. It is useful to consider such a collection both as individual spins acting independently (a “microscopic” picture) and as a single entity (a “macroscopic” picture). For many concepts, the two pictures provide equivalent results, even though the microscopic picture is more complete. Conversion between the two pictures requires the principles of statistical mechanics.

1.3.2 MRI Types

MRI is perhaps the best application of superconductivity which directly affected humanity across the globe. It is a common tool with the radiologist in diagnostic hospitals for imaging various soft tissue parts of the human body and for detecting tumors. The most used type of MRI images in brain tumor investigation are :

1.3.2.1 T1 weighted

T1 weighted MRI refers to a set of standard scans that depict differences in the spin-lattice relaxation time (known as T1) of various tissues within the brain. T1 weighted images can be acquired using either spin-echo or gradient-echo sequences. T1 weighted contrast can be increased with the application of an inversion recovery radiofrequency pulse. Gradient-echo-based T1-weighted sequences can be acquired very rapidly because of their ability to use short inter-pulse repetition times. T1-weighted sequences are often collected before and after infusion of T1-shortening MRI contrast agents Smith (1990).

1.3.2.2 T2 weighted

T2 weighted MRI is another basic type of MRI. Like the T1 weighted MRI, fat is differentiated from water, but in this case, fat shows darker and water lighter. For example, in the case of cerebral and spinal study, the cerebrospinal fluid (CSF) will be lighter in T2 weighted images. These scans are therefore particularly well suited to imaging edema with long echo time and repetition time. Because the spin-echo sequence is less susceptible to inhomogeneities in the magnetic field, they are widely used in clinical praxis. Freeman and Minch (1998)

1.3.2.3 Fluid Attenuated Inversion Recovery (FLAIR)

Fluid Attenuated Inversion Recovery (FLAIR) is an inversion-recovery pulse sequence used to null signal from fluids. It can be used in brain imaging to suppress cerebrospinal fluid (CSF) to bring out the periventricular hyperintense lesions, such as multiple sclerosis plaques. By carefully choosing the inversion time (the time between the inversion

and excitation pulses), the signal from any particular tissue can be suppressed De Coene et al. (1992).

1.3.2.4 Diffusion Tensor Imaging (DTI)

MR diffusion tensors are constructed from diffusion measurements obtained in non-collinear directions that describe the trajectory field of moving water molecules in three-dimensional space. A tensor matrix can be converted into three differential equations. DTI enables diffusion to be measured in multiple directions and the fractional anisotropy in each direction to be calculated for each voxel. This enables researchers to make brain maps of fiber directions to examine the connectivity of different regions in the brain (using tractography) De Coene et al. (1992), Figure 1.4 Network et al. (2008) illustrates the four types of MRI images for a GBM patient.

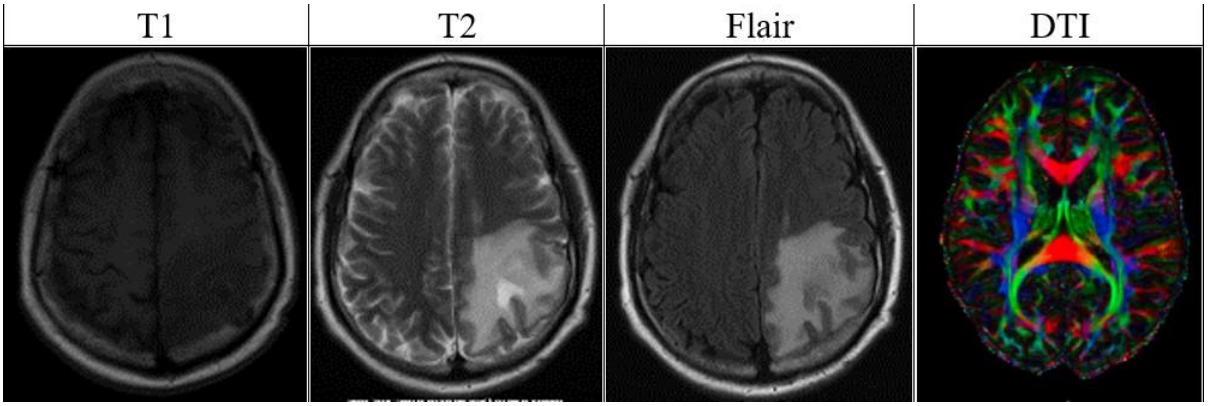

Fig. 1.4 An illustration of the four types of MRI images for the GBM patients

1.3.3 Challenge in medical images:

Medical image analysis for brain tumor studies is gaining attention in recent times due to an increased need for efficient and objective evaluation of large amounts of data. Indeed, the investigation in the medical field introduces new legal challenges in three interrelated areas: privacy of identifiable health information, reliability and quality of health data, and tort-based liability Coatrieux (2011).
In another viewpoint, we believe that the collaborative networks and data-sharing initiatives are broadening the opportunities for the advancement of science. These initiatives offer greater transparency in science, with the opportunity for external research groups to reproduce, replicate, and extend research findings. Furthermore, to identify homogeneous patterns within subgroups of individuals, a huge amount of data is needed, where

these patterns may be obscured by the heterogeneity of the neurobiological measure in smaller samples.

The absolute challenge appears in the three characteristics should be ensured:

- Confidentiality : is the property that ensures that only authorized users in normal conditions have access to the information. Remember that these purposes are legislatively specified and that disclosure may be made without the consent of the patient. It should also be noticed that if a particular emphasis is placed on patient data privacy, stakeholders' practitioners are themselves concerned Armoni (2000).

- Reliability : has two aspects: 1) Authenticity: the origin of the information and its attachment to the patient concerned; 2) Integrity: proof that the information has not been modified in a non-authorized way. It is either critical or non-critical. If the alteration of information is responsible for damage or inadequate treatment for the patient, integrity is critical. This is the case, but to a lesser extent, whether breaches of integrity induce legal or financial prejudices for the healthcare establishment. Otherwise, integrity may be considered as Jennett et al. (1996):

- The availability of personal medical information: the ability of an information system to be used under the normal conditions of access. Its absence may be the consequence of partial or total destruction of the information or a denial of access. The origins of the destruction may be different (physical or logical attack) and trigger immediate or delayed loss.Katsikas (2016)

It will be critical if, on one hand, the unavailability is a source of danger for diagnosis, treatment, and care for the patient and, on the other hand, it has consequences at financial or legal levels, or on other health care facility.

The Needs of data anonymization:

Within the framework of privacy protection, the degree of anonymization of the data is an important consideration and thus is an aspect incorporated in privacy regulations. Different rules apply to data, which are dependent on whether the data is considered personal data, fully anonymized, or de-identified. Fully anonymized data has all personalized data removed, is given a separate identification code, and the key between the fully anonymized dataset and any path back to the original data is deleted such that it would be extremely difficult to trace the data back to an individual. However, depending on the type and amount of data, machine learning algorithms could, within a specific probability distribution, trace back to a specific individual. Typically, various

techniques aim for fully anonymized data that can be shared without the consent of an individual (more details about our study in chapter 3). However, there are a set number of criteria that need to be met before data can be considered fully anonymized. These include taking actions to prevent the possibility of tracing, linking, or deducing individuals from the data. Each variable or combination of variables that could reasonably be used to identify an individual should be taken into account. For example, low rates of specific ethnic minorities in combination with other variables, such as age and gender, could be used to re-identify individuals. Also, more rare medical conditions coupled with other demographic features could be used to re-identify individuals. Within this context, there has been recent concern that large datasets with multiple variables cannot truly be anonymized. By merging with other large databases, algorithms can predict within a certain error margin, whether a specific dataset belongs to a certain individual. Thus, for some large datasets, it may be best to consider the dataset in the de-identified category when large numbers of variables will be shared.

1.4 Dataset (ADNI, BraTS, TCIA)

In this section, we will describe the three public datasets used in our work:

1.4.1 The Cancer Imaging Archive (TCIA)

The Cancer Imaging Archive TCIA Clark et al. (2013) Data Portal provides a platform for researchers to search, download, and analyze data sets generated by TCGA. current national Institutes of Health (NIH) research funding favors both collaborative efforts and sharable data in hopes of decreasing the time to achieve new levels of understanding and therapies. This, in turn, has stoked demands for collaborative initiatives to produce large and sharable data repositories, along with tools and resources to manage and analyze these data. The used collection Schmainda and Prah (2018) has 20 subjects with primary diagnosed GBM that are primarily diagnosed with glioblastoma each patient has two MRI scans within 90 days follow-up, where it contains T1(pre- and post-contrast agent), FLAIR, T2, and binary tumor masks (generated using T1 images). This dataset is collected to provide a way of training a deep learning algorithm for predict tumor progression tasks. Figure 1.5 shows an illustration of the MRI modalities used as inputs to our proposed TGP model with the aim to predict the tumor volume grown up from the first time scan (1st row tumor volume column) and the patient scan after 90 days (2nd row tumor volume column).

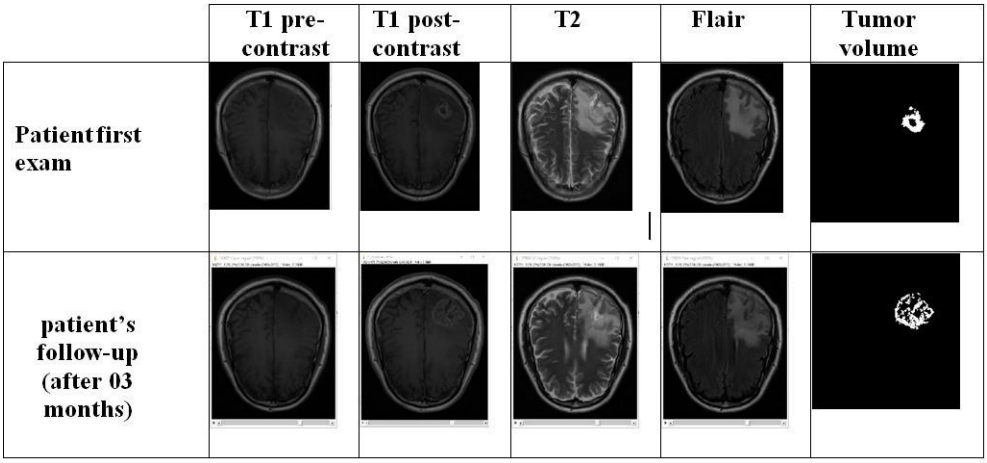

Fig. 1.5 illustration of the MRI provided by TCIA dataset, that contains T1(pre- and post-contrast agent), FLAIR, T2, and binary tumor masks (generated using T1 images)

1.4.2 Alzheimer's Disease Neuroimaging Initiative ADNI:

ADNI Petersen et al. (2010) The overarching aim of this dataset is to measure the progression of early Alzheimer's diseases based on MRI images and clinical data to determine the relationships between the clinical, cognitive, imaging, genetic and biochemical biomarker characteristics of the entire spectrum of Alzheimer's disease. The collection that we used contains 3416 pairs of T1 weighted MRI images and their ATLAS tissue (white/gray matter, and cerebrospinal fluid CSF).

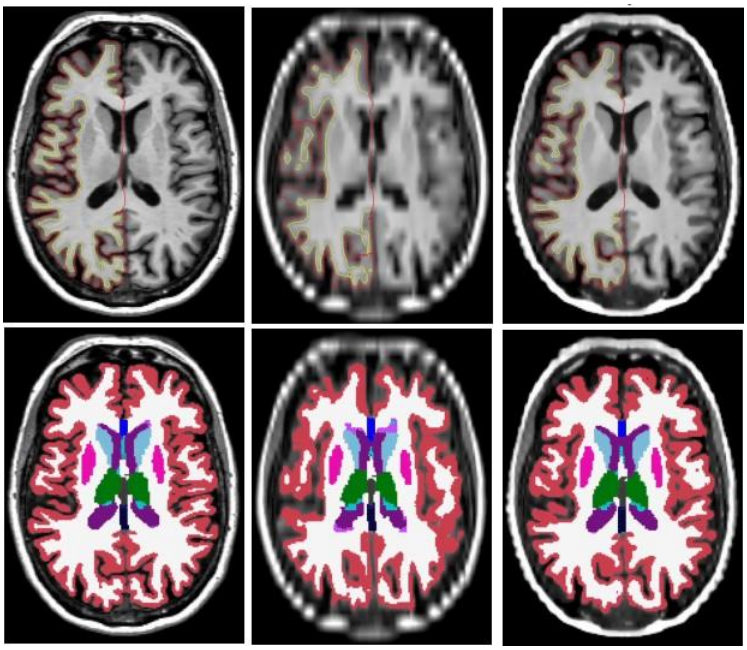

Fig. 1.6 Illustration of an example of ADNI dataset images

1.4.3 Brain Tumor Segmentation BraTS

BraTS Menze et al. (2014) scans are in NIfTI file format which contains a native (T1) , post-contrast T1-weighted (T1Gd), T2-weighted (T2), T2 Fluid Attenuated Inversion Recovery (T2-FLAIR). All the imaging datasets have been segmented manually, by one to four raters, following the same annotation protocol, and their annotations were approved by experienced neuro-radiologists. Annotations comprise the GD-enhancing tumor volume, the peritumoral edema, and the necrotic and non-enhancing tumor core.

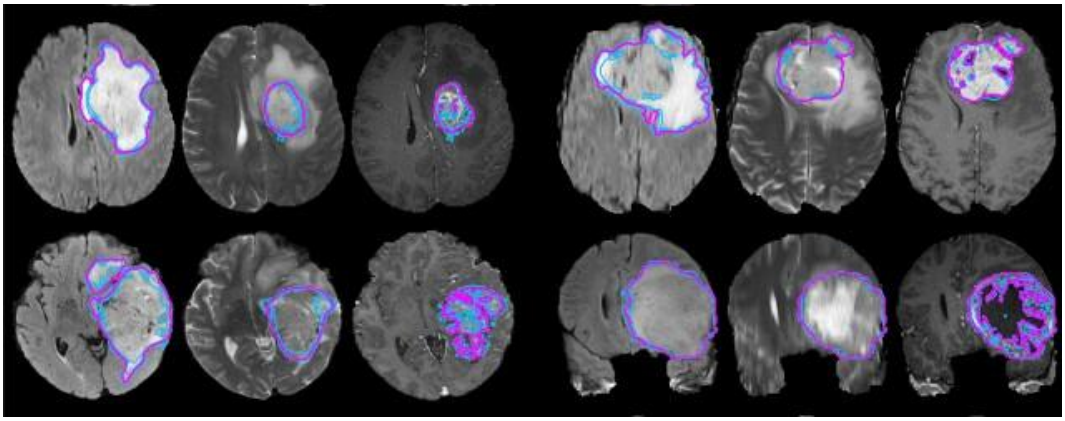

Fig. 1.7 Illustration of Brain Tumor Segmentation BraTS images

1.5 Conclusion

In this chapter, we presented a medical background for Glioblastoma tumor and statistics that motivate our investigation, We also showed the anatomy and the origin of Glioblastoma brain tumors, besides, how radiologists and oncologists diagnose and assess patients' MRI images with these tumors, besides the different level of investigation are presented and detailed.

The medical imaging and MRI techniques are presented, in addition to the challenges related to medical data in brain tumor studies. Moreover, we presented a set of three public datasets used in our work. In the next chapter, we present a survey on brain tumor growth modelling approaches. We also showed the the state-of-the-art modern approaches for genetic profile prediction, in addition to the limitation and the challenges of getting an accurate prediction result using mathematical modelling.

CHAPTER 2

Tumor growth modeling

2.1 Introduction

The Medical and surgical neuro-oncologists believed that it was almost impossible to remove this kind of tumor without generating functional deficits, especially when located within the so-called “eloquent areas”, as frequently observed. The surgical removal is mainly based on the subjective estimation of the extent of resection by neurosurgeons. It is only to achieve a biopsy that aims to obtain neuropathological examination in order to decide whether a simple follow-up could be considered or whether radiotherapy should be performed.

Indeed, a resection cannot be achieved according to “oncological” limits issued from radiological examination (as preoperative MRI, into surgical neuro navigation or intra operative neuroimaging) because this information is not the reflection of the entire glioma Duffau (2017*b*). It was previously thought that the abnormalities visible on neuroimaging corresponded to the whole disease (associated with edema), leading to consider a “normal brain” around these signal abnormalities.

In this context, Given a limited infiltrative character of the Glioma tumor, the resection imposes a major surgical challenge Pallud et al. (2012), Mandonnet et al. (2010).

The next section aim to demonstrate the effectiveness of the individual growth rate measurement, and the use cases of mathematical models before and after each therapy.

2.2 The math of GBM growth

In this section we aim to review the main known mathematical models in Brain cancer in particular the Glioma tumor. To reach this goal, we begin with models that describe the microscopic view of tumor cells and volume simulation of tumoral cell concentration at an earlier stage. Then, we discuss the macroscopic view with Reaction-Diffusion Equation (R-D) followed by some parameter estimation work, furthermore Swanson’s work to introduce specific parameters on R-D equation. Finally, we conclude by new investigation on mathematic modeling of the Glioma brain tumor using machine learning and deep learning methods.

A common feature of these tumors is the great heterogeneity in neuropathologic appearance, gene expression, and prognosis Weller et al. (2015). In 2007 WHO classification, the astrocytic tumor is the prototype referred to the description of the histologic grading. Grade I is assigned to localized tumors with low proliferative levels and potentially curable by surgical resection (pilocytic astrocytoma). Grade II includes diffusely infiltrative lesions, with cytologic atypia and low proliferative activity, which may recur and progress to higher degrees of malignancy (diffuse astrocytoma). Grade III consists of tumors with histologic evidence of malignancy, which express nuclear atypia and high mitotic activity (anaplastic astrocytoma). And grade IV includes tumors with malignant cytology, high mitotic activity, the tendency to necrosis and microvascular proliferation, with rapid growth, infiltration of surrounding tissues, skull and spinal dissemination, and unfavorable outcome (Glioblastoma multiforme). From literature brain tumor investigation, we distinguish three portmanteaux model, the first one is In Vivo in which researchers conducted tests and experiments on whole living organisms or cells, usually animals, secondly, In Vitro which was much faster than in vivo experiment but did not replace it completely. This method allows to carry out a biological procedure in a controlled environment outside of a living organism usually in test tubes or on Petri dishes, Finely, In Silico models (mathematic model and computer simulation), these models provide a testing proceeds on virtual patients, there is no risk of harm or threat to safety. Andre´ et al. (2004*b*). Following a brief overview of the main known Mathematical models, that allow describing the tumor as behavior, formulating and simulating the mechanisms of tumor growth over time. These models can be divided into two main levels of mechanism description, firstly, Microscopic where focus on biological interaction and interaction at the cell level. In the other hand, the Macroscopic models describe the full tumor behavior, velocity, and mass deformation based on information extracted from medical images. the next section will detailed each model and review the sate of the art in GBM mathematical modelling.

2.2.1 Microscopic models

The microscopic scale describes the evolution of individual cells based on division and invasion rules. This level studies the intra-cellular or biological interactions and chemical excretion. Each cell is considered independently as shown in figure 2.1. Hence, it presents the individual cells explicitly in space, time, and also the update of the individual cell according to a predefined set of biological and biophysical rules. These models are adequate when the tumor is in the early-stage (small lesion region). It focused on the study of tumor cell quantity and provided an estimation of the exact number of ab-

normal cells. However, when the number of cells increases, this microscopic scale will not fit due to the description obtained which is quite complicated.

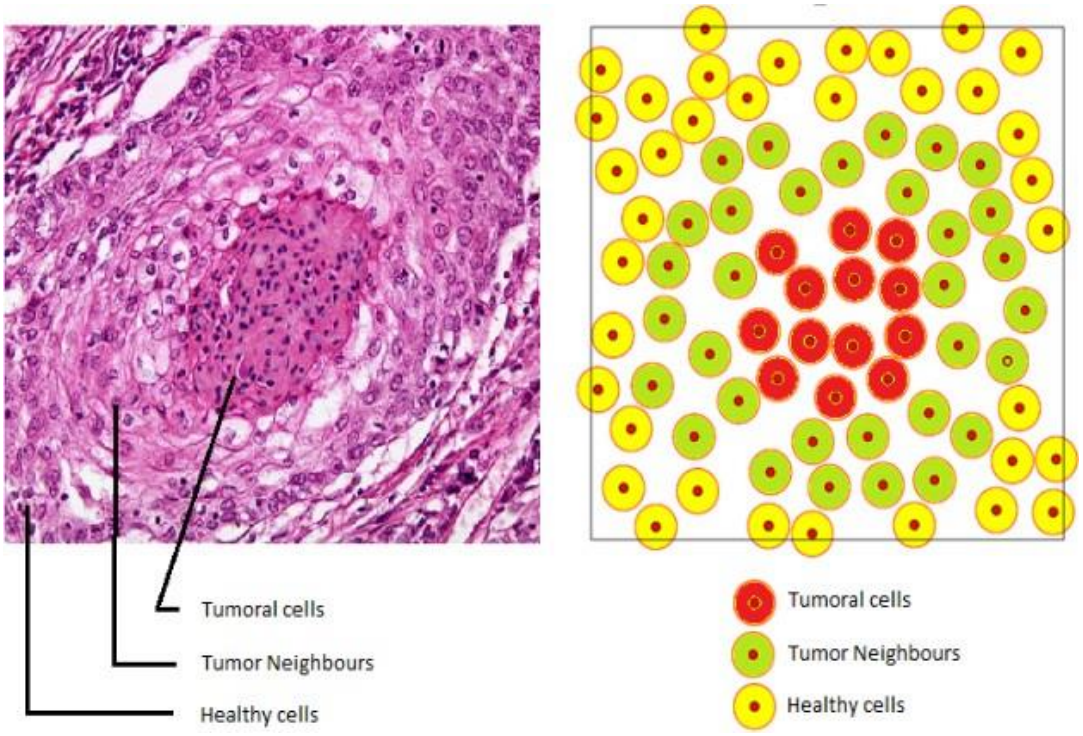

Fig. 2.1 Illustration of microscopic tumor tissue representation where each cell is considered independently, in the left a microscopic image for real tumor Fox et al. (2011), in the right is a schematic representation.

In literature, the study of tumor growth has been done by a series of microscopic models to quantify tumor cells.

The relationship of the cell cycle to tumor growth and control of cell division are describe and reviewed in Baserga (1965).The change of tumor area overtime led to the proposal of a 2D model by Lamia et al. Sallemi et al. (2015). The model provides a computer-aided prognosis for brain Glioblastomas tumor growth estimation. Such a model is based on cellular automata and fast matching Chaudhuri et al. (1997), Sethian (1996) in order to simulate the tumor growth and to predict the change of tumor size. Lamia's model used a dataset that contains MRI images for 80 patients. The evaluation of this model is based on a comparison between the obtained result and real tumor measurement by manual segmentation for successive patient scans. Besides, Kansal et al. Kansal et al. (2000) developed a three-dimensional cellular automaton (CA) model which describes proliferative GBM growth as a function of time. This approach is es-

pecially suited for a GBM, and it's designed with the evaluation of clinically important criteria in mind. The simulation data produced is in agreement with a test case derived from the medical literature, furthermore, Several GBM cell features have been incorporated into this model: the fraction of the tumor which can divide (proliferation), the non-proliferative quiescent, and necrotic fractions. As a major flaw of this approach, it's doesn't consider the spatial distribution of tumor cells or nutrients. As well, when the number of cells increases in the case of the advanced stage of the tumor, the analysis of the proposed model becomes more complicated. Al Mahmud et al. (2014) proposed a 2D cellular automaton to predict tumor growth at the microscopic level based on hypoxia (lack of oxygen) as a constraint on tumor growth, which is related to tumor invasion and cells number. Indeed, the proposed model is based on measure tumor invasion and dead cells number under different concentrations of oxygen. The obtained results demonstrate that although the cells die because of hypoxia environment (see figure 2.2(B)), it leads to increase the tumor invasion and to create a cell resistance to the drugs as shown in figure 2.2(A)

2.2.2 Macroscopic models

Magnetic resonance images MRI with its excellent soft-tissue contrast, high spatial resolution is currently the method of first choice for the diagnosis of cerebral glioma. Indeed, it is usually admitted that tumors appear on MRI only for cell densities above 500 cells/mm^3 Duffau (2017*a*). Despite technical advances, MRI (or even PET scan) still underestimates the actual spatial extent of gliomas, since tumoral cells are present several millimeters to centimeters beyond the area of signal abnormalities. For this, the macroscopic models are based on certain measurement information from the patient's MRIs in aim to estimate how fast the glioma cells are growing and where they will spread in each patient. The Gompertz model (or logistic model) Lo (2007) (goes back to 1825) allowed simulating the changing of cells from proliferative to non-proliferative according to the oxygen and nutriment of the environment thus providing a necrotic area (dead cells). Gompertz model allowed calculating the volume change in time and modeling the slowing of growth in the late-stage until product necrotic cells for the case of GBM. Based on Gompertz law Pollard and Valkovics (1992) Ri-Cha Hu Hu and Ruan (2002) proposed rules for the interaction of individuals which allows simulating the biological phenomena such as tumor growth. This model aims to show the process of tumor growth on a computer screen. In order to describe the spatiotemporal evolution of cell density a quantitative tool to predict the most probable location of tumor recurrences is proposed. Murray 1989 Murray (1989) proposed the first model for Glioma tumor growth as biological phenomena with mathematics equations. This model allows the integration of the spatial aspects and local quantities into the modeling such as the

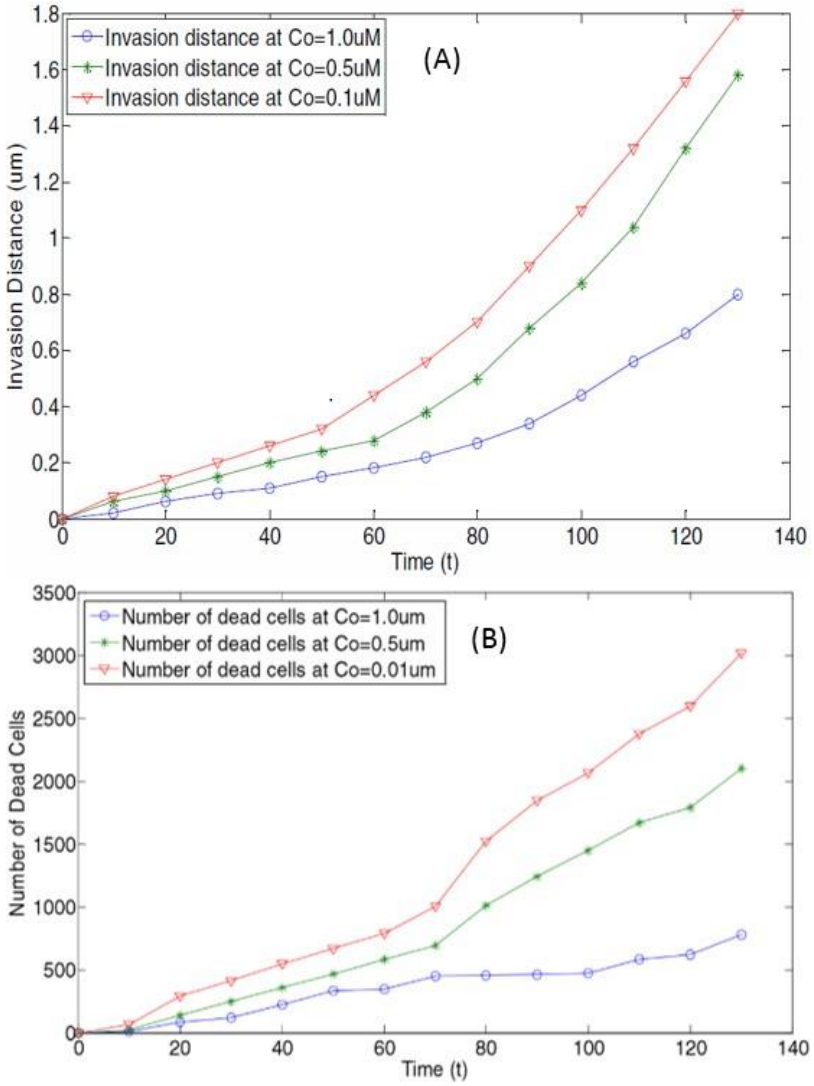

Fig. 2.2 Illustration of Al Mahmud et al. (2014) obtained results. The authors demonstrate the relation between the increase tumor invasion and the creation of cell resistance to the drugs.

tissue anisotropy, local density of cancer cells, or the spatial distribution of nutrients. These models are based on the use of Differential Equations Ordinary EDO DiPerna and Lions (1989) The model in Murray (1989) used a reaction-diffusion equation that allows estimating the cancer cells concentration in time where each patient can be characterized by two parameters: proliferation (ρ) and Diffusion (D). - The rate of change of tumor cell density is (c) = Diffusion (motility) of tumor cells + the proliferation (growth) of tumor cells as follows:

$$\frac{dc}{dt} = \nabla D(\nabla c) + \rho c \tag{2.1}$$

where ρ (1/day) represents the net rate of growth of cells including proliferation

and death (or loss), D (cm^2/day) is the diffusion coefficient of cells in brain tissue, and represents the spatial gradient. The diffusion term describes the active migration of the glioma cells using a simple Fickian diffusion Rehage et al. (1970) where cells move from regions of higher to lower densities. Tumor cells are assumed to grow exponentially.

Thereafter, Woodward et al Woodward et al. (1996) proposed a model that allows quantifying the Glioma tumor cell motility and invasion capabilities in vivo and in vitro. The obtained results suggest an average linear velocity of 12.5um/hr for human glioma cells in vitro and a minimum linear velocity of 4.8um/hr in vivo. Tracqui et al. Tracqui (1995) proposed a method to describe the invasive nature of gliomas with treatment regimes. This model simulates how tumor area is changing in time under-treatment based on the prior assumption that isotropic environment (the same diffusion coefficient). Cook et al Woodward et al. (1996) propose a mathematic model based on the Murray equation Murray (1989) to predict the resection effects on a patient's survival time. The obtained results led surgery to add little more than two extra months of life. Earlier, Traqui, et al Tracqui et al. (1995) developed a model that uses CT scans of a patient with Glioma tumors to quantify the effect of chemotherapy on Glioma tumor growth. The change of area and volume is measured while the patients undergoing chemotherapy treatment. Swanson team Swanson et al. (2000, 2003, 2008), Jackson et al. (2015), Randall et al. (2018) have a major contribution in mathematic modeling for glioma tumors. The first model Swanson et al. (2000) is based on the equation of Murray Murray (1989) and allows the introduction of the brain tissue heterogeneity (i.e. white and grey matters) to identify the accurate tumor region and their effects on cell migration velocity. Thus, based on Reaction-Diffusion (see equation 2.1) and the introduced parameters by Tracqui et al Tracqui (1995), Swanson's model specified for each brain tissue (i.e. white and grey matters) a fixed diffusion coefficient. Brain-Web database Kwan et al. (1999) is used to identify accurately the grey and white matter and the effects of the heterogeneity within brain tissue in tumor invasion in order to control the malignancy of gliomas regions.

The model in Swanson et al. (2000) take into account how fast is the tumor grows and spread through the mentioned brain tissue, also this equation could predict the mobility of the tumoral cells (see figure 2.3).

The equation of Swanson is based on the heterogeneity of the brain tissue. It has two diffusion coefficient parameters, where this equation (see equation 2.2) assumes that the diffusion in white matter(is equal to five times the diffusion in grey matter and tumoral cell position x, thats lead to five-fold difference in the diffusion coefficients in grey and white matter: Dw = 5 Dg.

$$\frac{dc}{dt} = \nabla D(x)(\nabla c) + \rho c. \tag{2.2}$$

$$D(x) = \begin{cases} D_W & \text{if } x \in \text{White matter} \\ D_G & \text{if } x \in \text{Gray matter} \end{cases}$$

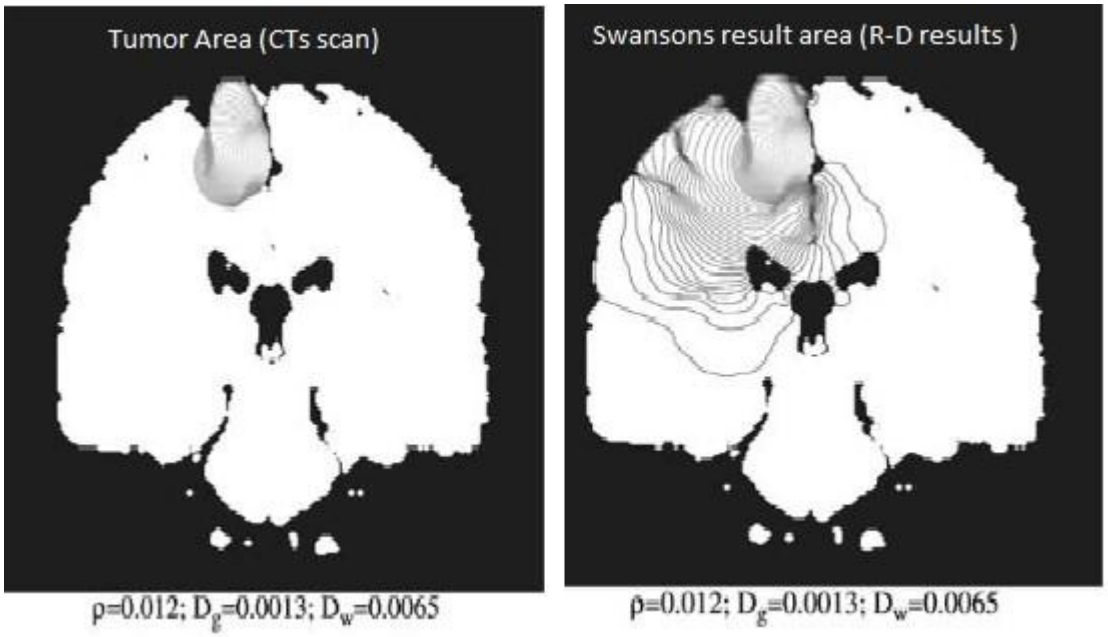

Fig. 2.3 Swanson Simulation of tumour invasion of a high-grade glioma in the superior cerebral hemisphere. the left side is the tumor area by the standard threshold of detection. Where the sensitive threshold of detection shown in the right side Swanson et al. (2000).

In 2003, Swanson et al. (2003) studied Glioma tumor growth in a virtual and real brain. The virtual Glioma model quantifies the spatiotemporal growth and invasion in 3-dimensional space on a virtual human brain from a diagnostic size of 3 cm to a fatal size of 6 cm in diameter. The features that affect the prognosis of a patient with Glioma tumors are the histological type, the grade of malignancy, the patient's age, and level of neurological functioning in which, those features may predict the individual tumor behavior (growth velocity). They Swanson et al. (2003) found the velocity of expansion is linear with time, where it increases 10 times faster, from 4 mm/year for low-grade Gliomas to 36 mm/year for high-grade Gliomas. Besides, Randall et al. (2018) developed a model that allows simulating the effects of the operation on the GBM lesions. The model predicts behavior similar to that observed clinically, their model based on given initial tumor size, grade, and location, in order to simulate the effects of various resection sizes and geometries on survival time. In 2008, Swanson Swanson et al. (2008) has developed virtual control for each patient with Glioblastoma

tumors. A software Swanson et al. (2008) program had been created using data from magnetic resonance imaging scans in order to simulate how fast is spread of tumoral cells in a patient's brain. In addition, this software has an accurate result in terms of precision, where it could predict the tumor growth and the survival time of each patient and under various treatment scenarios. In 2015 Jackson Jackson et al. (2015), developed patient-specific mathematical modeling enabling neuro-oncology to obtain optimized individualized treatment plans. Thereby an efficient and accurate prediction of tumor growth is proposed. These mathematical models are dedicated to improving the response of each patient to treatments. Despite the success of these models, they still have an issue of defining the parameters (i.e. p, D). Clatz Clatz et al. (2004) proposed a reaction-diffusion model to simulate Glioblastoma growth and brain anisotropy using DTI images. Clatz model Clatz et al. (2004) created a virtual tumor and a proved compression with real Glioblastoma at a different time point (6-month period). The model of Clatz Clatz et al. (2004) is oriented to address the tumor mechanical interaction. Also, this model allows simulating the mass effects inside the brain. Matthieu Leˆ et al. (2015) proposed a method for conducting the Bayesian personalization of the Glioblastoma growth model parameters. Their model estimates the parameters of the tumor growth model using posterior probability. The work of Leˆ et al. (2015) has contributed (1) to the estimation of the growth model parameters, which are difficult to predict due to the lack of identifiability of these parameters. On the other hand, the uncertainty in the tumor segmentation, and the model approximation cannot perfectly capture the dynamics of the tumor. The method of Leˆ et al. (2015) extracts the segmentation's of the visible abnormalities and uses the Bayesian method to estimate the parameters that control the tumor growth at different points of time.

2.2.3 Overview of mathematical modeling approaches

A wide variety of mathematical modeling approaches have been studied to simulate brain tumor growth. In this section, a chronological classification is provided. Figure 2.4 shows a history of Tumor growth model evolution.

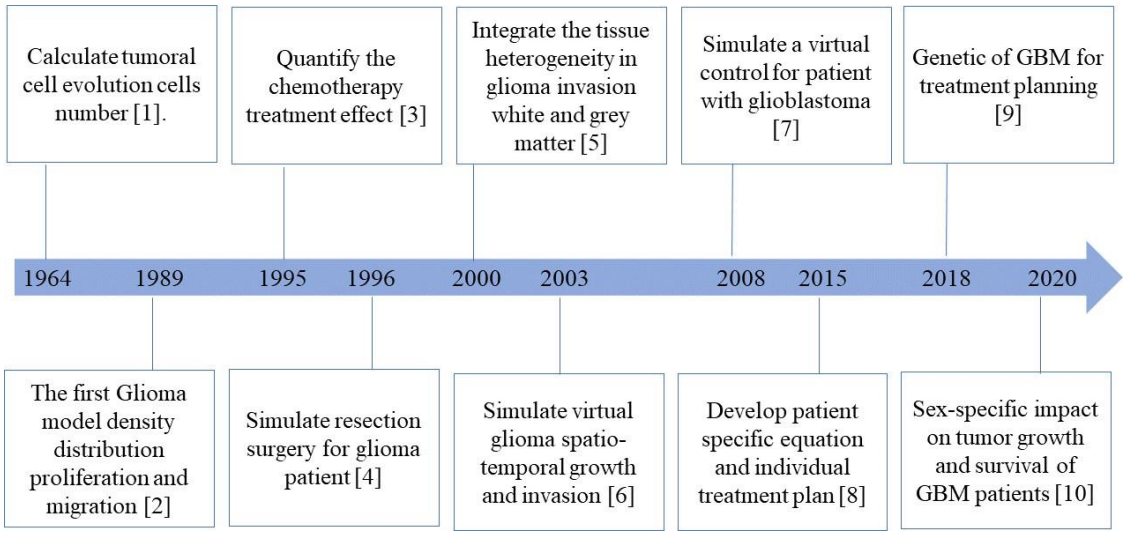

Fig. 2.4 Timeline of major mathematical models of brain tumor growth.

[1]: Baserga (1965) [2]: Murray (1989).
[3]: Tracqui (1995) [4]: Woodward et al. (1996).
[5]: Swanson et al. (2000). [6]: Swanson et al. (2003).
[7]: Swanson et al. (2008). [8]: Jackson et al. (2015).
[9]: Massey et al. (2018) [10]: Massey et al. (2020).

2.3 Genetic of Brain Tumor

Within the glioma brain tumor classification, genomic studies have described distinct molecular subtypes that tend to correlate with biological etiology, prognosis, and therapeutic response. The discovery of these subtypes indicates that, in addition to conventional histology, molecular genetic testing will and may be useful in the clinical assessment of glioma. In 2008, the Cancer Genome Atlas (TCGA) reported a comprehensive study of the molecular characteristics of glioblastomas Network et al. (2008), and demonstrated that glioblastomas aggressiveness and growth depends frequently on its molecular profile that contains the status of genes-set (markers), this molecular profile provides valuable information about prognosis and treatment response for GBM. During a diagnosis exam, a doctor may recommend a biopsy test in order to define the molecular profile of glioma patients using gene testing laboratory-based, in which a sample of blood or tissue is tested for changes in a chromosome linked to brain tumors and tested for the inherited syndrome. Predicting a single glioma reaction to a drug is a big aim of contemporary oncology, and it could eventually lead to individualized care. Multiple associations between genomic changes and drug responses have been discov-

ered by high-throughput screenings of potentially active compounds against a panel of genomically heterogeneous cancer cell lines. Several statistical methods to predict susceptibility based on genomic features have been suggested, while others have focused on the chemical properties of the drugs to assess their effect. A common method for identifying lead compounds with a beneficial impact on a given phenotype is to scan a large number of molecules in a high-throughput manner. In the field of cancer, libraries of chemical entities have been examined against panels of cell lines grown in various environments and with varying genomic histories in this manner.

2.3.1 State of the art for Genetic investigation:

For the genetic profile studies, Zhou Zhou et al. (2017) proposes a model to predict survival rate and molecular profile for Low-Grade Glioma (LGG) patients using TCIA dataset Pedano et al. (n.d.) contains 165 patient multimodel MRI scans (T1, T1C, T2, Flair). Zhou et al. (2017) study based on the Visually Accessible Rembrandt Image (VASARI) feature collection, conduct a systematic study of MR imaging characteristics of LGGs as they contribute to patient survival and molecular markers. Also uses a textural features derived from MR imaging to make binary predictions of wild-type IDH versus IDH1 mutation, IDH1 mutation with 1p/19q codeletion versus IDH1 mutation without 1p/19q codeletion, grade II versus grade III LGGs, and progression versus non-progression of LGGs.

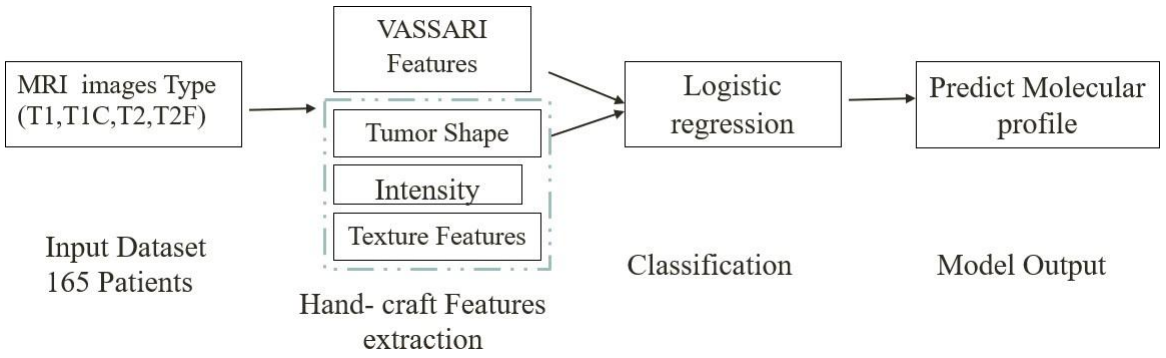

Fig. 2.5 Zhou et al. (2017) model to predict survival rate and molecular profile

As a result, IDH1 mutation, 1p/19q codeletion, histological rating, and tumor progression were all predicted with high precision using textural analysis of MR imaging results. In the same objective, Zeju Li et al. (2017) proposes a model to predict IDH for low-grade glioma patients, this model is based on Deep-Learning architecture to extract deep information from multiple modalities of magnetic resonance (MR) images and used private data. The private dataset yielded a cohort of 151 cases. Patients that have been diagnosed with grade II glioma. Every case's diagnosis of low-grade glioma

was verified by two pathologists independently, and the IDH1 mutation status was confirmed by Sanger sequencing Sanger et al. (1977).

Li et al. (2017) model's success was tested using various MR imaging modalities in the first cohort, which included 119 cases of both T2 flair and T1 contrast images. The second cohort, which included 110 cases with T2 flare images, was used to compare the IDH1 prediction performance of the model and the conventional radiomics approach. Figure 2.6 Li et al. (2017) illustrates and flowchart to recognize the tumor regions in the MR images to extract the deep filters. The molecular profile prediction was based on the deep filters and evaluated by a leave-one-out cross-validation SVM.

Zeynettin Akkus et al. (2017) proposes convolutional neural networks (CNN) model based on MR images from patients with LGG. The results obtained in this model is the prediction of 1p/19q without the need for surgical biopsy. Akkus et al. (2017) classification algorithm takes a mixture of two frequently acquired image forms as input: T2 and post-contrast T1-weighted images. Multi-modal image registration, tumor segmentation, data normalization, and data augmentation are among the pre-processing steps used in the classification algorithm. Segmented images are used to train a multi-scale CNN for 1p/19q status prediction after applying pre-processing steps to the data. Figure 2.7Akkus et al. (2017) depicts the multiscale CNN's flowchart and implementation info for the Zeynettin model.

Ken Zhang et al. (2017) propose a CNN model to predict IDH status for low and high-grade glioma patients, The model is based on Deep-Learning architecture to learn from MRI images for 446 patients. Zhang et al. (2017) uses a range of training heuristics and equipped a neural network for coronal, sagittal, and axial dimensions with comparable research set performance using the dimensional networks training heuristic. Finely, they trained a neural network for each MR series using the sequence networks training heuristic. As result, T1 post-contrast images had a higher predictive performance than other MR samples, and they proved to be responsible for the vast majority of the combined sequence model's precision, with additional sequences providing a smaller

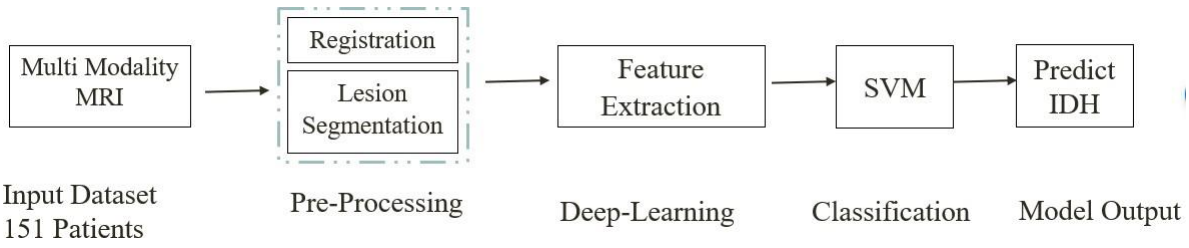

Fig. 2.6 Li et al. (2017) model diagram for IDH status prediction for low-grade glioma patients

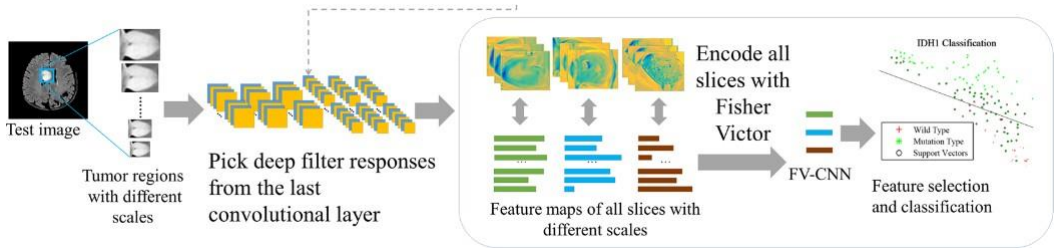

Fig. 2.7 Li et al. (2017) flowchart to recognize the tumor regions in the MR images to extract the deep filters

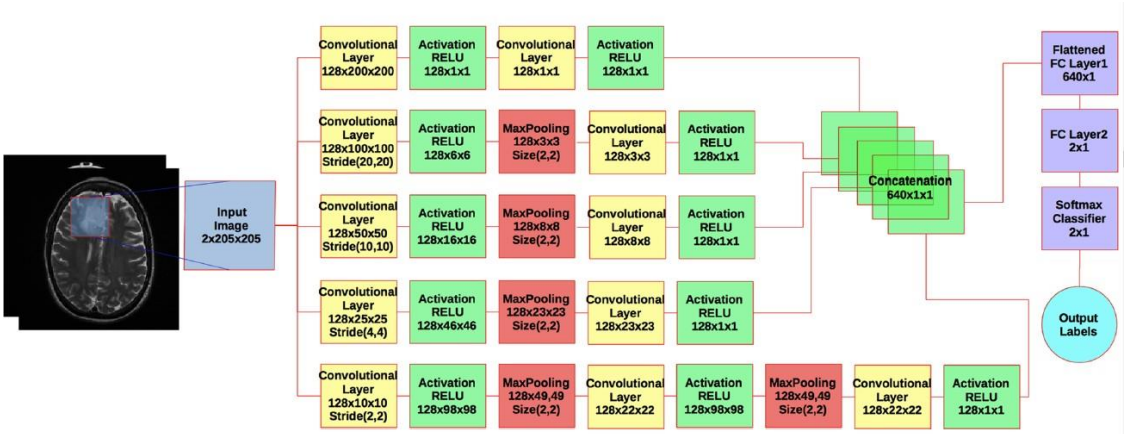

Fig. 2.8 Flowchart and implementation info for the Zeynettin model Akkus et al. (2017)

incremental gain. Javier Villanueva-Meyer et al. (2018) is a Radiologist studied for qualitative tumor characteristics for patients with LGG (grade2), this work aims to determine the MRI characteristics associated with IDH mutational status, Javier finds that age is an important characteristic for IDH prediction Chon Lao et al. (2017) propose to use deep features extracted via deep-learning with the aim to predict survival time for GBM patients. The goal of the Lao et al. (2017) study was to see whether radiomic feature-based imaging signatures would predict survival and stratify patients with newly diagnosed glioblastoma with compared precision with the clinical and radiologic risk models.

Furthermore, TP53 is a biomarker for glioma and allows to predict the high-risk (progression to high grade). Yiming Li et al. (2018) proposes a machine learning model to predict molecular information TP53 based on the radiomic features that are extracted images from the Chinese Glioma Genome Atlas database (http://www.cgga.org.cn), the content of the dataset is detail in table bellow.

Li et al. (2018) model based on the radiomic signatures extracted from conventional magnetic resonance (MR) images for the patient with primary grade II/III gliomas. Using the Least Absolute Shrinkage and Selection Operator LASSO regression and

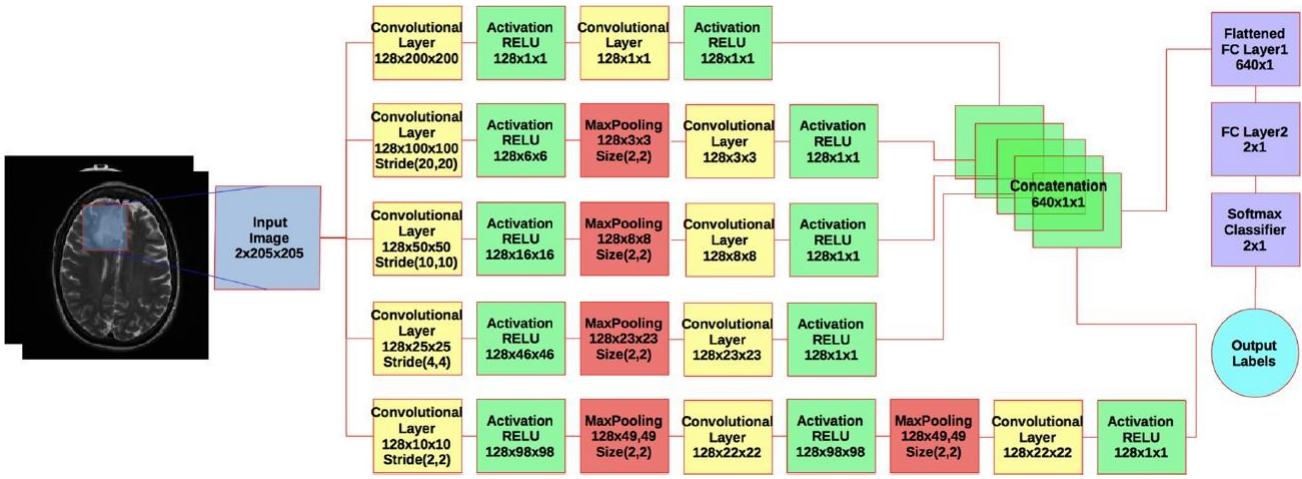

Fig. 2.9 Chon Lao et al. (2017) used a radiomic feature-based imaging signatures to predict survival

	Total (n = 272)	Training (n = 180)	Validation (n = 92)	p value
Age (years; mean)	40.1	39.2	41.9	0.054[a]
Sex (male/female)	169/103	111/69	58/34	0.825[b]
Grade II/Grade III	179/93	123/57	56/36	0.220[b]
P53 wild type/P53 mutation	151/121	104/76	47/45	0.293[b]
Tumor location (left/right/bilateral)	142/113/17	95/73/12	47/40/5	0.306[b]

Legends.
a T-statistical test.
b Chi-square test.

Table 2.1 Details data used in Yiming Li et al. (2018) model

Support Vector Machine SVM, to establish the radiomic signature that achieves non-invasive and efficient prediction of the p53 status in gliomas as shown in .9.

A strong correlation between p53 phenotype and the radiomic features in lower-grade gliomas with 80.0% of prediction accuracy is achieved. A satisfactory review for genetic investigations on glioma research is provided in Chong Suh et al. (2019) that study and review about 30 article works on predicting IDH status from patients image

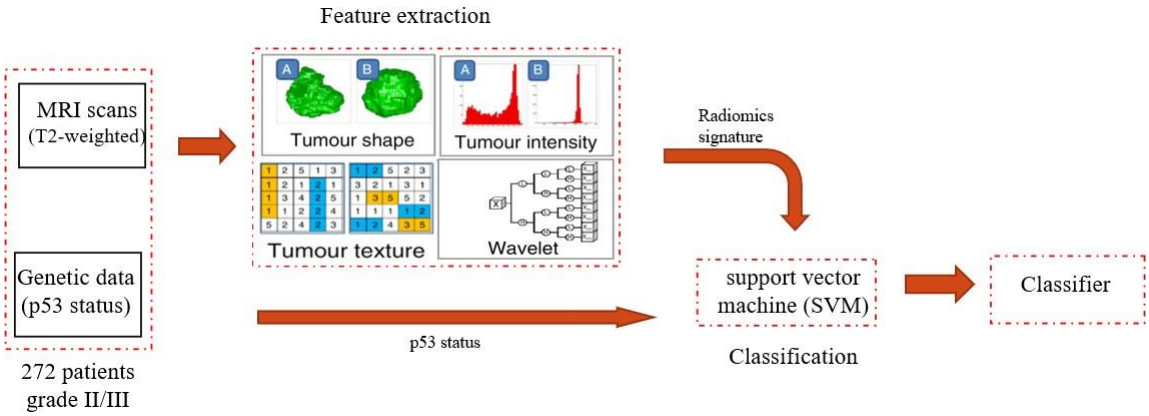

Fig. 2.10 Yiming Li et al. (2018) machine learning flowchart to predict molecular information TP53 based on the radiomic features

2.4 Proposed MLP for genetic profile prediction:

Gliomas are the most common primary brain tumors in adults ,where doctors in diagnosis step aim to :

- Detect the tumor lesion (detection).
- Define the tumor volume and contours (segmentation).
- Predict Treatment efficacy.
- Predict survival time.
- Risk of evolution to High grade.

Our aim is to develop non-invasive method to determine the genetic markers such as 1p/19q, IDH, EGFR, p53,witch provide valuable information about treatment response and prognosis in patients with low-grade gliomas (LGG) We aim to develop a Genetic Profile Predictor MLP which considered as a non-invasive model that provides genetic markers. the objective is to predict genetic markers and survival time for patients with low grade glioma based on series of features obtained from MRI images :

- IDH,1p19q,EGFR: Treatment response and treatment decision-making.
- TP53: High risk (progression from LGG to the HGG).
- Survival rate: As future work.

In 2016 The World Health Organization (WHO) classifies gliomas tumors entities based on molecular profile. The molecular information guided decision-making and has remained beneficial to determining treatment strategies. Among the genes used in the WHO classification, we cited :

Gene	Status possible	To predict
IDH	Mutant/wide-type	Treatment efficiency
1p/19q	co deletion/non-co-deletion	
EGFR	Mutant/wide-type	
p53	Mutant/wide-type	Progression to High grade

Table 2.2 The molecular information guided decision-making World Health Organisation 2020

Several reason lead to start with IDH1 gene prediction: (i) The Isocitrate DeHydrogenase (IDH) gene is identified in most diseases of Gliomas tumor, (ii) Recently, the Gene mutations (status) have been identified for this gene in more than 70% of grade II and III gliomas and also for secondary glioblastomas VI. (iii) Tumors with mutations in IDH have distinct clinical and genetic characteristics and generally have a better prognosis than similar tumors. Finally, IDH1 have two possible states: IDH Mutant that coded in the dataset "IDH-mut" and IDH wide-type coded in the dataset as "IDH-wt"

2.4.1 Materiel and methods:

We based on public available dataset that contain 30 Features called VASSARI features and their explications, and composed of 188 samples include :

- Patients' clinical data includes : age, sex, tumor grade (see figure 2.10).
- Features called VASARI features extracted by an expert from patients images namely : Tumor location, Side of Tumor, Lesion Size (see figure 2.11).
- Patients Image (T1,T1C,T2,T2Flair).

A	B	G	H	I	J	N	O	P
patient id	Tumor	IDH1	IDH/1p19q Subtype	death01	daystolastordeath	EGFR	PDGFRA	TP53
1	TCGA-CS-4938	1	2	0	143	wt	wt	Mutant
2	TCGA-CS-4941	0	0	1	234	wt	wt	wt
3	TCGA-CS-4942	1	2	1	1335	wt	wt	Mutant
4	TCGA-CS-4943	1	2	0	552	wt	wt	Mutant
5	TCGA-CS-4944	1	2	0	323	wt	wt	wt
6	TCGA-CS-5390	1	1	0	1966	wt	wt	wt
7	TCGA-CS-5393	1	2	0	1222	wt	wt	Mutant
8	TCGA-CS-5394	1	1	0	3	wt	wt	wt
9	TCGA-CS-5395	0	0	1	639	wt	wt	wt

Fig. 2.11 Patients' clinical data (age, sex, tumor grade, . . .)

patient	Tumor Location	Eloquent Brain	Enhanc	Satellites:	Calvarial remodeling:	Lesion Size
TCGA-CS-4938	1	1	1	1	1	9
TCGA-CS-4941	1	1	3	1	1	9
TCGA-CS-4942	3	1	2	1	1	11
TCGA-CS-4943	4	4	1	1	1	12
TCGA-CS-4944	2	1	2	1	1	18
TCGA-CS-5390	4	1	3	1	1	8
TCGA-CS-5393	2	3	3	1	1	18
TCGA-CS-5394	1	1	1	1	1	7
TCGA-CS-5395	4	1	1	1	1	7

Fig. 2.12 Patient's VASARI features extracted by an expert based on medical images includes : (Tumor location, Side of Tumor, Lesion Size . . .)

2.4.2 Data preparation

A step of digitization and normalization was applied to the dataset in order to be readable and usable, then we combine clinical features (histological type, neoplasm histological grade, gender, age at initial pathological . . .) and VASARI information. Eliminate Not Available features. Finely we eliminate Genetic status and survival rate (to be used as our model output). Here we list all the steps used to prepare the data file:

- Normalize file (to be usable with programming language "python").
- Combine clinical features (histological type, neoplasm histologic grade, gender, age at initial pathologic . . .) and VASSARI information obtained from images (Tumor location , Side of Tumor , Lesion Size . . .).
- Select relevant features.
- Eliminate features (Not Available).
- Eliminate Genetic status (to be used as model label).
- Eliminate survival time (May used as label as well).

The actual used dataset contain 160 patient with 38 available features (see figure 2.12).

2.4.3 Model Conception and Implementation :

Our model takes as input all relevant features provided by the TCIA dataset, and use the IDH1 Status as a model label (see figure 2.13).

After the step of data cleaning and preparing, we have a dataset containing 160 samples with 38 available features, We put our MLP model under series of different testing techniques to achieve the best prediction accuracy :

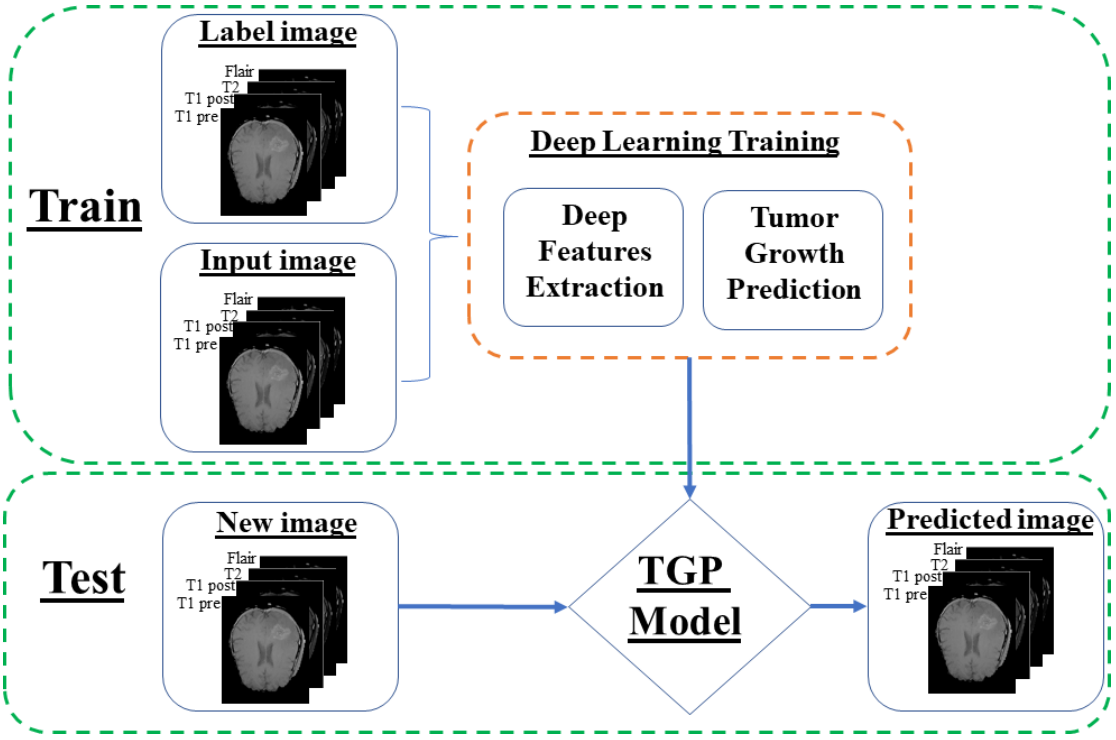

Fig. 2.13 Patient's features used for the model training : 38 features (VASSARI + clinical) in green color and IDH1 status in blue. Separate Dataset into two division (training and testing) green and yellow.

- Different combination of features as input
- The effect of adding layers and nodes to neural network
- Test different architecture (model size and dimension)

Our model train using a GPU and the obtained results were evaluated based on metrics known in the literature. One of the major challenges faced our model is the hyper-parameter selection, where the accuracy depends on a set of such parameters. A plage of testing hyper-parameter is used in our training, and each set of those parameters called 'Fit Case ' and give result (Accuracy, loss) we choose the best model when High Accuracy and low loss :

- Size of hidden layers [32 .. 1024]
- Activation function ['logistic', 'tanh', 'relu']
- Number epoch [10 .. 20 000]
- Patches size [2,4,8,16,32,64]
- Optimizer functions['SGD', 'RMSprop']

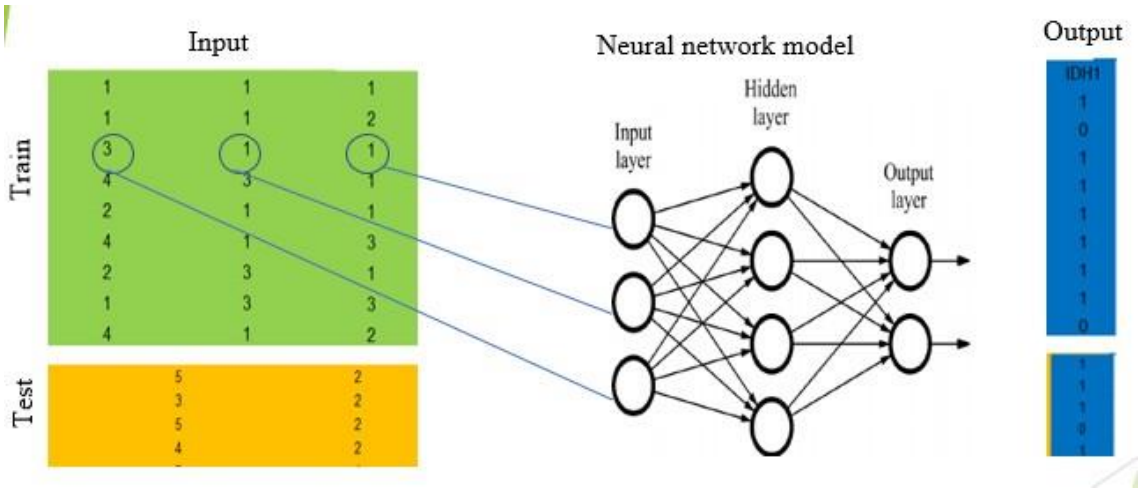

Fig. 2.14 Multilayer perceptron architecture (MLP). the green/yellow indicate the input feature for training and testing, the blue is the prediction output (binary classification of IDH status).

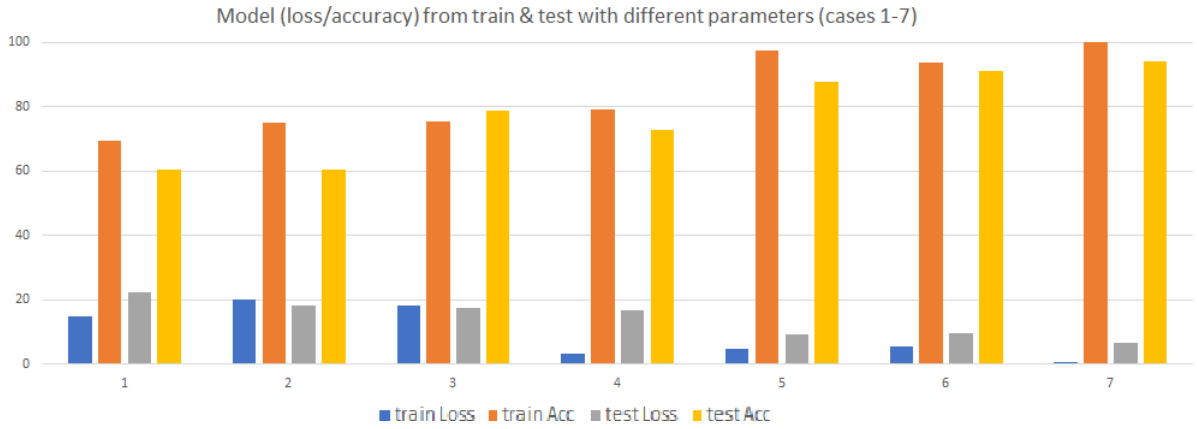

Fig. 2.15 Illustration of our classification results, we showed 7 result cases obtained using different training hyper-parameters. All result are based on BRATS 2017 dataset

- Learning rate = [1e-3,1e-4,1e-5,1e-6,1e-7,1e-8]

2.4.4 Our model classification results :

The aim is to find the best accuracy by trying different experiments (testing different hyper-parameters). From obtained results, the best experiment is the last case (07) when the training accuracy achieved 100% and test accuracy 93,9%. Case (07) parameters : hidden layers [128,256,512], Optimizer = 'SGD' , Learning rate = '0.001' activation function 'Relu ', figure 2.14 we list cases with all obtained results.

The major issue face our model is the problem Over-fitting, which the lack of model generalization- the so-called (over-fitting) is a term used to describe a model's ability to reach for new data. It makes the model useless even though it is able to make accurate

predictions for the training data. So the model will fail to make accurate predictions with new data. As Solution: we attend to enrich inputs data by adding patients images for model input.

2.5 Discussion and Conclusion

We have been motivated by the recent investigations in both GBM tumor prediction Morris (2005) and data generation Shin et al. (2018) in the field of brain tumor prediction, mathematical methods becomes more accurate and the inference time is decreased compared to the time spent by radiologists to predict the tumoral area growth. In addition, these automatic brain tumor prediction methods provide an objective, fast, and reproducible assessment of patients MRI analysis compared to radiologists who produce a subjective, slow, and difficult to reproduce even for the one patient MRI images. Table 2.3 shows a summary of state-of-the-art modern approaches for tumor growth modelling. These approaches are based on both mathematical modelling and machine learning techniques. Moreover, these approaches are applied to the GBM brain tumors growth and genetic profile prediction.

In this chapter, we presented a survey on brain tumor growth modelling approaches. We also showed the the state-of-the-art modern approaches for genetic profile prediction, in addition to the limitation and the challenges of getting an accurate prediction result using mathematical modelling. Through a variety of applications in medical image analysis, in particular, GBM brain tumors growth, Genetic profile prediction have proven their effectiveness in treatment planing and predicting all treatment response . In addition, they provide a promising prediction performance compared to classical approaches and state-of-the-art methods in terms of treatment planing.
In the next chapter, we present our first contribution based on Convolutional Autoencodeur Networks for Tumor Growth Prediction (TGP). Our model aim to solve and answer the questions related to the fully automatic manner GBM volume growth prediction. In addition, we sutdy and review preprocessing tools used for medical image preparation, and theier impact on TGP prediction performance.

Reference	Tumor	Study-l	Take into account			Under Treatment		
			D	N	M	chemo	Radio	Rese
Sallemi et al. (2015)								
Kansal et al. (2000)	GBM	Micro	√	√	√	√	√	√
Hu and Ruan (2002)	Solid-G	Micro	√	√	√	√	√	√
Murray (1989)	Glioma	Macro	√	√	√	√	√	√
Woodward et al. (1996)	Glioma	Macro	√	√	√	√	√	√
Tracqui (1995)	Glioma	Macro						
Swanson et al. (2000, 2003) Swanson et al. (2008) Jackson et al. (2015) Randall et al. (2018)	Glioma	Macro	√ √	√ √	√ √	√	√	√
Clatz et al. (2004)	GBM	Macro	√	√	√	√	√	√
Leˆ et al. (2015)	GBM	Macro	√	√	√			
Morris et al. (2006)	L.G.G	Macro	√	√	√	√	√	√
Lao et al. (2017)	GBM	Macro	√	√	√	√	√	√
Randall et al. (2018)	GBM	Macro						

Legends.
Study-l : Study level. Micro : Microscopic, Macro : Macroscopic, Gen : genetic.
D : take into account cells density changing.
N : take into account dead cells density.
M : take into account cells megration.
Chemo : chemiotherapy treatment.
Radio : Radiotherapy treatment.
Res : Resection and suregy treatment.

Table 2.3 Overview of state-of-the-art mathematical modelling approaches for brain tumor growth modelling

CHAPTER 3

Brain Tumor Growth Predictor

In this chapter, we present the issue of developing an efficient brain Tumor Growth Predictor (TGP) model that allows to predict how GBM tumor will look like after the follow-up step, TGP used multi-sequence MRI images publicly available and provided by TCIA datasetClark et al. (2013), (see figure 2.5). TGP is based on End-to-End Convolutional Neural Networks architecture LeCun et al. (1998) and it is inspired by convolutional autoencoder architecture Seyfioğlu et al. (2018).

TGP model takes input MRI image with four channels in the aim to predict the tumor volume in late-stage (i.e., tumor area after 90 days). To evaluate the effectiveness of our TGP proposed network we perform three common metrics: recall, precision, and Dice scores, each metric is described using four statistical values: True Positive (TP), True Negative (TN), False Positive (FP), and False Negative (FN) Volume Fractions are borrowed from statistical decision theory metrics (Sensitivity and Specificity) Yeghiazaryan and Voiculescu (2018) .

Getting an efficient and accurate prediction of Glioblastoma brain tumors growth gives an early clinical diagnosis, treatment plan, and follow-up. To the best of our knowledge, GBM growth prediction based mainly on mathematical modelling where the tumor lesion studied as the biological process and the growth calculated using the principe of mathematical biology invented by Pr. Murray (1989). . The mathematical modelling (MM) based on reaction-diffusion equation lead the majority of GBM growth prediction in 1990 and the early 2000, which uses the patients clinical data and details extracted for patients image to form the so-called patient-specific equation Jackson et al. (2015), as major limitations for this process is first: time consuming task, while GBM patients have short survival rate Buckner et al. (2007), the second limit is that this equation could used only for one specific patients due to the huge lot of parameters used in forming these equations. for this reason we believe that machine learning (ML) could contribute for the GBM growth with the same level as MM, and could be applied to many patients in the same time. in addition, ML didn't take into account details related to specific patient, thus show results in short time comparing to MM. In this chapter, we focus on the process of developing a machine learning algorithms, inspired by con-

volutional autoencoder architecture Seyfioğlu et al. (2018) for GBM growth prediction, we start by a brief introduction and background. In aim to prepare MRI image for TGP model, we review data pre-processing tools and techniques that are needed for an efficient prediction accuracy. Thus, we study the impact of pre-processing in TGP model prediction accuracy including the skull stripping, registration and resizing, normalisation/standardisation , and filtering/denoising process. TGP model take as input patients image in the diagnosis time point and aim to the tumor volume in late stage (after 90 days of followup).

3.1 Motivation and objectives

During the last two decades, the problem of GBM brain tumor growth prediction has attracted many researchers, in which a huge number of published papers study GBM behavior and involve the problem of its growth prediction, the creation of a smart brain tumor prediction system has always been a highly needed option. The motivation behind the need to create a smart system powered by Deep Learning and CNNs is that instead of waiting to collect all parameters needs for mathematical modelling. This way gives radiologists and oncologists more time with their patients in the therapy planning process, especially in the treatment and follow-up stages. The aim of this section is to propose a methodology to develop a fully automatic method for the GBM brain tumors growth prediction using MRI images. To achieve this goal, we propose the following contributions:

- We study and review the effect of MRI image quality on the performance of machine learning model, since we need to improve the quality of these images by first removing the skull, then applying a registration step, then normalizing these images, and finely denoising and filtering.
- We develop a fully automated tumor growth predictor TGP inspired by convolutional autoencoder architecture to solve the issue of GBM growth prediction and provide the tumor volume in late stage, TGP based mainly on multi-sequence MRI image for primary diagnosed GBM, each patient has two MRI scans within 90 days in two time points. TGP capable to predict the tumor volume in late-stage.

In the next section we present a brief introduction and background theory for machine learning, in addition to its applicability on health care field, also, we mention some research in brain tumor and GBM behavior.

3.2 Background theory: machine learning

Since the early days of Machine Learning (ML) in the 1950s Samuel (1959) the goal was to learn from data, to gain knowledge from experience, and to make predictions. The field accelerated by the introduction of statistical learning theory in the late 1960s; although it was at that time a purely theoretical analysis of the problem of function estimation from a given collection of data Vapnik (1999). With the advent of modern statistical learning algorithms (e.g. help vector machine Boser et al. (1992)) statistical learning theory becomes more and more interesting as a method for designing algorithms of realistic use for the estimation of multidimensional functions Hastie et al. (2009).

Today, ML is the most growing sub-field in computer science, and Health Informatics (HI) is the great application challenge Jordan and Mitchell (2015), Shen et al. (2017). In the health domain, we are confronted with probabilistic, uncertain, unknown, incomplete, heterogeneous, noisy, dirty, unwanted, and missing data sets which endanger the modeling of artifacts. Moreover, in the biomedical world, we are confronted with a further problem: time. Whilst most computational approaches assume homogeneity in time, people and processes in the health domain are not homogenous in time and cannot be forecasted, sometimes it can happen completely unexpected. That makes automatic solutions in this domain difficult, yet sometimes impossible. There are uncountable future challenges in the design, development, experimentation and evaluation of ML algorithms generally and in the application to health informatics specifically. The ultimate goal ever since is to develop algorithms that can automatically learn from data, hence can improve with experience over time without any human-in-the-loop. Many researchers in ML community are concentrating on automatic Machine Learning (AML), with the goal of excluding humans, hence making it fully automaticTenenbaum et al. (2011).

Artificial intelligence can be described as the field of designing and creating systems that can provide effective solutions for real-world problems by drawing inspiration from human thinking behaviors, as well as actions were taken by other living organisms and natural dynamics Cortes et al. (2020). Machine learning is a human-made product that offers very effective and efficient tools for automating real-world problems. As humanity has made many discoveries and innovations in the past, artificial intelligence is the most recent groundbreaking innovation that has driven technical advances since the mid-twentieth century. Taking the modern state of the 20th Century into account, there are no areas in which approaches, processes, and strategies dependent on artificial intelligence are not used. It has been a very simple task to solve complex (and sometimes almost impossible) problems using artificial intelligence in the form of only iterative code classes. Romportl et al. (2016) figure 3.1 Holzinger (2016*b*) represents

a broad overview of the relationship and the field of artificial intelligence in general. The perspective can be strengthened by adding further relationships, as artificial intelligence has a great good relationship with its surroundings. Today, artificial intelligence is a common combination of multiple solution approaches, strategies within these approaches, and techniques algorithms based on these approaches. Aside from comprehensive foundations, it is possible to suggest that an artificial intelligence-based system can accomplish the following while solving real-world problems Henning (2018).

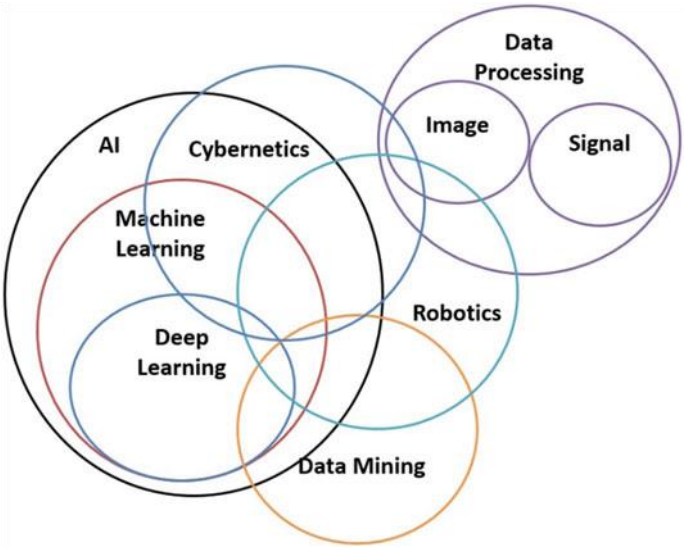

Fig. 3.1 A representation overview of the relationship and the field of artificial intelligence in general Holzinger (2016*b*)

Due to the characteristics of artificial intelligence, the area has become an important tool for various fields where problems can be modeled mathematically and logically, as existence itself is a traditional mess with definitions in terms of mathematics and modern logic. Detailed, artificial intelligence methods adopt the chance factor as a heuristic vision of solutions. By excluding technical information such as the processes and algorithms that are run in the system, the idea of the intelligent system can be used to objectively describe a whole artificial intelligence-based system. Since artificial intelligence is on the verge of becoming a commonplace phenomenon in everyday life, such broad terms are appropriate for indicating the active use of AI-based solutions in a variety of domains. An intelligent machine may be a problem-specific implementation of technology, a hybrid formation incorporating multiple artificial intelligence techniques, or a mixture of both artificial intelligence techniques and alternate methods from diverse fields. Returning to the rational definition of intelligent systems, these systems enable people to communicate with one another in order to find a solution.

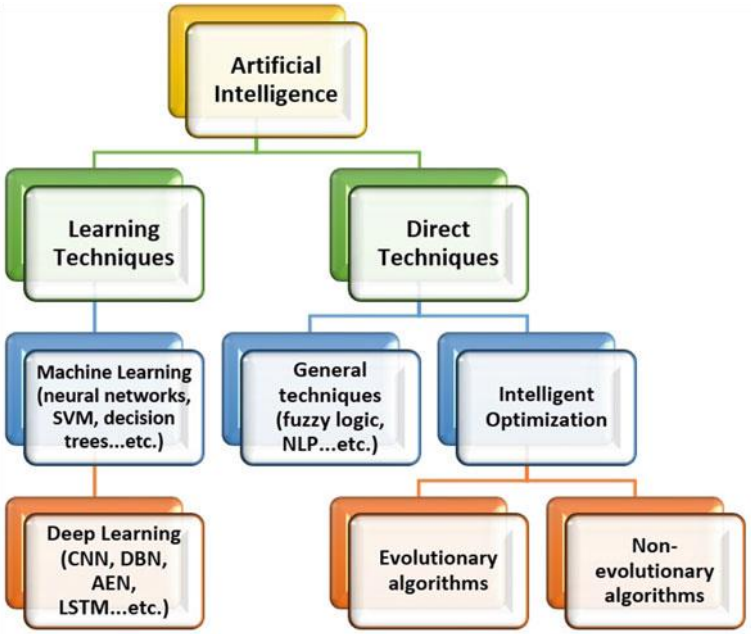

Fig. 3.2 a representation overview of the relationship and the field of artificial intelligence in general Holzinger (2016*b*)

3.2.1 Machine learning for health care

Recent advances in information technologies result in the evolution of decision support systems involving various techniques for analyses and handling big data. These systems are applied in a broad range of disciplines, e.g., in administration, engineering, and health systems Holzinger (2016*a*). In the field of medical informatics, designing and developing tools to support decision-making were highly motivated by advances in biometrics. Among different applications in health systems, medical diagnostics is especially important. Diagnostics is often challenging since many signs and symptoms are hidden and nonspecific. To cope with this problem, a correlation of the information must be analyzed, combined with recognition and differentiation of patterns. Algorithms for data analysis are among various techniques used in diagnostic procedures. Among them, neural networks and deep learning approaches play an important role. In medical diagnostics, deep learning frequently provides more robust results compared with artificial neural networks. The deep learning techniques were successfully used for cancer diagnostics. Many other fields of medicine are also open to high-level decision support systems that can diagnose and treat better than humans Holzinger (2016*b*).

3.3 Brain tumor growth prediction pipeline

The main objective of our TGP model is to predict the tumor volume in late-stage (tumor area after 90 days), based on multi-sequence MRI image for primary diagnosed

GBM, each patient has two MRI scans within 90 days. The input image is contains T1 (pre- and post-contrast agent), FLAIR, T2, where the label is to predict the follow-up image (volume after 90 days).
The result is a Tumor Growth Predictor model that is capable to predict the tumor volume in late-stage (see figure 3.3).

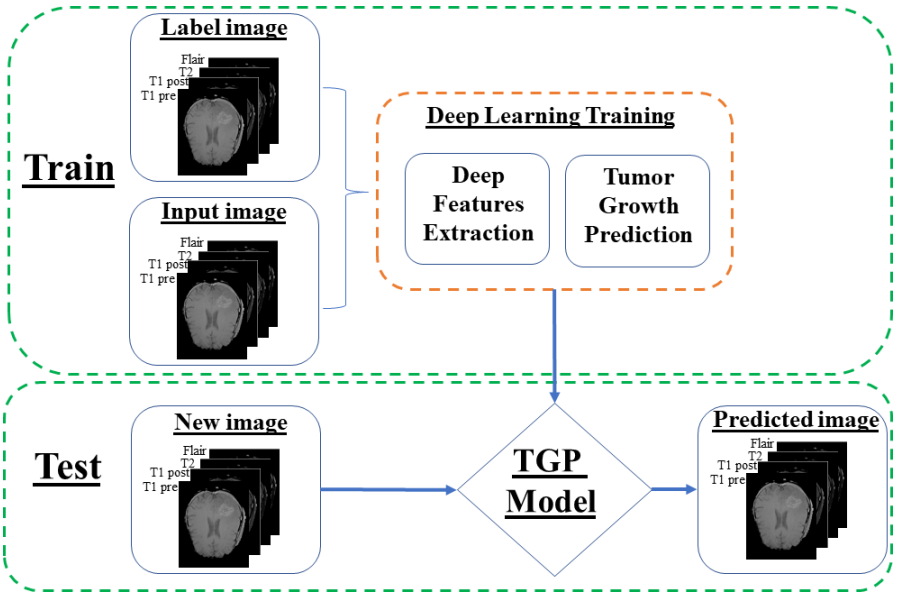

Fig. 3.3 Illustrate the workflow for TGP model,As input TGP take MRI image(four channels), the result is a model that capable to predict the tumor volume in late-stage (tumor area after 90days).

TGP model performance could be affected by MRI image quality, thus, image pre-processing is the basic stage that sets all input image for subsequent processes. That boost the MRI image improvement and enhance the set of relevant features extracted from patients images.

3.3.1 MRI image quality limitations

In recent years, magnetic resonance imaging (MRI) has proven to be an effective tool for clinical research, and it has been found useful in the detection of brain tumors. However, MRI images suffer from many issues such as:

- The presence of non-brain tissues or (Skull) is considered a major challenge in brain MRI image processing, which the high intensity of skull pixels fluctuate the machine learning algorithms in the process or features extraction Fennema-Notestine et al. (2006)
- Due to the diversity of MRI scanner, a different temporal and spatial sources images appears. Correlating these images in order to ensure spatial consistency

between given points is more than important due to its impact on ML algorithms Maintz and Viergever (1996).

- During MR image acquisition, the large variations in input parameters for MRI scanner, makes the intensity normalization an important pre-processing step in MRI image analysis Bağcı et al. (2010).
- Medical image acquisition, storage, or transmission, MRI images have been very sensitive to be affected by different types of noises. that is distributed across all the MRI images. Thus, Noise reduction is one of the challenging issues in medical data Sagheer and George (2020).

In order to reduce the effect of MRI image quality on the performance of machine learning model, we need to improve the quality of these images by first removing the skull, then applying a registration step, then normalizing these images, and finely denoising and filtering (See next section for more details).

3.3.2 Skull stripping

The presence of non-brain tissues is considered a major challenge in brain MRI image processing. The first step in the case of neurological MRI analysis is skull stripping. This step is very important for the remaining part of our proposed pipeline to remove the skull of the brain from all patients' MRI images, this step involves removing extra-meningeal tissue from patient MRI images. There are many ways to perform this operation Fennema-Notestine et al. (2006), in this section, we introduce the literature tools for skull stripping, also we show the result and its associated limitations.

3.3.2.1 FSL BET: Brain Extraction Tool (BET):

Brain Extraction Tool (BET) Woolrich et al. (2009) is a part of the FSLSmith (2002) package used to remove non-brain tissue from the patient MRI image of the whole head. BET is a commonly used tool for fully automated extracting of brain inner and outer skull and scalp surfaces from MR images. It provides an accurate result, that requires a pair of T1- and T2-weighted image BET uses a tessellated mesh to model the brain surface, which is allowed to deform according to various dynamic controlling terms until It reaches the brain edge, BET takes about 5–20 seconds to run on a modern desktop computer and is an open-source Smith (2002) As a major limitation of the BET tool is the resulting crude "skull" image contains a relatively large number of false negatives and positives (figure 3.4) shows an example of **T2** and **Flair** images).
As it is shown in figure 3.4, BET takes out undesirable brain extractions with **T2** and

Flair image type, which includes only part of the brain and in some cases part from non-brain tissue. The performance can be improved substantially with post-processing **T2** and **Flair** according to the result of the couple **T1** (pre and post-contrast).

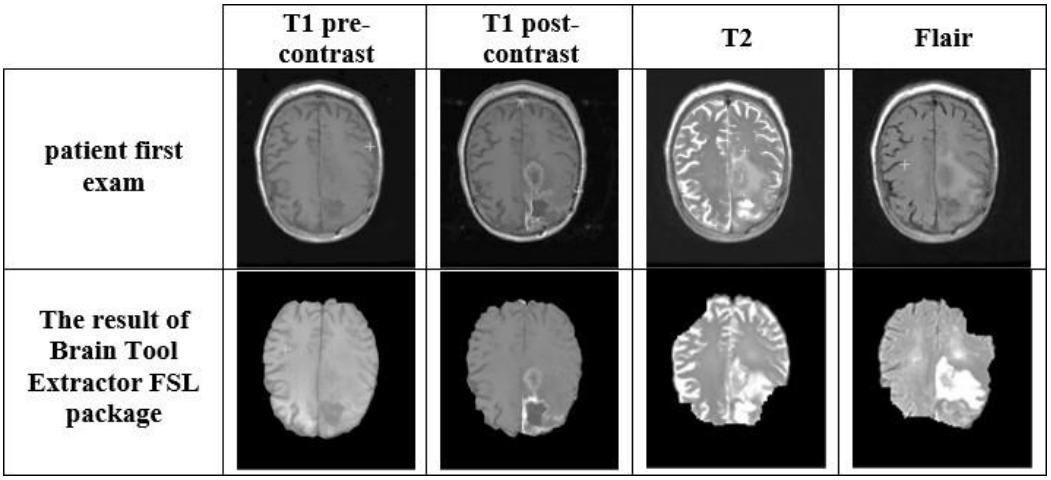

Fig. 3.4 illustration of skull stripping for patient's images using the BET-FSL tool, the original image in the 1^{st} row, and images result after skull stripping are shown in the 2^{nd} image row.

3.3.2.2 Brain-suit tools Brain Surface Extracto (BSE):

Brain Surface Extracto (BSE) Dogdas et al. (2005) from Brain-suit packageBhushan (2016) operates using a Marr-Hildreth Marr and Hildreth (1980) edge detector to find a boundary between the brain and the skull. Since the Cerebrospinal fluid (CSF) space and skull are dark on a T1 scan, the edges between the brain and the scalp are relatively well-defined.
Skull stripping using BES based on 04 steps:

- Filtration using anisotropic diffusion filter (See figure 3.5.1)
- Edge detection based on Marr-Hildreth algorithm (See figure 3.5.2)
- Finding the brain based on a series of mathematical morphological operators (See figure 3.5.3)
- The final step is extracting the brain by applying a mask (See figure 3.5.4)

The BSE allows mainly to adjust the parameters of the skull stripping process and according to the intermediate results. Several options and parameters are available for optimizing BES performance, thus, finding the right alternative BES settings can be a difficult and time-consuming task, which can introduce undesirable variability. figure 3.4 shows a visualization of skull stripping results using BSE tool, as it is shown visualization results of skull stripping obtained by Brain Surface Extractor (BSE) of brain

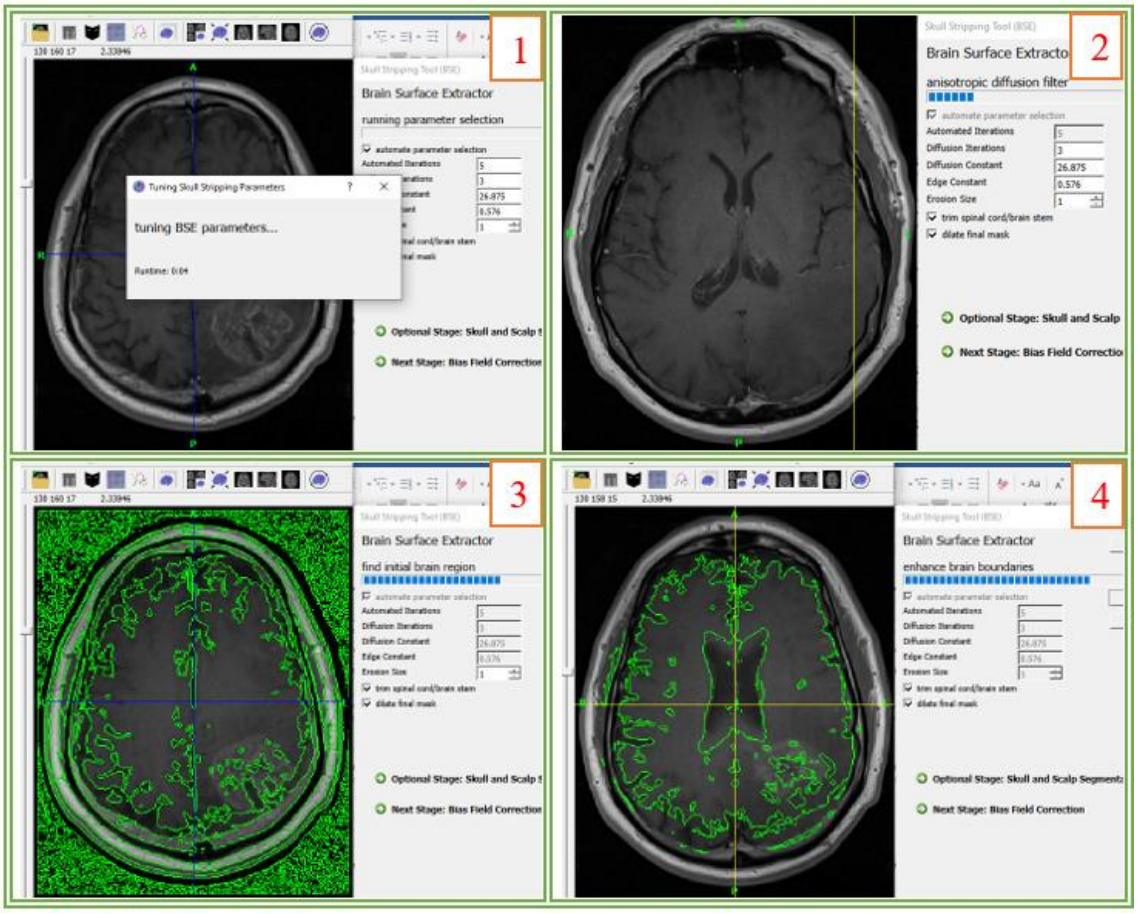

Fig. 3.5 Brain-suit skull stripping steps: (1) Filtration using anisotropic diffusion filter (2) Edge detection (based on Marr- Hildreth algorithm) (3) Finding the brain (based on a series of mathematical morphological operators (4) extracting the brain by applying a mask.

suit package, the original image is in the 1st row, the 2nd row shows the process of BES (detect the brain boundaries) and the 3rd row shows the brain surface. A major limitation of the Brain Surface Extractor (BSE) is rendering the poor-quality solutions on many occasions, in which the chosen manual parameter introduces undesirable variability. Therefore, it is a time-consuming, error-prone and almost completely human parameter choice dependent.

3.3.3 Registration and resizing

Due to the diversity of MRI images details (different sensors, different perspectives, and different shooting conditions), registration techniques essentially involve the process of correlating images from different temporal and spatial sources in order to ensure spatial consistency between given points in all images. Image registration is the process of transforming different sets of data into one coordinate system (image reference). The basic principle of registration is the process of finding a rigid body transformation

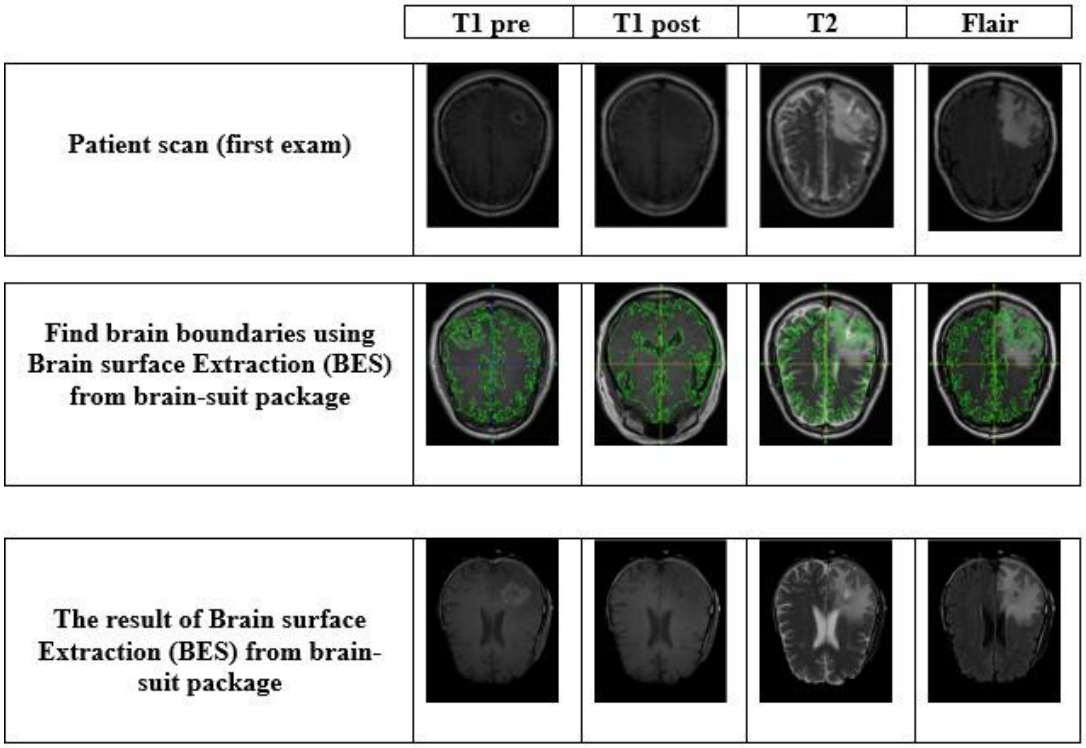

Fig. 3.6 Visualization results of skull stripping obtained by Brain Surface Extractor (BSE) of brain suit package, the original image is in the 1st row, the 2nd row shows the process of BES (detect the brain boundaries) and the 3rd row shows the brain surface

between two images or volumes through an optimization algorithm by minimizing a global image similarity metric. The matching anatomical points in image registration are considered as a critical optimization process aim to allow the learning models to improve their features extraction and classification process Maintz and Viergever (1996). figure 3.5 shows a registration example from the TCIA dataset, in the left the raw image (260*320*24) high*width*slices was registered to an image reference (256*256*23) where 256*256 the high*width choosing as the median of all our image dimensions and 23 is the median number of slices as well.

3.3.4 Normalization and standardization

The large intensity variations in MRI images due to using different MRI scanners and different parameters during MR image acquisition makes the intensity normalization an important pre-processing step in brain magnetic resonance image (MRI) analysisBağcı et al. (2010). Normalization is a process that changes the range of pixel intensity values, thus, calibrating the intensities of the different pixels into a normal distribution. wherein similar intensities achieve similar tissue meanings, and the lack of a standard image intensity scale in MRI leads to many difficulties in tissue characterizability (see equation 3.1). This process aims to get a similar range for features also the data center-

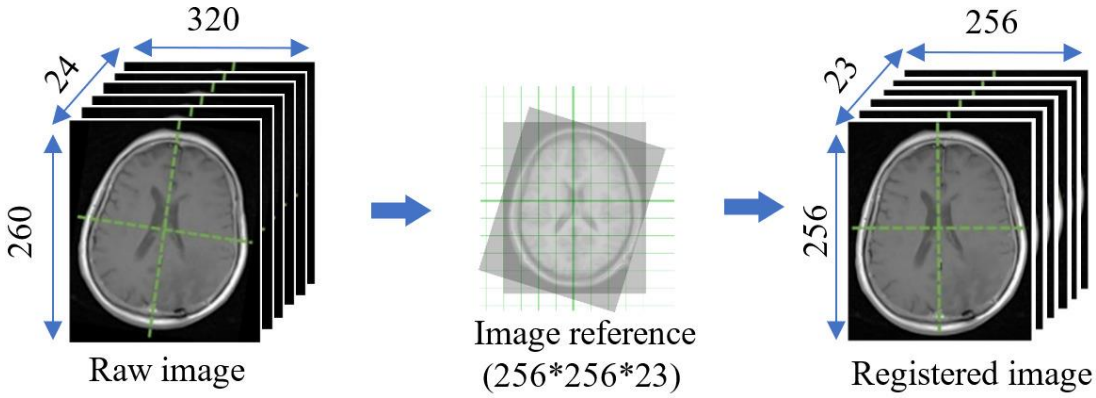

Fig. 3.7 An example of registration of the raw image with size (260*320*24) to the reference image with size (256*256*23)

ing normalization right can be a crucial factor in getting the model to train effectively. Besides, image standardization (see figure 3.8) is known as the process of bringing all images in the common format, in practice, Standardization has a mean value of 0 and a standard deviation equals to 1. Thus, assuming that the data has a Gaussian (bell curve) distribution. For the TCIA dataset, we standardize the intensity of the image (X) by subtracting the image Mean and divide by the standard deviation STD of the same image in all channels (see equation (3.1)):

$$(X - X.Mean())/X.STD()) \tag{3.1}$$

The lack of a standard image intensity scale in MRI leads to many difficulties in tissue characterizability.

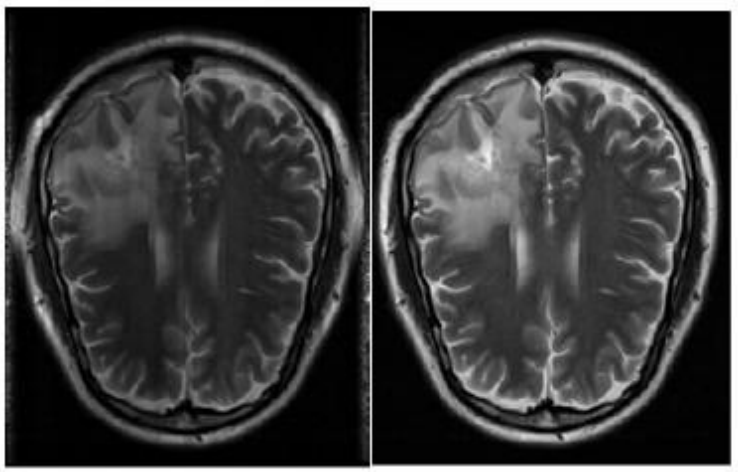

Fig. 3.8 Normalization- standardization result.

3.3.5 Filtering and denoising

During medical image acquisition, storage, or transmission, MRI images have been very sensitive to be affected by different types of noises. that is distributed across all the MRI images. Thus, Noise reduction is one of the challenging issues in medical data which is performed using various filter types: average, median, and wiener filter Sagheer and George (2020), an example of the result applying each filter is shown in figure 3.9. In our model, we apply in the preprocessing four steps as a fellow (skull stripping, normalization/standardization, registration then finely denoising). We notice that we used the combination of two skull stripping tools, the robust automated BET tool proceeded by BES that has four steps to prepare MRI images. The first step of the skull stripping using the BES tool is image filtering using an Anisotropic diffusion filter which preserves the edges and produces a filter depending on the significant parts of the image, hence, the result is its combination with the original image. After testing many experiments on the resulted images for the preprocessing step, we chose to apply the Wiener filter which is a linear estimation of the original image based on a stochastic process, it permits us to overcome the extra noise and flips the blurring at the same time. Besides, we apply the wiener filter due to its efficacy and its speed.

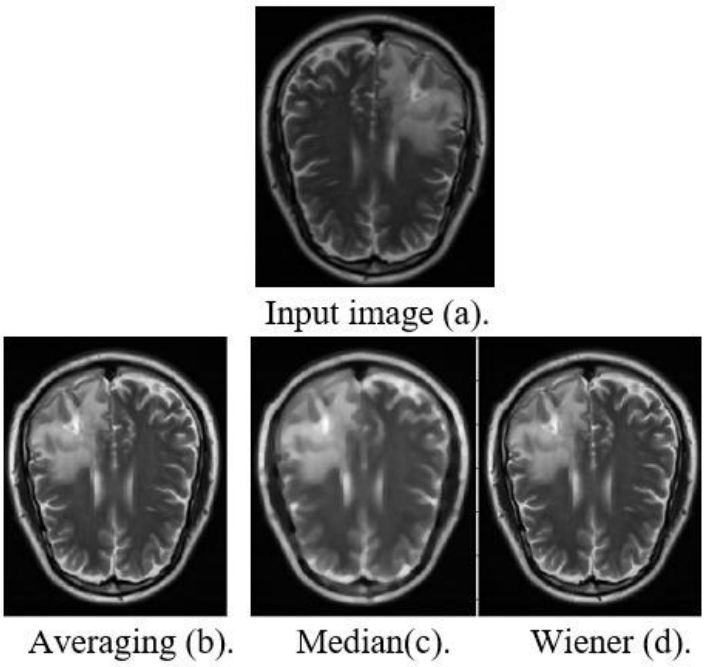

Fig. 3.9 Illustration of the resulted images after applying different filter: (a) the original input image (b), (c) and (d) the result of filtering average, median and wiener respectively.

3.4 TGP model conception and architecture

This section aims to illustrate more details of the new developed Convolutional Neural Networks architectures for the GBM brain tumors growth prediction. The proposed architectures may used to predict the brain tumors growth with both high- and low-grade, in our case, we used and tested in high-grade GBM in two time-points (scans within 90 days follow-up). Furthermore, the methodology and the steps to develop a fully automatic method for the GBM tumors prediction using MRI images.
figure 3.10 shows the flow of the proposed preprocessing steps and tools. The first step is the normalization to changes the range of pixel intensity values and making a normalised range. In addition, the standardisation is applied for correcting inter-subject intensity variations through transforming all images from the given image gray scale into a standard gray scale wherein similar intensities achieve similar tissue meanings . Besides, all TCIA medical image passed by registration step, whereas its crucial process of transforming different sets of image data into one coordinate system. Furthermore, skull stripping, where the brain tissue (cortex and cerebellum) segmented and speared from surrounding region (skull and non-brain area). This step is based on two public available tools BET (BET) Woolrich et al. (2009) and BES Dogdas et al. (2005). Also, we perform the combination of both tools, the result of each skull stripping method pass by three steps: the first, slices selection (selecting 10 slices where tumor appear), the last step is patches extraction to prepare data as input for CNN model. Also, we explains in detail the prediction of brain tumor growth in based MRI image. The input brain images are provided by TCIA dataset Clark et al. (2013) and passed throw the preprocessing steps (See figure 3.10).

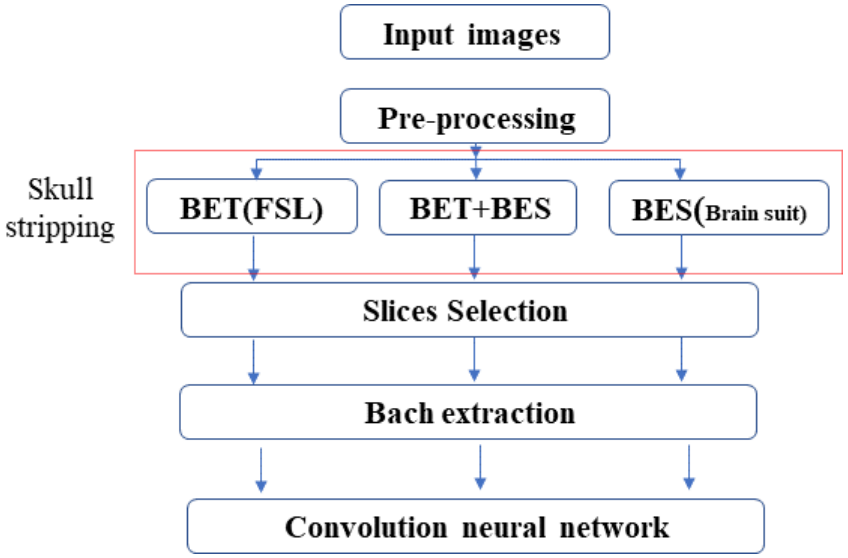

Fig. 3.10 Diagram illustrates the outline that is used in our work starting with preprocessing (normalization, standardization and registration), then skull stripping (based on BET and BES and the combination of them). The result of each skull stripping method pass by three steps: the first, slices selection (selecting 10 slices where tumor appear), the last step is patches extraction to prepare data as input for CNN model.

The encoder has used the convolutional layer and max-pooling function which reduces the dimensions of the feature maps. After a specific number of layers, when the encoder is complete the feature maps are flattened and a dense layer is used for the latent-space representation. Now, the transpose convolution is used for the upsampling of the incoming feature maps, which is followed by the batch normalization and the activation function.

Figures 3.11 and 3.12 show the detailed conception architecture for the developed TGP model. Our proposed TGP model is based on End-to-End Convolution Neural Networks architecture And inspired by convolutional auto-encoder architecture. The convolution step creates many small pieces called the feature maps (image size 32*32*4 in figure 3.11), where the de-convolution step reproduce the original image size based on the feature maps. many small pieces called the feature maps These squares preserve the relationship between pixels in the input image. Let each feature scan through the original image like what's shown in Figure 3.12. An autoencoder consists of two parts: encoder and decoder.

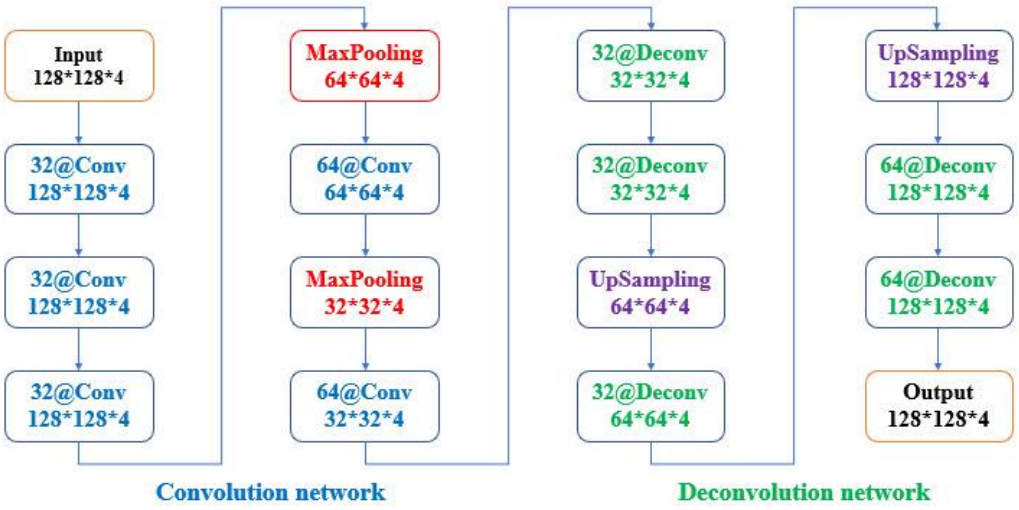

Fig. 3.11 A schematic representation of the principal idea of convolution aut-oencoder, where its start by compressing the input image to a small piece called feature map (convolution part). The compression uses MaxPolling layers (in red color). The second part is responsible of reproduce the original image size based on the feature maps (de-convolution part). The decompression based on Up-samplling layers (green color)

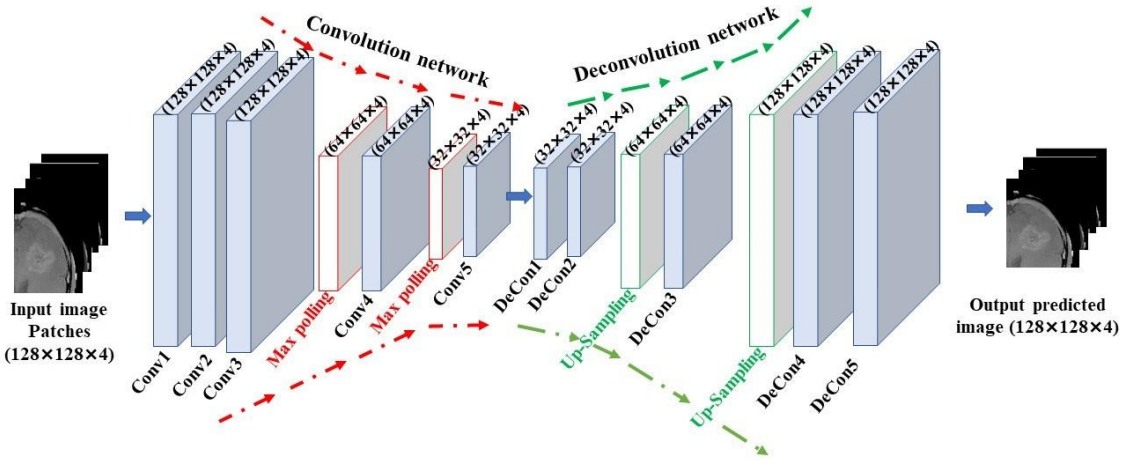

Fig. 3.12 Our TGP model conception inspired by convolution auto-encodeur.

3.4.1 Training parameters

When researching the most common methods used to train deep learning architectures. Interestingly, there is no specific method for training the CNN architecture. Many hyper-parameters should be selected before starting the training phase of the CNN architecture, and there is no guarantee that the success or failure of the architecture will

converge to the global minimum. For these reasons, we choose to based on a new strategy called ELOBA Naceur et al. (2019) to unify the training method of CNNs architectures. The algorithm of ELOBA takes into account the most influencing hyper-parameters (i.e., Epochs, Batch size, Learning rate and Optimizer).

3.4.2 Implementation and working environment

In this work, all our results are obtained using Python environment on windows 64 bit, Intel Xeon processor CPU @2.10 GHz with 24 GB RAM. For the training phase, it is done on Nvidia Quadro GPU K1200 with 4 GB memory. Our proposed **TGP** model is developed using Anaconda environment, *Keras* [1] and *Theano* [2] as a backend, Keras is a high-level open-source deep learning library that runs on top of Theano which can benefit from a massively parallel architecture such as Graphics processing unit (GPU) for the deep learning network optimization.

3.5 TGP Experimental results

In this work, we propose an End-to-End method to improve the prediction of Glioma brain tumor growth based on an MRI image of the brain from the TCIA public dataset Clark et al. (2013) and integrating several data augmentation techniques. TGP model takes as an input MRI images with four channels, where the aim is to predict the tumor volume in late-stage (i.e., tumor area after 90-days).

Accuracy metric is not sufficient to evaluate efficiency the complete model effectively. Hence, we perform Dice, Precision, Recall for every predicted image. So, we evaluate the effectiveness of TGP model we measure the three common metrics (recall, precision, and Dice scores). Each metric is described using four statistical values: True Positive (TP), False Positive (FP), and False Negative (FN) , True Negative (TN) Yeghiazaryan and Voiculescu (2018).
False positive (FP) case happens when the pixel in the predicted image is indicated by the classification model to be as tumor, but it actually does not belong to the tumor region. If a non-tumor pixel in ground-truth image is suggested as non-tumor by the classifier, it is the case of true negative(TN) (See figure 3.14).

1. Recall/Sensitivity is also called as the True Positive Rate (TPR) or Recall. It answers the following question: What proportion of actual positives was identified correctly? And it is defined as:

$$Recall = \frac{TP}{TP + FN}$$

[1] https://keras.io/
[2] http://deeplearning.net/software/theano/

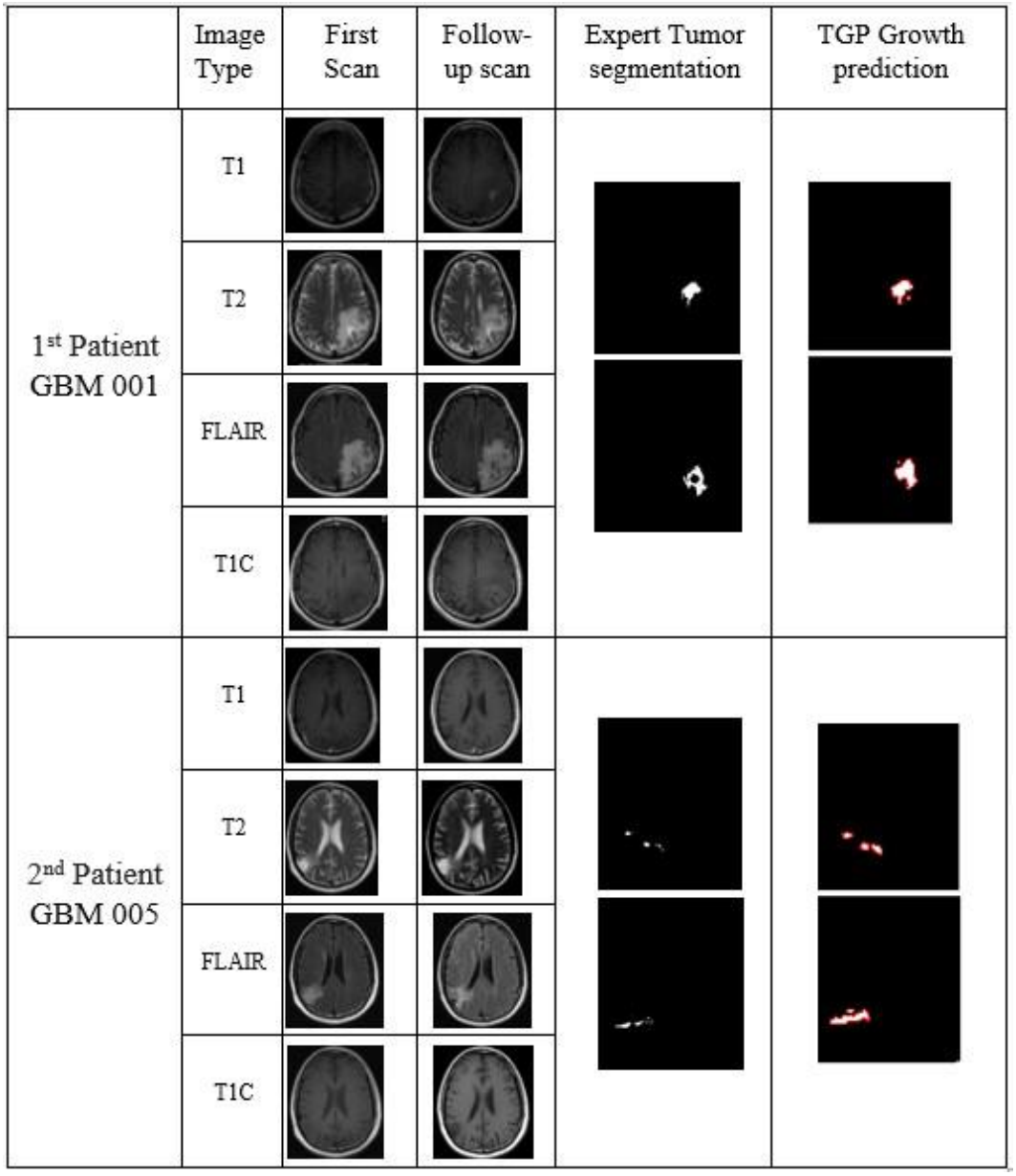

Fig. 3.13 An example of the TGP model prediction results compared to the segmentation provided by TCIA expert. We illustrate two GBM patient scans (T1, T2, FLAIR and T1C). The two last columns represent the binary lesion mask provided by the expert and TGP prediction.

2. Precision metric answers the following question: What proportion of positive identifications was actually correct?
   It is defined as:

$$Precision = \frac{TP}{TP + FP}$$

3. Dice Similarity Coefficient (DSC)is used to measure the similarity of two samples.

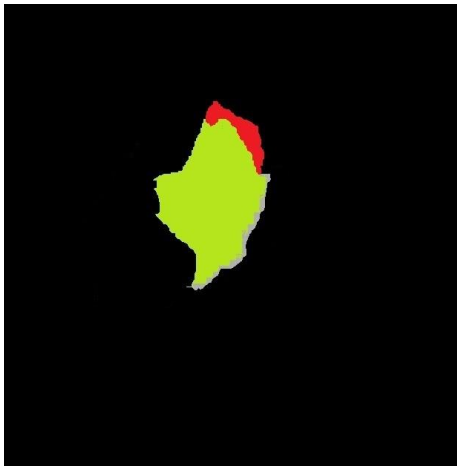

Fig. 3.14 An example of the validation result which shows True Positive, False Positive, True Negative, and False Negative, that are indicated by colors in the order of green, black, red, gray and represent the number of pixels in each class.

It is defined as:

$$Dice = \frac{2TP}{TN + FN + TP + FP}$$

3.5.1 Evaluating TGP performance

We evaluate our proposed TGP model based on cross-validation K-fold (See figure 3.15) in which the validation performed using 03 samples never seen by the model in training (also not used in the process of data augmentation and generation of synthetic image). Then, we change the selected patients for the 40 evaluation experiments. The chose 17 samples are used as training and 03 as a test is are carefully trialed in a variety of different portion (train-test) in which using more patients for test will reduce the number of training cases entered to the model, thus the model performance will be affected, in the other hand using less than 03 samples will not establish the reached results. This operation helps to provide a better evaluation for the obtained results.
All training experiments took 500 epochs to convergence to the best parameters.

3.5.1.1 Review the impact of preprocessing on **TGP** performance

With the purpose of measuring the performance of our proposed **TGP** model under different preprocessing techniques. The first training strategy is to evaluate our TGP model on 04 composite datasets with different variants of the preprocessing techniques.

- Experiment 01: Training **TGP** model using raw data (Original TCIA data).
- Experiment 02: Training **TGP** model including pre-processing (registration, normalization, standardization, and denoising) and using BET Woolrich et al. (2009) as a skull stripping tool.

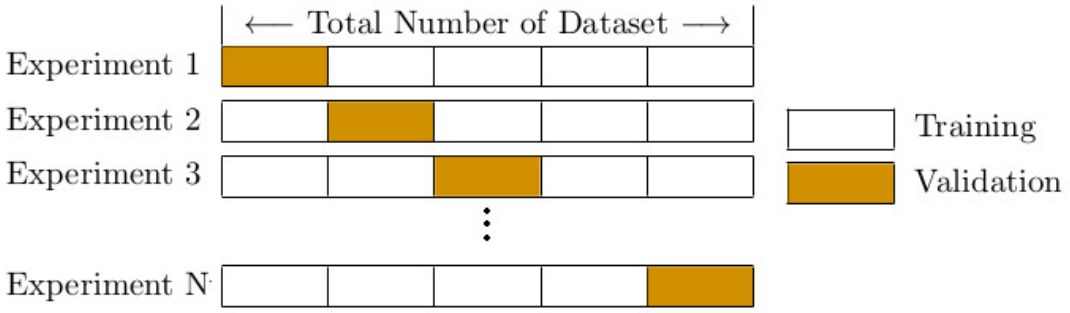

Fig. 3.15 A schema representation for the Cross-validation testing procedure that used to evaluate TGP performance

- Experiment 03: Training **TGP** model including pre-processing (registration, normalization, standardization, and denoising) and using BES Dogdas et al. (2005) as a skull stripping tool.
- Experiment 04: Including pre-processing (registration, normalization, standardization, and denoising) and using the combination of BET and BES for skull stripping.

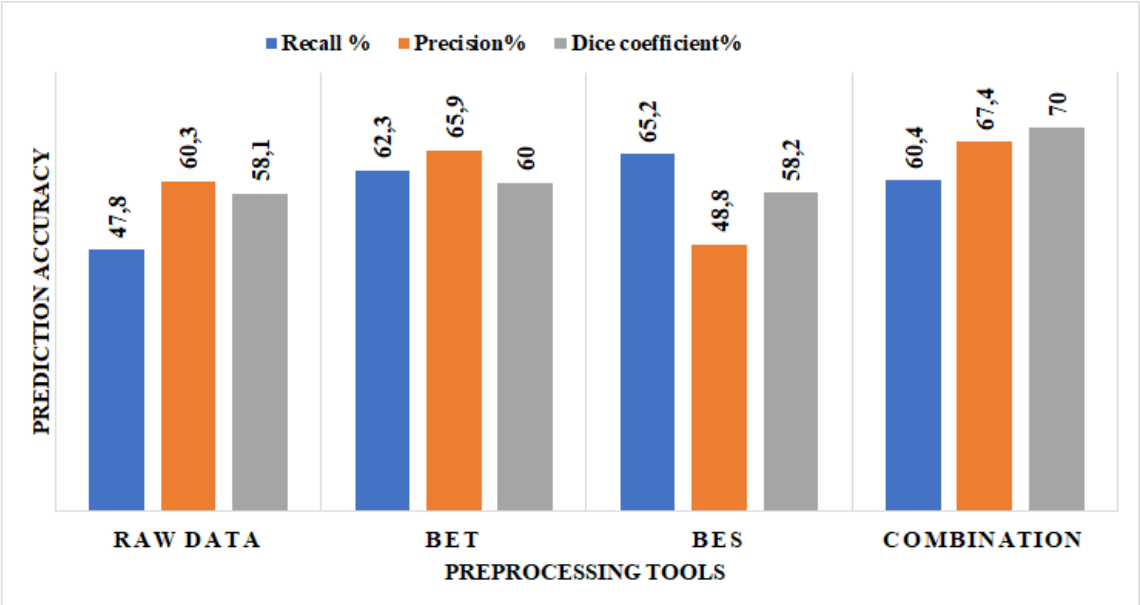

Fig. 3.16 Evaluating TGP model and measuring the impact of pre-processing on TGP performance

Figure 3.16 shows the evaluation results of TGP model based on three metrics (recall, precision, and dice coefficient scores). As it is shown, we observe that training our TGP model with raw data gives 60.3%precision in the best case; besides a low value of

recall (47.8%) and 58.1% in dice coefficient score. While applying the pre-processing and the skull-stripping using BET improve the model precision accuracy to achieve 65.3% and obvious change in recall score (+15% compared to training with raw images) and achieve to 65.9%and 60.0%dice coefficient, alongside the BES shows lower precision (mean score 48.2%) beside 56.2% and 58.2% in recall and dice coefficient respectively. Finally, our model accuracy achieve 67.4% of precision 60.4% in dice coefficient and 70.0% in recall metrics when the combination of the two skull stripping tool used (BES Dogdas et al. (2005) followed by BETWoolrich et al. (2009)), all results and the standard deviation of the experiment are shown in table 3.1.

Experiment Metrics	Recall % ± STD	Precision % ± STD	Dice % ± STD
Experiment 01	47.8 ± 8.3	59.1 ± 7.2	55.1 ± 3.0
Experiment 02	62.3 ± 3.9	46.2 ± 5.2	58.2 ± 5.9
Experiment 03	62.3 ± 5.9	63.4 ± 7.6	69.1 ± 5.4
Experiment 04	48.3 ± 6.1	56.1 ± 3.2	49.4 ± 7.7

Table 3.1 Table illustrates TGP model result and the impact of different pre-processing tools on TGP performance.

3.6 Discussion and Conclusion

In this section, we proposed three fully automatic models for GBM tumor growth prediction (TGP), Our model is capable to predict GBM tumor volume growth based on patients MRI images.

In addition, we review the impact of using different preprocessing tools for TGP the accuracy result. Through the empirical experiments, we proved that using the combination of BET and BES for skull stripping gives the best performance. We illustrate that the combination improve +10% in terms of prediction accuracy. And the volume prediction achieve 67.3%, 68.4%, 70.0% in recall and dice coefficient respectively.

Our intuition behind the proposed TGP model is to overcome the issue of using mathematical equation for simulating GBM growth volume, and provide a fully automatic model for brain tumor prediction using Multi-sequence MRI images.

We believe that TGP may overcome the issue of the tumor prediction. Moreover, it will provide a new tool for tumor growth prediction.

The main challenge that face TGP model is the lack of sufficient training data due to limit number of publicly available dataset for GBM growth. In the other hand, Generative Adversarial Networks (GANs) prepare a future seeing to grant freely public medical image dataset.

For these reasons, we propose a new method for generating and Anonymization of medical image that may be used as training data to deep learning models.

In the next chapter, we present the issue of training GANs to generate and anonimize medical image data.

CHAPTER 4

Synthetic Medical Image Generator

4.1 Introduction

The investigations in brain tumor growth is keeping an active area of research, and providing sufficient study data is the major challenge due to the data privacy and the lack of publicly available data-set in which Generative Adversarial Networks (GANs) prepare a future seeing to freely guarantee public medical image dataset.

Generative Adversarial Networks (GANs) are known as the combination of two types of networks; the first network is a type of generative model Oord et al. (2016) which makes use of detailed prior information associated with the appearance and spatial distribution from different features in the image. The second is a Discriminator Beyerlein (1997) classifier, which classify the two input images according to their characteristics and appearance differences (more details in section 4.2).

GANs could be trained to use unlabeled data as they learn the internal representations, which produces new content based on training data. A variety of applications in the literature are based on GANs and fairly useful practical applications; such as Image generation Wang and Gupta (2016) which use GANs based architecture to generate new images that are different from the images in the training dataset, also text-to-image synthesis Xu et al. (2018) GANs allows to generate an image based on text descriptions, also used to generate sequences of a story based on made text. Face aging and older image generationAntipov et al. (2017) is another application for GAN, in which provides an effective way to imagining how the face will look like when the person gets older which help in security systems (face detection), In addition complete the missing parts of imagesLi et al. (2019); where GAN allows recovering the missing part from existing image.

Generating new realistic data is a common use case of GANs especially in the medical image where the GANs provide an effective method of synthetic data generation and data anonymizing, the reason why several approaches are based on GANs in medical Fields.

4.2 Motivation and objectives

We focus our interests on machine learning investigation in brain tumor growth prediction. However, providing sufficient study data is a challenging task, the data medical data privacy and the lack of publicly available datasets. Generative Adversarial Networks (GANs) prepare a future seeing to generate a synthetic medical image, also, GANs provide data anonymizing and guarantee a free public dataset. That's what unroll a huge need for the generative model, that provide a way of data augmentation and medical image anonymizing.
In the next section we present a brief introduction and background theory for Generative adversarial network, in addition to its applicability on health care field and medical data generation, also, we mention some researches that based on GANs as data augmentation technique for brain tumor investigations.

4.3 Background Theory : Generative adversarial networks (GANs)

Generative Adversarial Networks (GANs) are a type of Neural network composed of two network types: generative and discriminator networks that are trained in an adversarial manner to generate data according to given data distribution. GANs have emerged as powerful computational models since they were introduced by Ian Goodfellow in 2014 Goodfellow et al. (2014), and have shown good results and very large applications such as Image-to-image translation Isola et al. (2017), Super-resolution, and synthetic Goodfellow et al. (2016) image.

4.3.1 Generative adversarial networks: Model conception

GANs are unsupervised generative models which implicitly learn an underlying distribution (such as a uniform or Gaussian) using two neural network models trained in the same time together: The Generator (G) network creates synthetic images from noise vectors and the Discriminator (D) network to make the difference between fake images generated by the generator G and real images of the dataset. The GANs game training may be resumed as two networks: the first is a generator G which take a given standard random input noise vector (z) from a prior distribution Pz and generates a fake sample G(z) corresponds of distribution D' which close as much as possible from the true distribution D. The second is the Discriminator D network which aims to discriminate between two different class of data, D receives as input a data (x) which could be from the true samples or generated by G model and outputs the estimation probability that (x) was sampled from the real data rather than the model G as shown in figure 4.1.

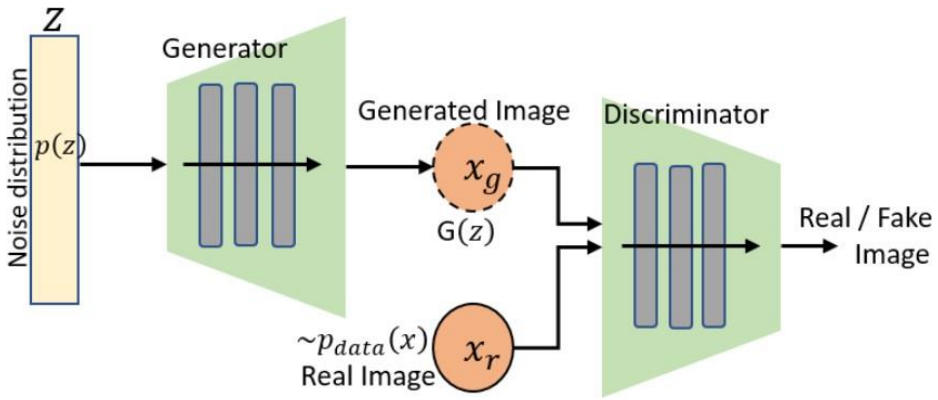

Fig. 4.1 The illustration of GANs workflow Goodfellow et al. (2016).

4.3.2 Generative adversarial networks: Training strategy

GANs is based on the concept of a non-cooperative game of two networks generator G and discriminator D, where each player(G, D) uses a gradient-based optimization technique in aim to minimizing its cost and continue simultaneously until leads to Nash equilibrium Maskin (1999).

During the training of GANs model, the objective of discriminator D is to correctly classify the real image input (which labeled 1) and the fake input (labeled 0) as a binary classification where the loss function L corresponds to the binary cross-entropy Mao et al. (2016):

- For the real image

$$L(D(x), 1) = [logD(x)] \tag{4.1}$$

- For the generated image

$$L(D(G(z)), 0) = [1 - logD(G(z)))] \tag{4.2}$$

Where D(x) is the discriminator classification probability of input (x), G(z) is the generator model output for z random input from Pz distribution. The objective of the discriminator is to form a correct classification by maximizing Eq (4.1) and Eq (4.2):

$$Max_D[logD(x)] + [1 - logD(G(z)))] \tag{4.3}$$

At the same time the generator G has the objective of fooling on the discriminator by minimizing the same objective function:

$$Min_G[logD(x)] + [1 - logD(G(z)))] \tag{4.4}$$

GAN training simultaneously keeps trying to move the generated samples towards the real data based on gradient information following the equation:

$$Min_{\vartheta_G} Max_{\vartheta_D} V(G, D) = Min_G Max_D [E_{x\ p_{data}}[log D(x)] \tag{4.5}$$

$$+ E_{z\ p_z}[log(1 - D(G(z)))]$$

Where ϑ_D and ϑ_G represent the set of parameters in the Generator G and the discriminator D respectively, Pdata(x) correspond with the real data distribution, PZ (z) is a random distribution of the data, and V(D, G) is a binary cross-entropy function Mao et al. (2016). The Discriminator D and the Generator G are performed by back-propagating the error signal via their respective models and the update rule is defined in Eq 4.5 and The optimization equation is solved by alternating two gradient updates as described in function Eq 4.6:

$$\{\vartheta_D^{t+1}, \vartheta_G^{t+1}\} \leftarrow \begin{cases} \text{Update if D(x) predicts wrong} \\ \text{Update if D(G(z)) predicts wrong} \\ \text{Update if D(G(z)) predicts correct} \end{cases}$$

$$\vartheta_D^{t+1} = \vartheta_D^t + \lambda^t \nabla_{\vartheta_D} V(D^t, G^t) \tag{4.6}$$

$$\vartheta_G^{t+1} = \vartheta_G^t + \lambda^t \nabla_{\vartheta_G} V(D^{t+1}, G^t) \tag{4.7}$$

Which ϑ_D and ϑ_G are the parameters of D and G, respectively, is the learning rate and t is the iterations number**?**, and ϑ_G^{t+1} is the updated set of parameters for the generator G, and ϑ_D^{t+1} is the updated set of the Discriminator D, t is the iterations number. λ is the learning rate, and t is the iteration number. The final objective function of Eq 4.3 and 4.4 is to train the Discriminator D and the Generator G to have enough capacity that can reach a point at which both cannot improve (Nash Equilibrium **?**), that's provide a Generator G able to transform a simple prior distribution P_G to more complex distributions i.e., P_G converges to P_{data}, such as $P_G = P_{data}$. And the Discriminator D is incapable to distinguish between the two distributions, i.e. D(x)=1/2 and cannot distinguish whether a sample is generated by the G or generated from the real data distribution.

4.3.3 Game theory

The adversarial method of training GANs based on a min-max game, where two players make simultaneous updates (back-propagation [Hecht-Nielsen (1992)]), in which there is a single value function of classification, and the discriminator is trained to maximize the classification accuracy (i.e. well classification image real and fake) and adversely the generator is trained to minimize the probability of discriminator being well taken. The major problem of the min-max game is when the discriminator saturated and the

generator failed to fool the discriminator completely. Then, the generator no longer has an update for the gradient, the advantages of the cross-entropy loss function that it trains Sigmoid classifiers and SoftMax classifiers are that whenever the classifier fails in choosing the right class, the gradient of cross-entropy with the respect of logits is guaranteed to nonzero (the gradient approaches to 1 as probability assigned to the correct class approach is zero). Besides, cross-entropy [De Boer et al. (2005)] provides the possibility to flip the order of argument in the cost function (i.e. the generator tries to maximize the log probability of the miss-classification rather than trying to minimize the classification accuracy). Although, it is known that GANs are facing the problem of training instability and failure to converge due to the min-max strategy and the cost function in the original work.

4.4 State of the art: GANs in Medical investigation

Machine learning is experiencing explosive growth that provides a better way to exploit the massive volume of medical data received. Nevertheless not all machine learning (ML) approaches are capable for brain tumor growth prediction due to the complex tumor behavior and the absence of sufficient training data.
The investigations in brain tumor growth is keeping an active area of research, and providing sufficient study data is the major challenge due to the data privacy and the lack of publicly available data-set in which Generative Adversarial Networks (GANs) prepare a future seeing to freely guarantee public medical image dataset.
GANs could be trained to use unlabeled data as they learn the internal representations, which produces new content based on training data. A variety of applications in the literature are based on GANs and fairly useful practical applications; such as:

- Synthetic image generation [Wang and Gupta (2016)], this type of model use GAN-based architecture, and aim to generate a new and synthetic image that's conserve the input data distribution, and contain different features compared to the images in the training dataset

- Text-to-image synthesis [Xu et al. (2018)]. GANs allows to generate an image based on text descriptions, also used to generate sequences of a story based on made text.

- Face aging and older image generation [Antipov et al. (2017)]. Another application for GAN that provides an way to imagining how the face will look like when the person gets older. This technique used the most in security systems as face detection.

- Complete the missing parts of images [Li et al. (2019)]. GAN allows also recovering the missing part from existing image.

In this section, we present the state of the art of GANs in medical works. There is two major categories for GANs models in the medical in investigations:

4.4.1 Synthetic medical image generations:

Generating new realistic data is a common use case of GANs especially in the medical image where the GANs provide an effective method of synthetic data generation and data anonymization, the reason why several approaches are based on GANs in medical Fields.
Frid-Adar et al. (2018) combines a GANs model with CNN architecture in order to develop a liver lesion classification network, Frid model aim to demonstrates the impact of GANs generated data on liver lesion classification task, and its allows achieving an improvement of $\sim 7\%$ of classification accuracy using synthetic data augmentation over classic augmentation. In addition, Iqbal and Ali (2018) proposes a GAN-based framework to generate realistic images, Iqbal generated image used as the additional training dataset, and aim to enhance the retinal vessel image segmentation performance. For brain image generation, Han et al. (2018) proposes to generate a multi-sequence brain MR images using GANs to increase diagnostic reliability, their result are approved by physician Geman et al. (2015). Shin et al. (2018) proposes to generate synthetic medical images based on two publicly available datasets (*ADNI* [1], *BRATS* [2]) which aims to provide more data to train tumor segmentation architecture also an effective tool to medical images anonymizing, the model trained to generate synthetic images from labels, where it allows to generate multi-series abnormal brain MRIs based on the brain map and tumor label separately to generate various synthetic data (changing tumor location, size . . .).
For brain tumor MR image segmentation, Bowles et al. (2018) proposes a model that allows augmenting the training data with an aim to improve the brain tumor segmentation accuracy. The model is based on GANs and trained using BraTS dataset, and the validation is performed by using the augmented annotated training sets for the segmentation tasks which show the impact of using the generated image in the network.
In the case of brain tumor prediction task, the accuracy remains always a challenging task due to the lack of sufficient training data and the complexity of GBM tumor behavior. Generative Adversarial Network (GAN) achieve exceptional success in the medical investigations Yi et al. (2019).

[1] 1: Alzheimer's Disease Neuroimaging Initiative(ADNI)
[2] 1: Brain Tumor Segmentation (BraTS)

4.4.2 Medical image quality enhancing.

GANs not only used in new image generation, also ability to enhance quality and provide high resolution images. Zhou et al. (2021) developed a model augment performance of a classifier trained using the generated MRI images. To achieve this goal, Zhou processed brain MRI scans of multiple magnetic field strengths (1.5 Tesla (1.5T) and 3 Tesla (3T)) from the ADNI dataset. Using these generated data, Zhou demonstrates a proof of principle that GAN frameworks can be constructed to augment classification performance and improve image quality.

4.5 Synthetic Medical Image generator (SMIG) pipeline

The main objective of SMIG model is to generate synthetic MRI images based on GANs. SMIG model is inspired by Shin work Shin et al. (2018) that uses (Alzheimer's Disease Neuroimaging Initiative) ANDI and BraTS datasets to generate a synthetic image. In our work we don't change the tumor size as done in Shin work (see figure 5 row 3 and 4 Shin et al. (2018)), the save the tumor size and shape, is critical in our work, Since to predict tumor growth, size and shape are more than important. Also any change in tumor size will surely affect the prediction performance. Another difference between SMIG and Shin work is in the used dataset, where SMIG based on the TCIA dataset Schmainda and Prah (2018) instead of Brats Menze et al. (2014) used by Shin et al. (2018). SMIG model is trained to generate different types of synthetic MRI images such as; (1) Abnormal brain (See Fig 4.4(A)) that is based on using a healthy brain and tumor volume (See figure 2.5 tumor volume column). (2) Besides, the tumor in a new location (see Fig 4.4(B)) by taking as input the original and the tumor volume. The image-to-image translation conditional-GAN (pix2pix) model introduced in Shin et al. (2018) is adopted to translate label-to-MRI (synthetic image generation) and MRI-to-label (image segmentation). For brain segmentation, the generator G is given a T1-weighted image of ADNI as input and is trained to produce a brain mask with white matter, grey matter and CSF. The discriminator D on the other hand, is trained to distinguish "real" labels versus synthetically generated "fake" labels. During the procedure (depicted in figure 4.2 (a)) the generator G learns to segment brain labels from a T1-weighted MRI input. Since we did not have an appropriate off-the-shelf segmentation method available for brain anatomy in the BRATS data set, and the ADNI data set does not contain tumor information, we first train the pix2pix model to segment normal brain anatomy from the T1-weighted images of the ADNI data set. We then use this model to perform inference on the T1 series of the BRATS data set. The segmentation of neural anatomy, in combination with tumor segmentation provided by the BRATS

data set, provide a complete segmentation of the brain with tumor.

The synthetic image generation is trained by reversing the inputs to the generator and training the discriminator to perform the inverse task (i.e., "is this imaging data acquired from a scanner or synthetically generated?" as opposed to "is this segmentation the ground-truth annotation or synthetically generated?" – figure 4.2 (b)). We generate synthetic abnormal brain MRI from the labels and introduce variability by adjusting those labels (e.g., changing tumor size, moving the tumor's location, or placing tumor on a otherwise tumor-free brain label).

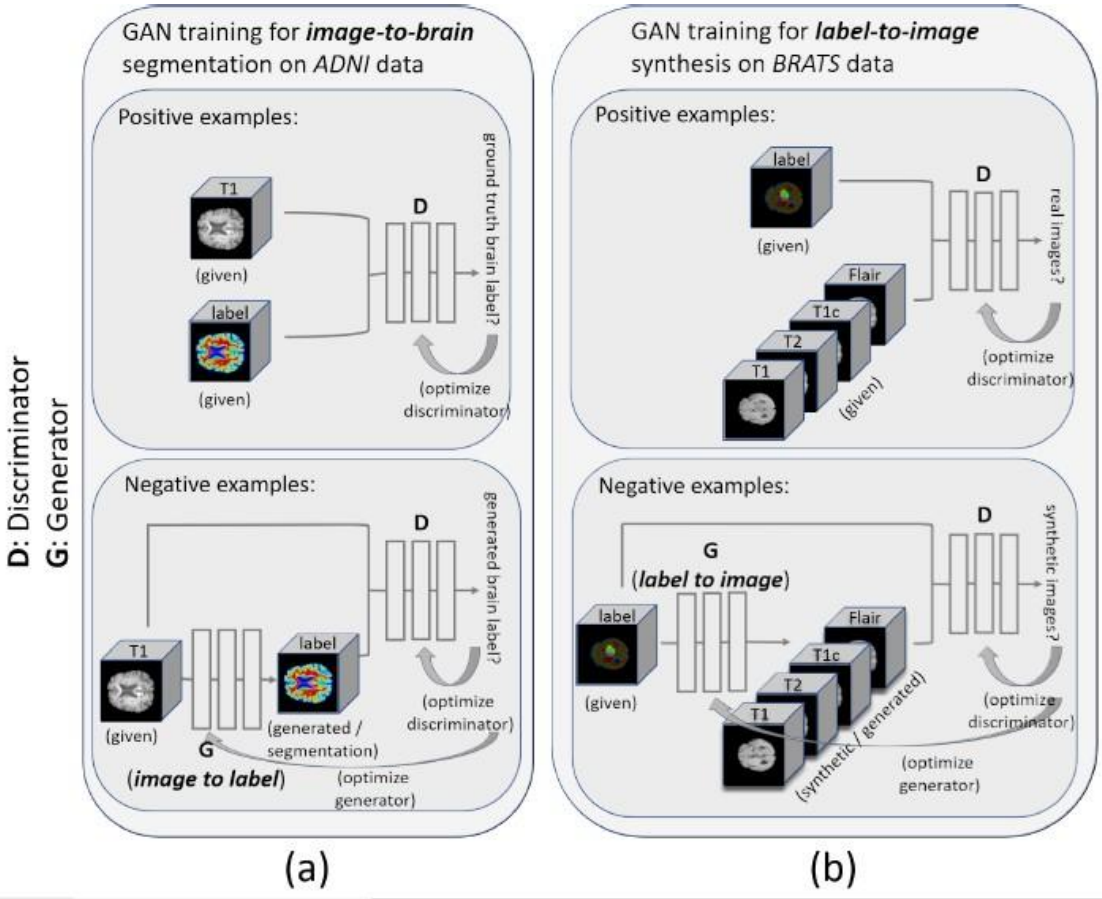

Fig. 4.2 Illustration of training GAN for (a) MRI-to-brain segmentation; (b) label-to-MRI synthesis Shin et al. (2018).

The SMIG trained to generate synthetic images from labels allows for the generation of arbitrary multi-series abnormal brain MRIs. Since we have the brain anatomy label and tumor label separately, we can alter either the tumor label or the brain label to get synthetic images with the characteristics we desire. For instance, we can alter the tumor characteristics such as size, location of the existing brain and tumor label set, or place tumor label on an otherwise tumor-free brain label. Examples of this are shown in figure 4.3.

The effect of the brain segmentation algorithm's performance has not been evaluated in this study. Since the GANs was first trained on 3,416 pairs of T1-weighted (T1) images from the ADNI data set, generated T1 images are of the high quality, and, qualitatively difficult to distinguish from their original counterparts. BRATS data was used to train the generation of non-T1-weighted image series. Contrast-enhanced T1-weighted images use the same image acquisition scheme as T1-weighted images. Consequently, the synthesized contrast-enhanced T1 images appear reasonably realistic, although higher contrast along the tumor boundary is observed in some of the generated images. T2-weighted (T2) and FLAIR image acquisitions are fundamentally different from the T1-weighted images, resulting in synthetic images that are less challenging to distinguish from scanner-acquired images. However, given a sufficiently large training set on all these modalities, this early evidence suggests that the generation of realistic synthetic images on all the modalities may be possible.

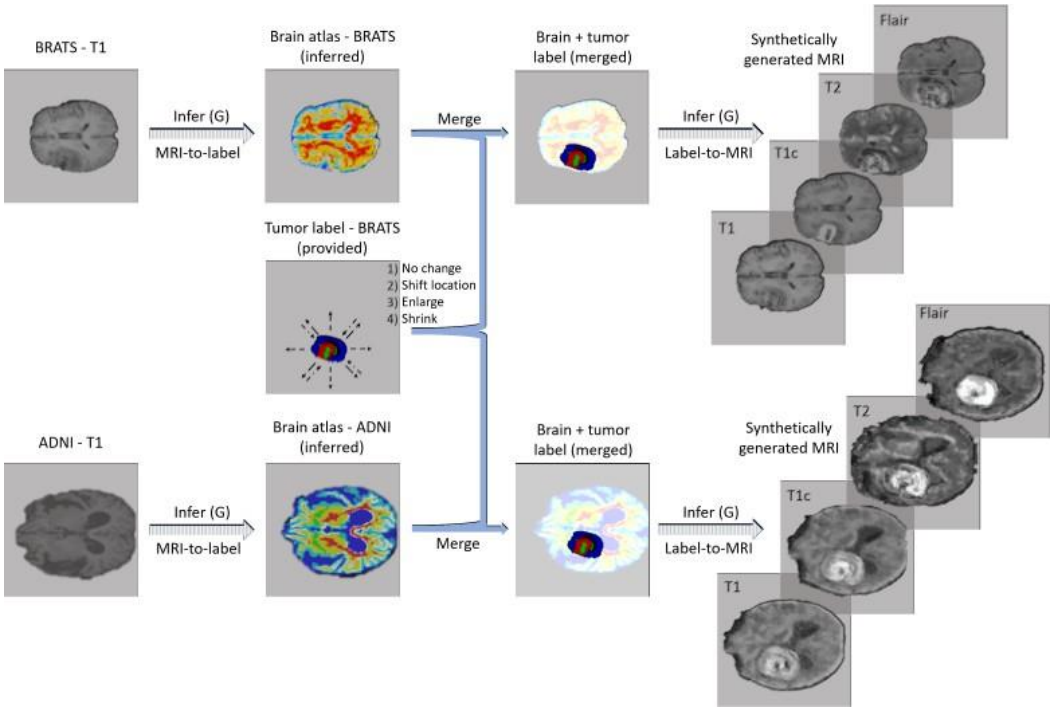

Fig. 4.3 Workflow of getting synthetic images with variation. On BRATS data set, MRI-to-label image translation GAN is applied to T1-weighted images to get brain atlas. It is then merged with the tumor label given in the BRATS data set, possibly with alterations (shift tumor location; enlarge; shrink). The merged labels (with possibly alterations) are then used as an input to label to- MRI GAN, to generate synthetic multi-parametric MRI with brain tumor Shin et al. (2018).

4.5.1 SMIG Model Training

As it is shown in 4.4(A), the generator is trained to place the tumor volume into a healthy brain from ADNI. Then, the discriminator D is trained to classify images as fake (from the generator) or real from the original dataset. Moreover, SMIG produces a synthetic abnormal brain with the same size as input (e.g. see figure 4.4(A)). Furthermore, as it is shown in figure 4.4(B), Generator G is trained to generate a tumor in a new location while discriminator D helps to improve the quality of generated images.

The main objective of the SMIG model is to generate synthetic images (changing the

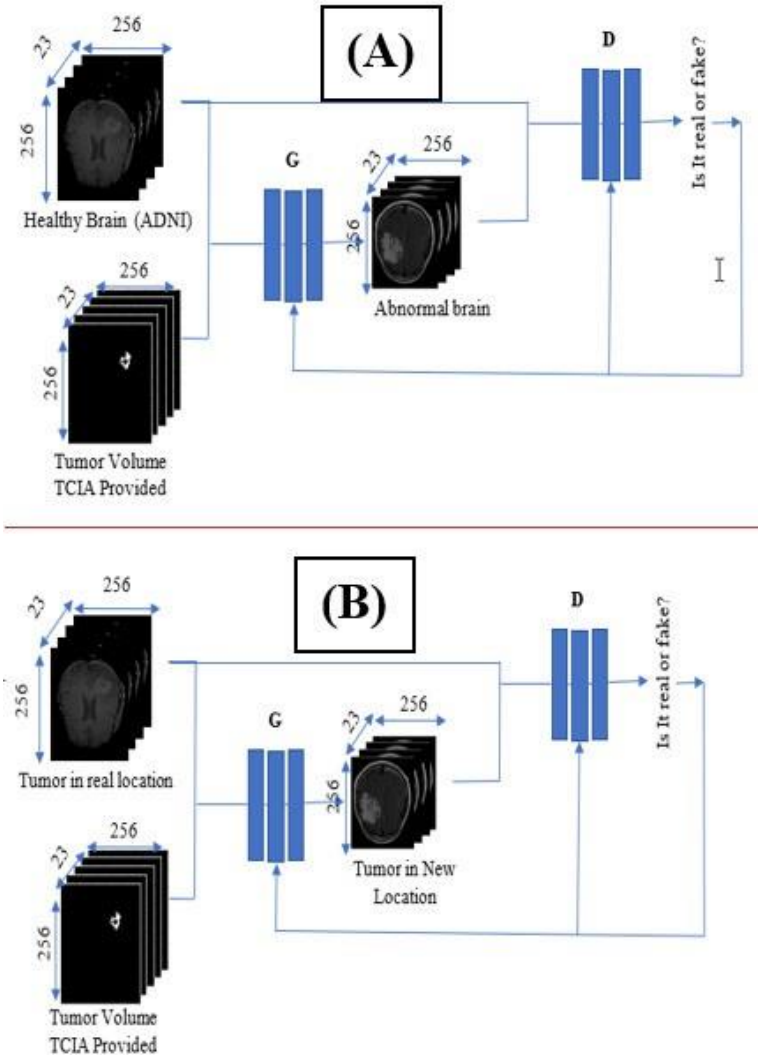

Fig. 4.4 Illustration of our proposed Synthetic Medical Image Generator (SMIG) training workflow, (A) SMIG trained to generate abnormal brain based on a healthy brain from ADNI dataset and tumor volume provided by TCIA, (B) SMIG trained to change the tumor location Kamli et al. (2020)

tumor location and setting a tumor in a healthy brain region) to give us new MRI images. While traditional data augmentation techniques apply a geometric transformation to

produce the augmented image, i.e., geometric transformation does not change the tumor information it only gives the same image with some modifications while SMIG helps the model to generalize by providing quite different images (tumor information).

4.5.2 SMIG model Results

The application of SMIG model to generate data produces images at high resolution that are both realistic and phenotypically diverse. Figure 4.5 shows a comparison between real and synthetic image (generated by SMIG). As figure shows, no noticeable differences between the two images. Also the mathematical model behind GANs guarantee that no differences in the data distribution for both images. Furthermore, to ensure that such qualities hold for SMIG in medical imaging data, we trained a neural network to calculate approximate similarity between all generated images.

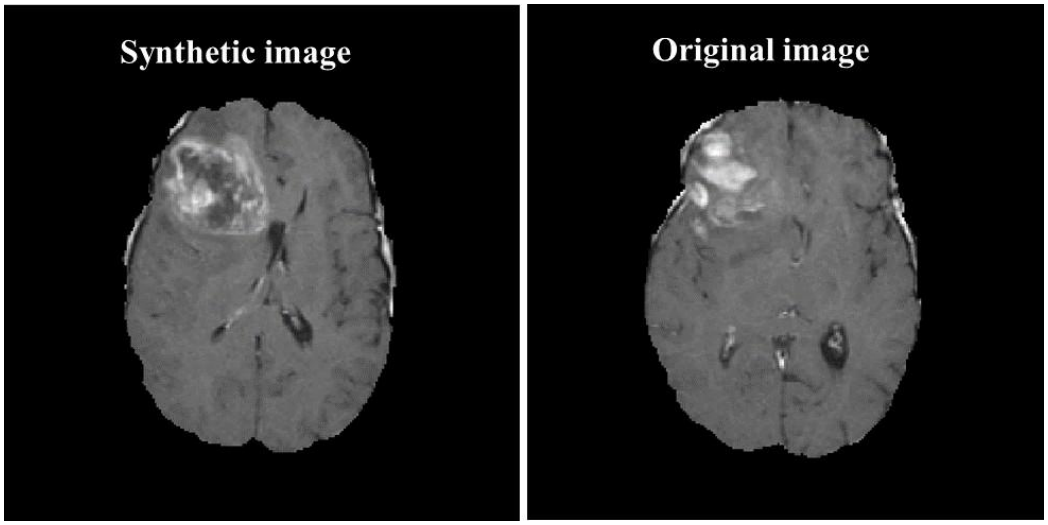

Fig. 4.5 An example of SMIG synthetic generated image compared to the original patient images from the BraTS dataset.

Figure 4.5 shows an an example of the application of SMIG model on a single patient images from the BraTS dataset to augment its number of images, and we compare them to the traditional data augmentation techniques in which the four rows depict the four image type(T1 , T1C, T2, and Flair). The original images are shown in the first raw the second and the thired depicts the result of generating an image with changing the tumor location, the fourth row is the result of generating a synthetic abnormal brain by integrating the tumor in a healthy brain(set tumor volume on a healthy brain from the ADNI. The last rows illustrates examples of the application of traditional data augmentation techniques on the original image.

SMIG can generate synthetic images of unprecedented size, and be used via its latent to space to learn imaging features in an unsupervised manner. Its application will open new avenues for synthetic image generation in medical imaging, which has thus far been limited by an inability to synthesize images at native resolution.

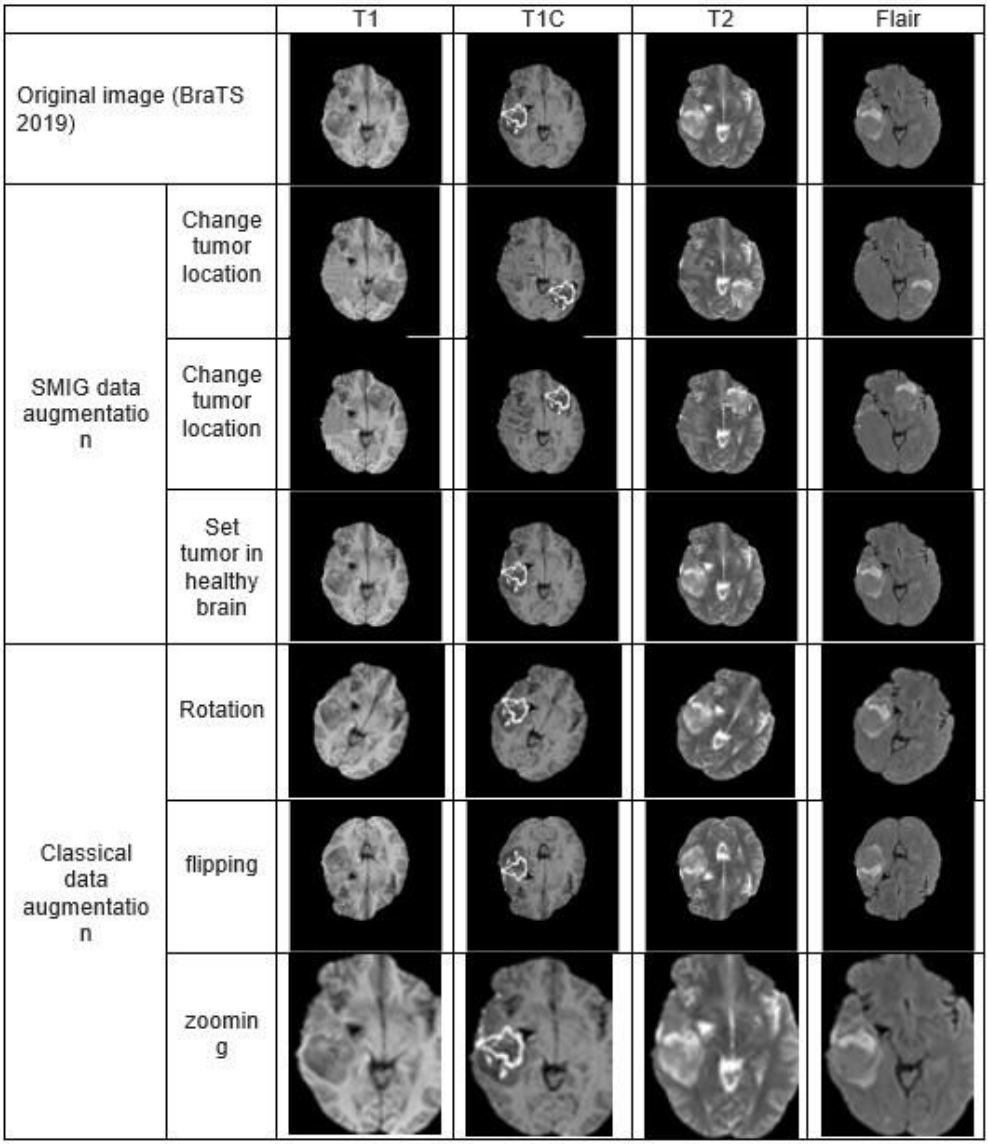

Fig. 4.6 An example of the application of SMIG model on a single patient images from the BraTS dataset compared to the traditional data augmentation techniques

4.5.3 model limitation and future work

4.5.4 Conclusion

In this chapter, we introduced our novel method that is based on GANs model for the aim to obtain synthetic medical images. The lack of public medical training data is known in medical sector due to two main reasons: (i) privacy of patients identity, and (ii) poorly labeled data. Our proposed SMIG model (See section 4.5) is developed specifically to solve these two issues. The SMIG model is composed of two networks: generator and discriminator networks. One the one hand, the generator network is responsible to generate medical images from the same distribution of the training data. Moreover, the generator network is based on the idea of central limit theorem, where the lack of training data makes the training phase diverge from the expectation point. Furthermore, generating and using medical data makes the expectation point of the training data closer to the expectation point of the real distribution. From the other hand, the discriminator network is responsible to classify the generated data into fake or real classes. When the discriminator network reaches the point where it cannot be fooled by the generator network, at this point we can say it reached the Nash equilibrium point.

SMIG model effectively generates synthetic multi-sequences MRI images from the acquired one, which saves time slots for GBMs patients. The second reason may be the large number of MRI data set available in the public domain allowing researchers to have a surplus sample size for better model training. Further, a large fraction of studies conducted in the area of tumor growth prediction are due to better adversarial training and regulation on the generator's output of the GAN model for image-to-image translation framework. Although, conditional generation provides flexibility over augmentation and high resolution for training data. A very limited number of studies have been reported for the challenge of generating GBM tumor MRI images. As future work, we intend to test our proposed SMIG model with the Wasserstein loss function Arjovsky et al. (2017) that theory-justified to be more informative and more stable in training the GANs model. Wasserstein uses 1-Wasserstein distance, instead of the JS-Divergence (used in cross-entropy) to measure the difference between the real distribution and goal distribution.

In addition, we attend to use generated and Anonymized medical image training data for TGP models.

In the next chapter, we present the proposed method of training TGP using generate and anonimize medical image data provided by SMIG model.

CHAPTER 5

Synthetic MRI images to predict GBM growth

5.1 Introduction

GBM brain tumors are heterogeneous brain tumors with a high risk of being lethal, the complex behavior of theses tumor lead to many challenges in lesion segmentation and growth prediction.
In the other hand, generating new realistic data is a common use case of GANs especially in the medical image where the GANs provide an effective method of synthetic data generation and data anonymization, the reason why several approaches are based on GAN in medical fileds.
The lack of public available dataset and the limit number deep-learning of investigations in GBM growth prediction motivate us to use SMIG model (see chapter4) to generate synthetic data and use them as training for our TGP model (see chapter 3).
The combination of the two models to improve GBM growth prediction accuracy, that inspired by the ability of SMIG to generate data in different time point that could be used as data augmentation for TGP model.

5.1.1 Problem statement

The complex tumor behavior and the absence of sufficient training data create a challenge for machine learning (ML) approaches to be capable in brain tumor growth prediction. The investigations in brain tumor growth is keeping an active area of research, and providing sufficient study data is the major issue due to the data privacy and the lack of publicly available data-set. Moreover, GBM growth prediction need a historical data (MRI scans from different time point) to help ML model to improve the prediction accuracy.

5.1.2 Objectives and motivation

In this chapter, we solve the limits of training GMB growth models, in particular, TGP model performance with two issues independently. The first issue is the lack of training data where we find a class of interest has a minority of data compared to other classes.

The second issue is the complex behavior of GBM growth; where SMIG model allow to provide historical image from single patient scan. Consequently, our main objective is to provide an accurate prediction for GBM growth, by generate patients historic data and improve TGP performance. In addition, we compare training result using synthetic data with reel patients image.
Finally, we combine multiple models through various data and MRI modalities to empirically evaluate and report the improvements of TGP results over divers models combination.

5.2 Related work

In literature, plentiful investigations in mathematical modeling of GBM tumor are proposed Swanson et al. (2000, 2003, 2008), Jackson et al. (2015) which provide a useful manner toward patients' specific model to personalized treatment for each patient , also to build a personalized models for tumor growth prediction. As major limit for the mathematical models is the necessity of an experts annotation and quantification of the tumor cell density. In the other hand, machine learning is experiencing explosive growth that provides a better way to exploit the massive volume of medical data received. Nevertheless not all machine learning (ML) approaches are capable for brain tumor growth prediction due to the complex tumor behavior and the absence of sufficient training data. As one of machine learning investigations, Morris et al. (2006) proposes a model trained to learn and predict Glioma tumor growth, that is based on the features of the tumor-adjacent voxels and their probability to become a tumor. In which, they pre-processed patients MRI images to reduce noise and to extract relevant features. Afterwards, they developed a model in aiming to determine what is exactly the tumor region of the brain diagnosed with primary glioma to treat in the occult tissue. The model is trained to classify the adjacent voxel according to their features (such as tissue type, voxel intensities . . .), where the classification is based on two different classifiers (Support Vector Machine and Logistic Regression). As a major limitation of the Morris et al. (2006) model is that the validation and the model performance are based only on one sample due to the lack of training data and reach 59 % in the best case, also the model required Handcrafted features extraction that includes many difficulties and human error margin.
The investigations in brain tumor growth is keeping an active area of research, and providing sufficient study data is the major challenge due to the data privacy and the lack of publicly available data-set in which Generative Adversarial Networks (GANs) prepare a future seeing to freely guarantee public medical image dataset.

5.3 SMIG data based on TCIA dataset

The main objective of this thesis is to provide a high prediction accuracy for GBM tumor growth, for that reason we based or test on TCIA dataset that contain 20 GBM patients; each sample include scans for tow time point (diagnosis and 90 days of follow up).

Due to limit data size, we will use SMIG model to generate synthetic samples that contain two time point scans (the same as TCIA data diagnosis and 90 days of follow up).

The SMIG trained to generate synthetic images from labels allows for the generation of arbitrary multi-series abnormal brain MRIs. Since we have the brain anatomy label and tumor label separately, we can alter either the tumor label or the brain label to get synthetic images with the characteristics we desire. For instance, we can alter the tumor characteristics such as size, location of the existing brain and tumor label set, or place tumor label on an otherwise tumor-free brain label (more details in chapter 4). As shown in figure 5.1, no difference can be observed between the synthetic (generated) and the original image. In the same way learning model couldn't differentiate between the image due to the equilibrium state provided by the training strategy of GAN models.

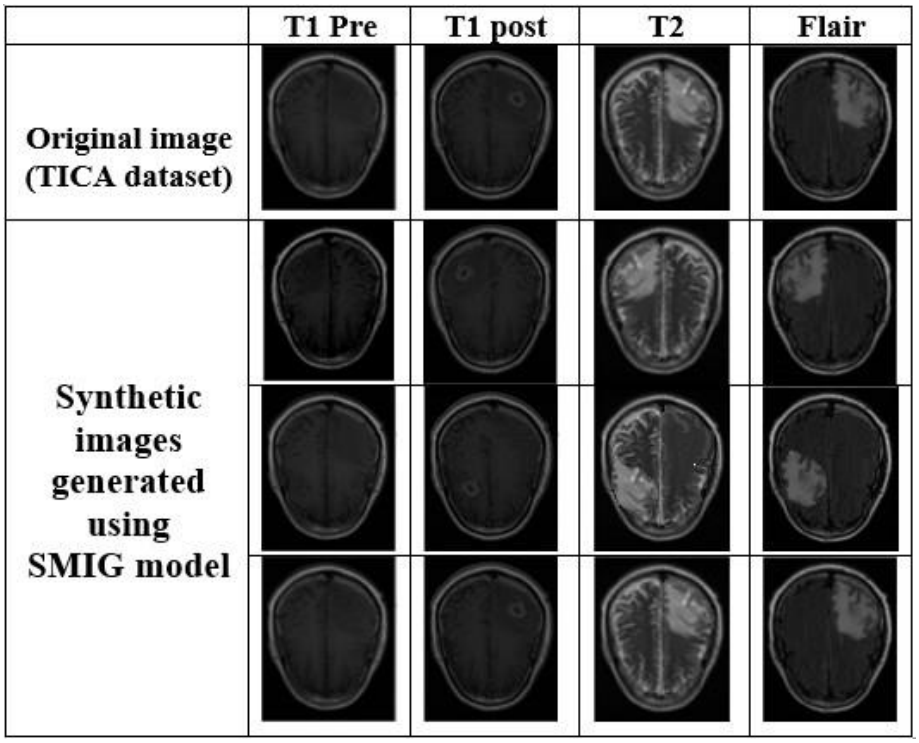

Fig. 5.1 Illustration of an example of synthetic image generated using SMIG model based on TCIA dataset

5.4 Tumor Growth Prediction Based on SMIG data

Noise reduction, image shaping, and registration are the biggest issues in medical image analysis, thus, enhancing image quality and relevant information extraction continue being a difficult challenge and mostly depends on the exact application objectives and the result of experiments.
In our model, we apply in the preprocessing four steps as a follow (skull stripping, normalization/ standardization, registration and denoising). We notice that we used the combination of two skull stripping tools; the robust automated BET tool proceeded by BES that has four steps to prepare MRI images (Filtration, Edge detection, Finding the brain contours, and extracting the brain). The choice of the combination is motivated by the suggestion of the author of BET Woolrich et al. (2009) that the performance of an automated methods could be improved by pre-processing (which is the role of step 1 of BES). As the final step, we apply the wiener filter due to its efficacy and its speed; we provide a measurement of the most known metrics of noise. All steps of preprocessing applied and the used tool and the image output are shown in figure 5.2.

The variety of raw images in intensity, size, noise, and spatial resolution was treated as a pre-processing step to achieves a uniform image dimension (256*256*23) High*width*Slices. For the issue of skull stripping, we evaluate the result of the BET Woolrich et al. (2009) and BES Dogdas et al. (2005) tools and the combination of them.
In addition, to focus on the region of interest we select the slices from number 07 to slices number 17 among the whole 23 slices to omit initial/final slices, since they convey a negligible amount of useful information and negatively affect the training of our model.
The output dimensions (256*256*10) High*width*Slices (10 slices is the max number of slices contain tumor portion based on the tumor mask provided by TCIA)).
SMIG model is used to provide sufficient data and generate synthetic images (change tumor location and tumor in the free-tumor brain from the ADNI dataset).

Finally, we create a new 3D volume, in which it contains one slice and its corresponding one from every image type (i.e., slice from T1 pre, the second from T1 post, the third from T2 and the forth from Flair). As a result, we got 3D volume (256*256*4) High*width*channel where the channel is the four images type, then we extract the patch area of 128*128 from the image. This step is important to help our CNN model to focus on the local information by sub-dividing all existing images into rectangle size (128,128,4) to be as an input for the Convolution neural network as (see figure 5.3).

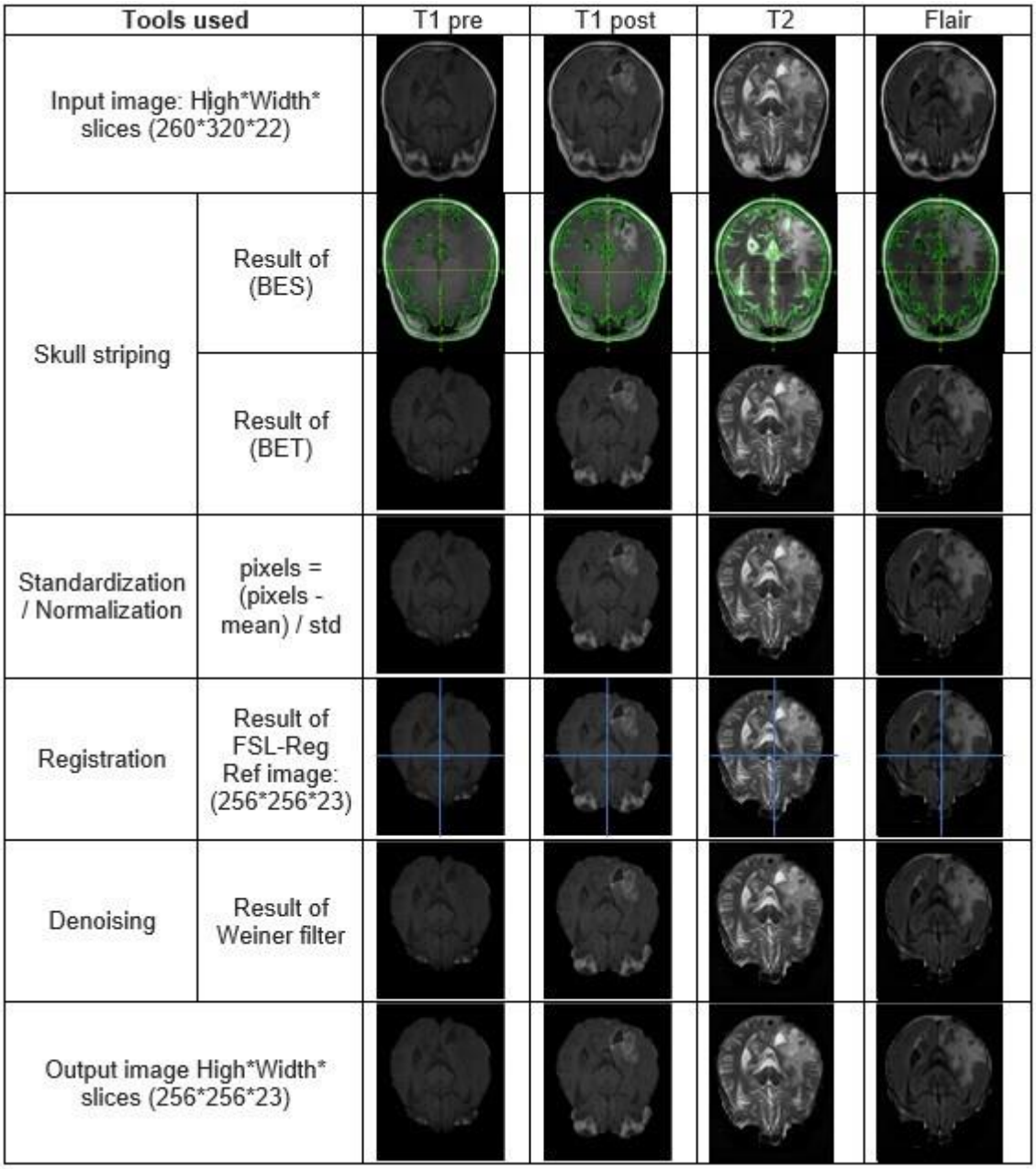

Fig. 5.2 Preprocessing steps applied to prepare the input images for TGP model

Figure 5.4 shows a schematic representation of the final step before launching our **TGP** Convolution architecture, where we extract image patches with size (128*128*4). 128*128 represents the width*height and 4 is the four image type (T1 pre, T1 post, T2, Flair). This step has two main reasons, the first is to reduce the size of the input image due to the limited GPU capacity. The second is to help the proposed model to focus on the local information in the specific area from the input image.

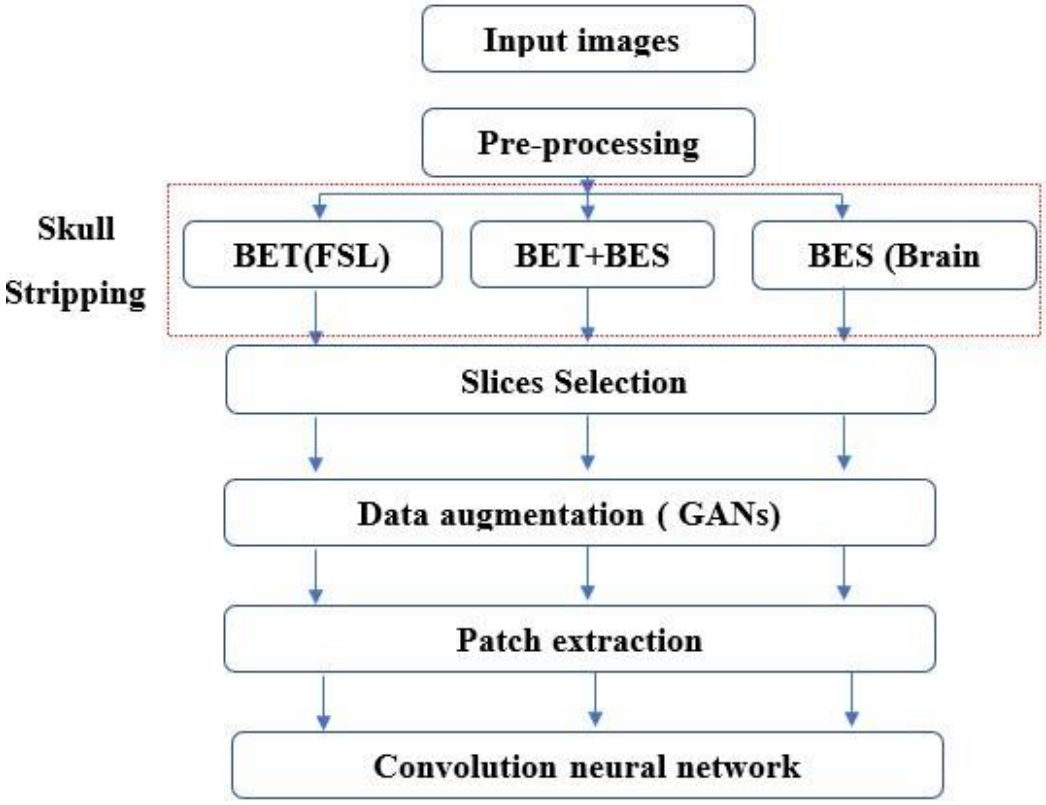

Fig. 5.3 diagram illustrate the outline that used in our work starting with preprocessing (normalization, strandarisation and registration) then skull stripping (based on BET and BES and the combination), the result of each skull stripping method pass by three steps: the first, slices selection (select 10 slices where tumor appear), the second is data augmentation based on traditional technique beside GAN, the last step was patches extraction to prepare data as input for CNN model.

5.5 Evaluating strategy

We propose an End-to-End method to improve the prediction of GBM growth based on MRI images with several data augmentation techniques. TGP model takes as input MRI image (four channels) with an aim to predict the tumor volume in the late-stage (tumor area after 90 days) in terms of three metrics **?**: recall, precision, and Dice scores, each metric is calculated using four statistical values:

- True Positive (TP): is the correctly classified tumoral region (number of pixels).
- False Positive (FP): is the healthy tissue (number of pixels) identified incorrectly as a tumoral region.
- True Negative (TN): is the correctly classified healthy tissue (number of pixels).
- False Negative (FN): is the tumoral region (number of pixels) identified incorrectly as healthy tissue.

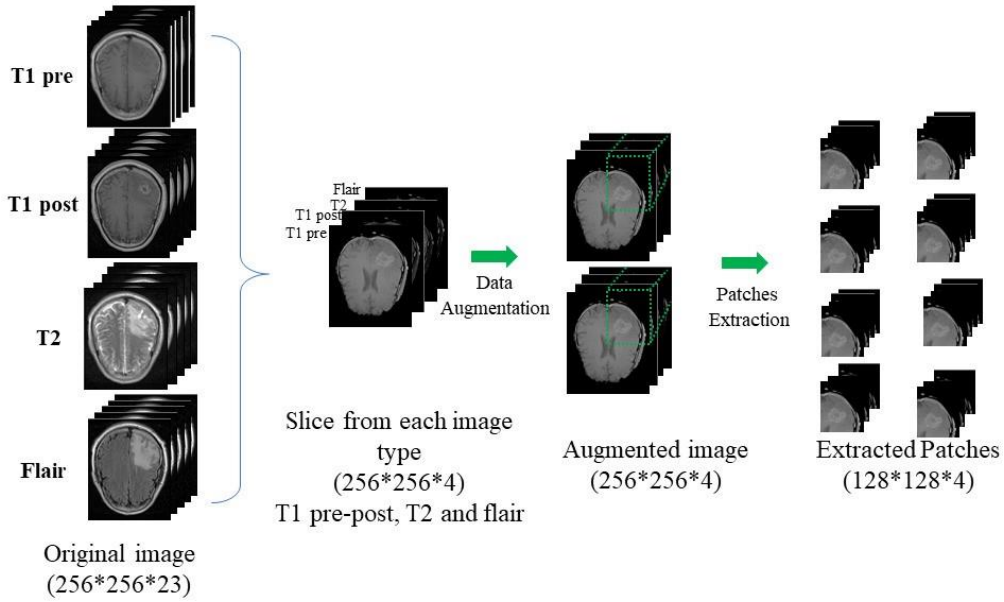

Fig. 5.4 Patch extraction diagram from the input image size(256*256*23) high*width*slices to data augmentation the patch extraction to get image size (128*128*4) where 128*128 is high*width and four is the channel number(T1 pre,T1 post, T2, and Flair).

- Recall = TP /TP+FN, Precision= TP /TP+FP, Dice Similarity Coefficient (DSC) = 2TP / TN+FN +TP+FP.

5.5.1 Combination result validation

The validation of TGP model is based on image processing techniques to compute the tumor volume, and we intent to get the affirmation from an expert from medicine. Firstly, we trained TGP model to take as input image from TCIA dataset and to predict the tumor volume in the late stage (tumor volume after 90 days), then, we segment the lesion volume using Brain Intensity AbNormalities Classification Algorithm (BIANCA) tool implemented in FSL package for the two compared images:

- The predicted image transformed to a binary lesion mask (TGP output lesion volume).
- The original patient image after 90 days from TCIA dataset transformed to a binary lesion mask for the target image (the target lesion volume).

Afterward, we compare the two output masks in terms of three metrics **?**: recall, precision, and Dice scores.

figure 5.5 shows an example of the basic idea of TP, FP, TN, FN that are indicated by colors in the order of green, black, red, and gray for each class. The green/black colors represent the tumor/healthy pixels that are well classified by TGP model. And the misclassified parts are: (1) in red represents the pixels that are classified as tumors only by TGP model, (2) in gray which the part of the tumor that is considered healthy tissue by TGP model. To overcome the issue of segmentation influence on the validation results, we perform the segmentation using the same tool for the two compared images (The predicted image and the original image).

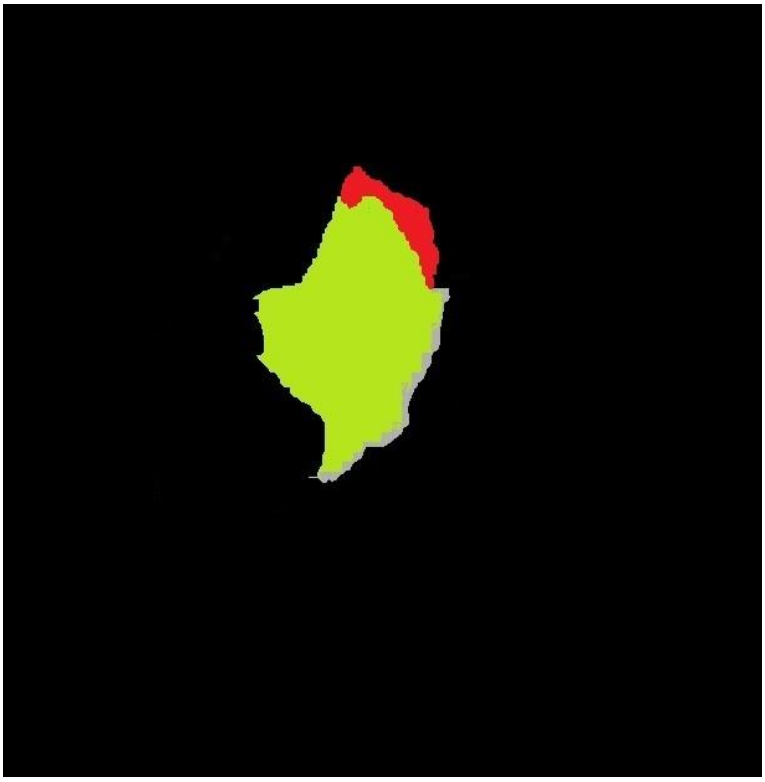

Fig. 5.5 An example of the validation result which True Positive, False Positive, True Negative, False Negative, that are indicated by colors in the order of green, black, red, gray and represent the number of pixels in each class in the binary lesion mask on the compared images.

The evaluation of TGP model is based on cross-validation K-fold (see figure 3.10) in which it performed using 03 patients never seen by the model in training (also not entered in the process of data augmentation and generation of synthetic image), then, we change the selected patients for the 40 evaluation experiments. The chosen of 17 patients as training and 03 as a test is are carefully trialed in a variety of different portion (train-test) in which using more patients for test will reduce the number of training cases entered to the model thus the model performance will be affected, in the other hand using less than 03 patient will not establish the reached results. This operation helps to provide a better evaluation for the obtained results. All training experiments

took 500 epochs to converge to the best parameters.

5.6 Experimental results

Review the result of our model while trained on a different ratio of synthetic data and its impact on TGP prediction performance:
This strategy aims to measure the performance of our TGP model in the readjustment of the synthetic image produced by SMIG generator and the impact of training with different proportion data generated by SMIG model. For this experiment we use the best result given by TGP model trained with real data (section 4.1.1), while we are based on using the combination of two skull stripping tools BET Woolrich et al. (2009) and BES Dogdas et al. (2005) in order to separate non-brain tissue for all image in the training data:

- Experiment 01: Training **TGP** model with only original data (0% synthetic)
- Experiment 02: Training **TGP** model with 75 % original data and 25% synthetic image produced by **SMIG**
- Experiment 03: Training **TGP** model with 50 % original data and 50% synthetic image produced by **SMIG**
- Experiment 04: Training **TGP** model with 80 % original data and 20% synthetic image produced by **SMIG**
- Experiment 05: Training **TGP** model with 100% synthetic data and produced by **SMIG** image (0 % Original)

Figure 5.6 shows the result of evaluating our TGP model under different ratios of the synthetic images in training data, synthetic images are produced with our proposed SMIG model with an aim to provide more extra training data for our TGP model.
The impact of changing the ratio of synthetic data in the training is measured which 0% of synthetic data is achieved 69.3%, 67.8%, and 68.9% of recall, precision and dice coefficient score respectively, and improvement of model performance were observed with the addition of synthetic data to achieve 75.8%, 80.2%, 82.1% of recall, precision and dice coefficient respectively (ie a mean of +13% of accuracy).

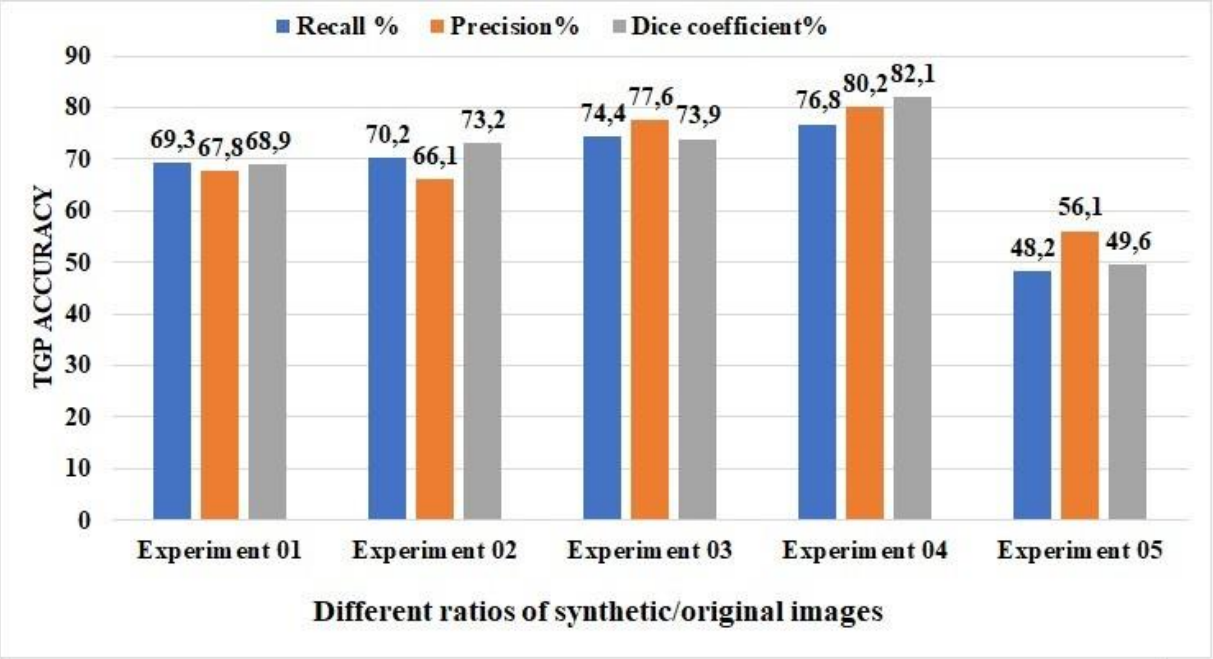

Fig. 5.6 Recall, Precision, and Dice metric evaluation of the performance of our **TGP** models trained on 05 datasets with different ratios of synthetic/original images. We observe that 80% ratio of synthetic data generated by SMIG and 20% from TCIA data have a greater effect on model accuracy 76.8%, 80.2%, 82.1%

We observe that 80% ratio of synthetic data generated by SMIG and 20% from TCIA data have a greater effect on model accuracy 76.8%, 80.2%, 82.1% of recall, precision and dice coefficient respectively when 50% of synthetic achieve 70.2%, 77.6%, 73.9% of recall, precision and dice coefficient, and less accuracy is noticed when training the model only on the synthetic data in which 48.2% ,55.1%, and 49.6% of dice coefficient, recall, and precision in order. As it is shown in table 5.1, which provides the numerical value that was measured within the change of synthetic data ratio, we observe an improvement of model performance (+13%) due to using SMIG generated data as data augmentation and providing more training sample.

Experiment Metrics	Recall % ± STD	Precision % ± STD	Dice % ± STD
Experiment 01	69.3 ± 5.3	67.8 ± 7.2	68.9 ± 4.0
Experiment 02	70.2 ± 4.9	65.1 ± 5.2	73.2 ± 5.9
Experiment 03	74.4 ± 5.9	77.6 ± 7.6	73.9 ± 5.4
Experiment 04	**75.8 ± 5.1**	**80.2 ± 4.2**	**82.1 ± 7.7**
Experiment 05	48.2 ± 5.1	55.1 ± 4.2	49.6 ± 7.7

Table 5.1 Table illustrates Recall, Precision, and Dice metric evaluation of the performance of our **TGP** models trained on 04 datasets with different ratios of synthetic/original images.

5.7 Discussion

Comparison of TGP performance with the literature model for the issue of tumor prediction

TGP model aims to predict the tumor volume growth, comparing to the majority of the prediction model based on mathematical modelling. Moreover, the TGP model do not require any supplement input data, it is based only on patient's MRI images.

Morris et al. (2006) trained a model to predict the future Glioma tumor growth; Morris model based on support vector machine and logistic regression, where they extract handcrafted features such as Growth rate of tumour mass, Percentage of edema, Volume increase between 2 scans. All extracted features used for the for the classification of voxel around the active tumour border to tumour or non-tumour class. Morris et al. (2006) model achieve 59% of prediction accuracy, and the test phase is performed on a single patient images.

Furthermore, Nathan et al. (2019) proposes a GBM tumor cell density prediction model that achieve 51.8% using a machine learning model combined with mathematical model, where they achieved 83,8 accuracy.

The advantages of TGP model are: (i) fully automatic, and (ii) reach better results despite the small size of data. TGP trained also on the generated data by SMIG model and achieve a valuable performance compared to the state-of-the-art methods. SMIG model solves the issue of the lack of sufficient training data, and provides a way to anonymize the data, in addition, to protecting patient's privacy and allowing the share of training data.

figure 5.7 shows the evaluation results of the state-of-the-art machine learning methods for the issue of tumor prediction with our proposed TGP model.

In order to determine the performance of our TGP model , we first compared the accuracy of TGP between the all training strategies to get the optimal ration of synthetic data, Table 5.1 shows the comparison result using two metrics: Recall, precision and Dice coefficient between the predicted and the expert volume measurements. As a second comparison, we aim to compare to state of the art (ML model for GBM growth prediction) with TGP result, as shown in figure 5.7 all metrics metrics show a clear improvements of the prediction accuracy. where a mean of +20% of accuracy improvement observed with TGP model to achieve 76.8%, 80.2%, 82.1% of recall, precision and dice coefficient respectively.

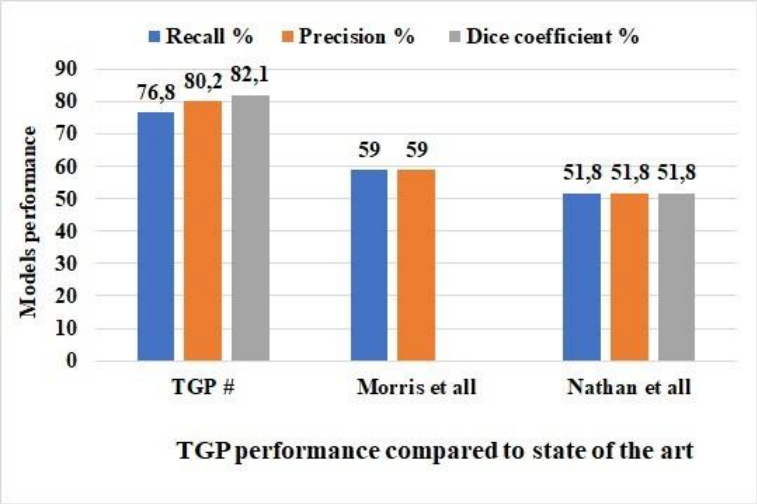

Fig. 5.7 Comparison of the state-of-the-art methods for the issue of tumor prediction with our proposed TGP model (which is noted by adding *J*.

5.8 Conclusion

In this chapter, we introduced a use case for our developed SMIG model. The main objective is to obtain synthetic medical images that can be used as training data for TGP model.

The combination of SMIG generated data and TGP model help to improve the prediction accuracy, a mean of +13% in the three metrics; which achieve 75.8%, 80.2%, 82.1% of recall, precision and dice coefficient.

SMIG model provides a super realistic data as shown in figure 5.1, where no difference can be observed between the synthetic (generated) and the original image. In the other hand during the TGP training; the match between images features (due to the training strategy of GAN models) ensure the high performance of the prediction accuracy (82,1% Dice coefficient).

In addition, for the GBM growth prediction, we need to train on historical data (i.e. scans from different times points) where its generated using our SMIG model.

It is well accepted that GBM tumor growth prediction accuracy didn't achieve a very high precision, however, TGP model result show an improvement of 20% all metrics compared to state of the art. We have to note that an exact comparison in the medical image domain is not possible, as different datasets are used in each work.

Despite our prediction results still need to be improved by introducing other regions MRI images and improve the generated data quality by using new loss function during the training of SMIG model. We hope that this finding will be successfully used by the research community for medical image generating and the prediction tasks.

General Conclusion

In this dissertation, we studied the challenge of GBM tumor growth prediction using the MRI multi-modal imaging technique. These imaging tools can accurately diagnose GBM condition and its growth for a while, whether in clinical assessment or research settings.

Machine learning algorithms have produced emerging results for various domain applications; among which is the medical field. At this stage, there is no doubt about the advantages and benefits of using ML models for GBM growth prediction.

Thus, in the current Ph.D. work, we study and propose two models; First model: Tumor Growth Predictor (TGP) based on an End-to-End CNN network aiming to predict GBM tumor growth. TGP is a high automatic prediction model to help clinicians predict the volume of GBM in the late-stage based on the patients scans. Besides, TGP does not require any prior feature extraction or signature generation process and adopts them for brain MRI imaging. Second model: SMIG to generate synthetic data based on GANs architecture. SMIG provides an efficient method for a low-cost dataset generation, protects patients' privacy and medical data anonymizing, and provides a way for future sharing of the training data.

Through this work, we aim to show the effectiveness of developing a fully automatic GBM growth predictor that is trained on synthetic data, we review the combination of the two models (TGP and SMIG), we also study the impact of changing the preprocessing tools which have a valuable impact on the prediction accuracy.

However, the deep prediction methods necessitate huge datasets for training models; overall, they consist of millions of parameters. This can be a big challenge in the medical field, since datasets are not often readily available. Thus, we addressed two main crucial points: how to deal with the constraint of limitation of the available dataset using synthetic data, and how to conceive adaptable architecture designs for the GBM growth prediction challenge.

In chapter 1, we first introduced the medical background and necessary information about Glioblastoma multiforme (GBM) and brain tumor imaging, we also we provided a complete description of the public dataset used in this work.

In chapter 2, we covered a detailed presentation of tumor growth modeling and the mathematical viewpoint of GBM growth. It includes a the studies in the microscopic and macroscopic levels that are briefly discussed and reviewed. We also presented an overview of GBM tumor growth investigation based on artificial intelligence. We highlighted the investigations on treatment planning and genetic profile prediction to study treatment efficacy.

In chapter 3, we present our TGP model, which is an adapted architecture that aims to predict GBM tumor growth (volume changing) based on multi-modal images. TGP model takes into account the complexity of computing that needs to be low, whereas increasing the accuracy of results, which is achieved by using convolution auto-encoder. Besides, we made various analyses with different settings in order to study the impact of pre-processing tools on the model prediction accuracy; including the important methods for separating the brain from the skull, resizing, and registration, and image denoising. We highlight the effect of using BET and BES as skull stripping and their combination results. As a result, we obtained a high accuracy for GBM tumor prediction: 69,9%, 71,7%, 72,3% of recall, precision, and dice coefficient respectively.

In chapter 4, we presented our SMIG model which is based on generative adversarial networks (GANs). The mathematical theory behind the GANs is also detailed, and the contribution is compared to related work as well. Then we demonstrated all results and examples of generative images. SMIG model provides an efficient method that has several advantages: (1) Protecting patients' privacy by generating synthetic images to be used for researches. (2) Medical data anonymizing and allowing for future sharing of the training data. (3) A low-cost dataset generation (provide sufficient data for learning model). (4) SMIG model is capable of augmenting medical dataset images with realistic and high-quality generated MRI images.

In chapter 5, we further extended our proposed SMIG model, we introduce its capability to generate scans at different time points. The generated images were used in TGP training to improve its prediction accuracy. We took advantage of the combination methods (TGP and SMIG) using different settings and strategies to enhance our TGP models' robustness. We showed the effectiveness of using multiple ratios of synthetic data and its impact on the TGP model performance. TGP model achieves a means of +10.28 % more accuracy by using the generated data; thus GBM tumor prediction accuracy achieves 75,8%, 80,2%, 82,1% of recall, precision, and dice coefficient respectively. Moreover, we exhibited the improved results provided by the majority of applied metrics in medical image investigations. The obtained results demonstrate promising

prediction performance and simplicity compared to the state-of-the-art. We conclude this thesis by identifying and discussing potential future research lines, where we intended to train our SMIG model to generate scans from various datasets, also, we also worked to implicit the mathematical model of GBM growth in TGP and combine the Reaction-Diffusion (RD) model with machine learning.

Finally, the one interesting research line that we have not covered in this thesis is the use of the Wasserstein loss function Arjovsky et al. (2017) that theory-justified to be more informative and more stable in training the GANs model. Another approach would be interesting to investigate, is to use multi-model MRI image as input for TGP model; This would develop more comprehensible and valuable systems that bring the concept of covering all tumor feature for better prediction result.

Limitations and perspectives

We attempt to overcome some limitations of our model in future works such as :

- Using a large number of training data that is important to improve and to generalize on new cases. In our experiments we used a dataset with only 20 subjects. Moreover, the dataset that we used does not have to normalize data time points over all subjects.
- Small tumoral regions might get lost due to the use of many down-sampling and upsampling layers in our TGP model.
- As Shin et al. (2018) we believe that using T2/flair images can improves the quality of generated synthetic images, because T2/flair contain more relevant features related to the tumor area.

REFERENCES

Akil, M., Saouli, R., Kachouri, R. et al. (2020), 'Fully automatic brain tumor segmentation with deep learning-based selective attention using overlapping patches and multi-class weighted cross-entropy', *Medical image analysis* **63**, 101692.

Akkus, Z., Ali, I., Sedlář, J., Agrawal, J. P., Parney, I. F., Giannini, C. and Erickson, B. J. (2017), 'Predicting deletion of chromosomal arms 1p/19q in low-grade gliomas from mr images using machine intelligence', *Journal of digital imaging* **30**(4), 469–476.

Al Mahmud, M. A., Bhadra, S., Haque, A., Al Mamun, M. E. and Haider, S. S. (2014), 'Development and validation of hplc method for simultaneous determination of gliclazide and enalapril maleate in tablet dosage form', *Dhaka University Journal of Pharmaceutical Sciences* **13**(1), 51–56.

André, S., Unverzagt, C., Kojima, S., Frank, M., Seifert, J., Fink, C., Kayser, K., von der Lieth, C.-W. and Gabius, H.-J. (2004*a*), 'Determination of modulation of ligand properties of synthetic complex-type biantennary n-glycans by introduction of bisecting glcnac in silico, in vitro and in vivo', *European journal of biochemistry* **271**(1), 118–134.

André, S., Unverzagt, C., Kojima, S., Frank, M., Seifert, J., Fink, C., Kayser, K., von der Lieth, C.-W. and Gabius, H.-J. (2004*b*), 'Determination of modulation of ligand properties of synthetic complex-type biantennary n-glycans by introduction of bisecting glcnac in silico, in vitro and in vivo', *European journal of biochemistry* **271**(1), 118–134.

Antipov, G., Baccouche, M. and Dugelay, J.-L. (2017), Face aging with conditional generative adversarial networks, *in* '2017 IEEE international conference on image processing (ICIP)', IEEE, pp. 2089–2093.

Arjovsky, M., Chintala, S. and Bottou, L. (2017), Wasserstein generative adversarial networks, *in* 'International conference on machine learning', PMLR, pp. 214–223.

Armoni, A. (2000), Diabetes mellitus-evaluating the diagnostic probabilities, *in* 'Healthcare information systems: challenges of the new millennium', IGI Global, pp. 169–177.

Bağcı, U., Udupa, J. K. and Bai, L. (2010), 'The role of intensity standardization in medical image registration', *Pattern Recognition Letters* **31**(4), 315–323.

Bailey, D. L., Maisey, M. N., Townsend, D. W. and Valk, P. E. (2005), *Positron emission tomography*, Vol. 2, Springer.

Baserga, R. (1965), 'The relationship of the cell cycle to tumor growth and control of cell division: A review', *Cancer research* **25**(5 Part 1), 581–595.

Beyerlein, P. (1997), Discriminative model combination, *in* '1997 IEEE Workshop on Automatic Speech Recognition and Understanding Proceedings', IEEE, pp. 238–245.

Bhushan, C. (2016), Correction, coregistration and connectivity analysis of multi-contrast brain MRI, PhD thesis, University of Southern California.

Black, P. (2000), 'Surgery for cerebral gliomas: past, present, and future', *Clinical neurosurgery* **47**, 21–45.

Boser, B. E., Guyon, I. M. and Vapnik, V. N. (1992), A training algorithm for optimal margin classifiers, *in* 'Proceedings of the fifth annual workshop on Computational learning theory', pp. 144–152.

Bowles, C., Chen, L., Guerrero, R., Bentley, P., Gunn, R., Hammers, A., Dickie, D. A., Hernández, M. V., Wardlaw, J. and Rueckert, D. (2018), 'Gan augmentation: Augmenting training data using generative adversarial networks', *arXiv preprint arXiv:1810.10863* .

Brem, S. and Abdullah, K. G. (2016), *Glioblastoma E-Book*, Elsevier Health Sciences.

Buckner, J. C., Brown, P. D., O'Neill, B. P., Meyer, F. B., Wetmore, C. J. and Uhm, J. H. (2007), Central nervous system tumors, *in* 'Mayo Clinic Proceedings', Vol. 82, Elsevier, pp. 1271–1286.

Buzug, T. M. (2011), Computed tomography, *in* 'Springer handbook of medical technology', Springer, pp. 311–342.

Chaudhuri, P. P., Chowdhury, D. R., Nandi, S. and Chattopadhyay, S. (1997), *Additive cellular automata: theory and applications*, Vol. 43, John Wiley and Sons.

Clark, K., Vendt, B., Smith, K., Freymann, J., Kirby, J., Koppel, P., Moore, S., Phillips, S., Maffitt, D., Pringle, M. et al. (2013), 'The cancer imaging archive (tcia): maintaining and operating a public information repository', *Journal of digital imaging* **26**(6), 1045–1057.

Clatz, O., Bondiau, P.-Y., Delingette, H., Malandain, G., Sermesant, M., Warfield, S. K. and Ayache, N. (2004), In silico tumor growth: application to glioblastomas, *in* 'International Conference on Medical Image Computing and Computer-Assisted Intervention', Springer, pp. 337–345.

Coatrieux, G. (2011), Contribution au contrôle d'intégrité des images médicales, PhD thesis, Universite´ de Rennes 1.

Cortes, E., Rabelo, L., Sarmiento, A. T. and Gutierrez, E. (2020), 'Design of distributed discrete-event simulation systems using deep belief networks', *Information* **11**(10), 467.

Dale, B. M., Brown, M. A. and Semelka, R. C. (2015*a*), 'Mri: basic principles and applications'.

Dale, B. M., Brown, M. A. and Semelka, R. C. (2015*b*), 'Mri: basic principles and applications'.

De Boer, P.-T., Kroese, D. P., Mannor, S. and Rubinstein, R. Y. (2005), 'A tutorial on the cross-entropy method', *Annals of operations research* **134**(1), 19–67.

De Coene, B., Hajnal, J. V., Gatehouse, P., Longmore, D. B., White, S. J., Oatridge, A., Pennock, J., Young, I. and Bydder, G. (1992), 'Mr of the brain using fluid-attenuated inversion recovery (flair) pulse sequences.', *American journal of neuroradiology* **13**(6), 1555–1564.

DeAngelis, L. M. (2001), 'Brain tumors', *New England journal of medicine* **344**(2), 114–123.

DiPerna, R. and Lions, P. (1989), 'Ordinary differential equations, sobolev spaces and transport theory', *Invent. Math* **98**(3), 511–547.

Dogdas, B., Shattuck, D. W. and Leahy, R. M. (2005), 'Segmentation of skull and scalp in 3-d human mri using mathematical morphology', *Human brain mapping* **26**(4), 273–285.

Duffau, H. (2017*a*), *Diffuse low-grade gliomas in adults*, Springer.

Duffau, H. (2017*b*), Introduction: From the inhibition of dogmas to the concept of personalized management in patients with diffuse low-grade gliomas, *in* 'Diffuse Low-Grade Gliomas in Adults', Springer, pp. 1–9.

Elazab, A., Wang, C., Gardezi, S. J. S., Bai, H., Hu, Q., Wang, T., Chang, C. and Lei, B. (2020), 'Gp-gan: Brain tumor growth prediction using stacked 3d generative adversarial networks from longitudinal mr images', *Neural Networks* **132**, 321–332.

Fennema-Notestine, C., Ozyurt, I. B., Clark, C. P., Morris, S., Bischoff-Grethe, A., Bondi, M. W., Jernigan, T. L., Fischl, B., Segonne, F., Shattuck, D. W. et al. (2006), 'Quantitative evaluation of automated skull-stripping methods applied to contemporary and legacy images: Effects of diagnosis, bias correction, and slice location', *Human brain mapping* **27**(2), 99–113.

Fox, B. D., Cheung, V. J., Patel, A. J., Suki, D. and Rao, G. (2011), 'Epidemiology of metastatic brain tumors.', *Neurosurgery clinics of North America* **22**(1), 1–6.

Freeman, R. and Minch, M. J. (1998), *Spin choreography: basic steps in high resolution NMR*, Oxford University Press Oxford.

Frid-Adar, M., Diamant, I., Klang, E., Amitai, M., Goldberger, J. and Greenspan, H. (2018), 'Gan-based synthetic medical image augmentation for increased cnn performance in liver lesion classification', *Neurocomputing* **321**, 321–331.

Geman, D., Geman, S., Hallonquist, N. and Younes, L. (2015), 'Visual turing test for computer vision systems', *Proceedings of the National Academy of Sciences* **112**(12), 3618–3623.

Goodfellow, I., Bengio, Y. and Courville, A. (2016), *Deep learning*, MIT press.

Goodfellow, I., Pouget-Abadie, J., Mirza, M., Xu, B., Warde-Farley, D., Ozair, S., Courville, A. and Bengio, Y. (2014), Generative adversarial nets, *in* 'Advances in neural information processing systems', pp. 2672–2680.

Han, C., Hayashi, H., Rundo, L., Araki, R., Shimoda, W., Muramatsu, S., Furukawa, Y., Mauri, G. and Nakayama, H. (2018), Gan-based synthetic brain mr image generation, *in* '2018 IEEE 15th International Symposium on Biomedical Imaging (ISBI 2018)', IEEE, pp. 734–738.

Hastie, T., Tibshirani, R. and Friedman, J. (2009), *The elements of statistical learning: data mining, inference, and prediction*, Springer Science and Business Media.

Havaei, M., Davy, A., Warde-Farley, D., Biard, A., Courville, A., Bengio, Y., Pal, C., Jodoin, P.-M. and Larochelle, H. (2017), 'Brain tumor segmentation with deep neural networks', *Medical image analysis* **35**, 18–31.

Hecht-Nielsen, R. (1992), Theory of the backpropagation neural network, *in* 'Neural networks for perception', Elsevier, pp. 65–93.

Henning, K. (2018), How artificial intelligence changes the world, *in* 'Developing Support Technologies', Springer, pp. 277–284.

Hoang-Xuan, K., Idbaih, A., Mokhtari, K. and Sanson, M. (2005), 'Towards a molecular classification of gliomas', *Bulletin du cancer* **92**(4), 310–316.

Holzinger, A. (2016*a*), Machine learning for health informatics, *in* 'Machine learning for health informatics', Springer, pp. 1–24.

Holzinger, A. (2016*b*), *Machine learning for health informatics: state-of-the-art and future challenges*, Vol. 9605, Springer.

Hu, R. and Ruan, X. (2002), A logistic cellular automaton for simulating tumor growth, *in* 'Proceedings of the 4th World Congress on Intelligent Control and Automation (Cat. No. 02EX527)', Vol. 1, IEEE, pp. 693–696.

Iqbal, T. and Ali, H. (2018), 'Generative adversarial network for medical images (mi-gan)', *Journal of medical systems* **42**(11), 231.

Isola, P., Zhu, J.-Y., Zhou, T. and Efros, A. A. (2017), Image-to-image translation with conditional adversarial networks, *in* 'Proceedings of the IEEE conference on computer vision and pattern recognition', pp. 1125–1134.

Jackson, P. R., Juliano, J., Hawkins-Daarud, A., Rockne, R. C. and Swanson, K. R. (2015), 'Patient-specific mathematical neuro-oncology: using a simple proliferation and invasion tumor model to inform clinical practice', *Bulletin of mathematical biology* **77**(5), 846–856.

Janelidze, S., Bexell, D., Badn, W., Darabi, A., Smith, K.-E., Fritzell, S., Gunnarsson, S., Milos, P., Bengzon, J., Salford, L. G. et al. (2009), 'Immunizations with ifnγ secreting tumor cells can eliminate fully established and invasive rat gliomas', *Journal of Immunotherapy* **32**(6), 593–601.

Jennett, P., Watanabe, M., Igras, E., Premkumar, K. and Hall, W. (1996), 'Telemedicine and security. confidentiality, integrity, and availability: a canadian perspective.', *Studies in health technology and informatics* **29**, 286–298.

Jordan, M. I. and Mitchell, T. M. (2015), 'Machine learning: Trends, perspectives, and prospects', *Science* **349**(6245), 255–260.

Kamli, A., Saouli, R., Batatia, H., BenNaceur, M. and Youkana, I. (2020), 'Synthetic medical image generator for data augmentation and anonymisation based on generative adversarial network for glioblastoma tumors growth prediction', *IET Image Processing* **14**(16), 4248–4257.

Kansal, A., Torquato, S., Harsh Iv, G., Chiocca, E. and Deisboeck, T. (2000), 'Cellular automaton of idealized brain tumor growth dynamics', *Biosystems* **55**(1-3), 119–127.

Katsikas, S. (2016), *Information systems security: facing the information society of the 21st century*, Springer.

Kwan, R.-S., Evans, A. C. and Pike, G. B. (1999), 'Mri simulation-based evaluation of image-processing and classification methods', *IEEE transactions on medical imaging* **18**(11), 1085–1097.

Lao, J., Chen, Y., Li, Z.-C., Li, Q., Zhang, J., Liu, J. and Zhai, G. (2017), 'A deep learning-based radiomics model for prediction of survival in glioblastoma multiforme', *Scientific reports* **7**(1), 1–8.

Lê, M., Delingette, H., Kalpathy-Cramer, J., Gerstner, E. R., Batchelor, T., Unkelbach, J. and Ayache, N. (2015), Bayesian personalization of brain tumor growth model, *in* 'International Conference on Medical Image Computing and Computer-Assisted Intervention', Springer, pp. 424–432.

LeCun, Y., Bottou, L., Bengio, Y. and Haffner, P. (1998), 'Gradient-based learning applied to document recognition', *Proceedings of the IEEE* **86**(11), 2278–2324.

Li, S. C.-X., Jiang, B. and Marlin, B. (2019), 'Misgan: Learning from incomplete data with generative adversarial networks', *arXiv preprint arXiv:1902.09599* .

Li, Y., Qian, Z., Xu, K., Wang, K., Fan, X., Li, S., Jiang, T., Liu, X. and Wang, Y. (2018), 'Mri features predict p53 status in lower-grade gliomas via a machine-learning approach', *NeuroImage: Clinical* **17**, 306–311.

Li, Z., Wang, Y., Yu, J., Guo, Y. and Cao, W. (2017), 'Deep learning based radiomics (dlr) and its usage in noninvasive idh1 prediction for low grade glioma', *Scientific reports* **7**(1), 1–11.

Lima, F. R., Kahn, S. A., Soletti, R. C., Biasoli, D., Alves, T., da Fonseca, A. C. C., Garcia, C., Romão, L., Brito, J., Holanda-Afonso, R. et al. (2012), 'Glioblastoma: therapeutic challenges, what lies ahead', *Biochimica et Biophysica Acta (BBA)-Reviews on Cancer* **1826**(2), 338–349.

Lo, C. (2007), 'Stochastic gompertz model of tumour cell growth', *Journal of Theoretical Biology* **248**(2), 317–321.

Louis, D. N., Perry, A., Reifenberger, G., Von Deimling, A., Figarella-Branger, D., Cavenee, W. K., Ohgaki, H., Wiestler, O. D., Kleihues, P. and Ellison, D. W. (2016), 'The 2016 world health organization classification of tumors of the central nervous system: a summary', *Acta neuropathologica* **131**(6), 803–820.

Maintz, J. A. and Viergever, M. A. (1996), An overview of medical image registration methods, *in* 'Symposium of the Belgian hospital physicists association (SBPH/BVZF)', Vol. 12, Citeseer, pp. 1–22.

Mandonnet, E., Pallud, J., Fontaine, D., Taillandier, L., Bauchet, L., Peruzzi, P., Guyotat, J., Bernier, V., Baron, M.-H., Duffau, H. et al. (2010), 'Inter-and intrapatients comparison of who grade ii glioma kinetics before and after surgical resection', *Neurosurgical review* **33**(1), 91–96.

Mao, X., Li, Q., Xie, H., Lau, R. Y. and Wang, Z. (2016), 'Multi-class generative adversarial networks with the l2 loss function', *arXiv preprint arXiv:1611.04076* **5**, 1057–7149.

Marr, D. and Hildreth, E. (1980), 'Theory of edge detection', *Proceedings of the Royal Society of London. Series B. Biological Sciences* **207**(1167), 187–217.

Maskin, E. (1999), 'Nash equilibrium and welfare optimality', *The Review of Economic Studies* **66**(1), 23–38.

Massey, S. C., Rockne, R. C., Hawkins-Daarud, A., Gallaher, J., Anderson, A. R., Canoll, P. and Swanson, K. R. (2018), 'Simulating pdgf-driven glioma growth and invasion in an anatomically accurate brain domain', *Bulletin of mathematical biology* **80**(5), 1292–1309.

Massey, S. C., Whitmire, P., Doyle, T. E., Ippolito, J. E., Mrugala, M. M., Hu, L. S., Canoll, P., Anderson, A. R., Wilson, M. A., Fitzpatrick, S. M. et al. (2020), 'Sex differences in health and disease: A review of biological sex differences relevant to cancer with a spotlight on glioma', *Cancer Letters* .

Menze, B. H., Jakab, A., Bauer, S., Kalpathy-Cramer, J., Farahani, K., Kirby, J., Burren, Y., Porz, N., Slotboom, J., Wiest, R. et al. (2014), 'The multimodal brain tumor image segmentation benchmark (brats)', *IEEE transactions on medical imaging* **34**(10), 1993–2024.

Moore, M. P., Rodney, S. B., Michael, L. H. and Gavin, P. R. (1996), 'Intracranial tumors', *Veterinary Clinics of North America: Small Animal Practice* **26**(4), 759–777.

Morris, M. (2005), 'Classification-based glioma diffusion modeling.'.

Morris, M., Greiner, R., Sander, J., Murtha, A. and Schmidt, M. (2006), 'Learning a classification-based glioma growth model using mri data.', *JCP* **1**(7), 21–31.

Murray, J. D. (1989), 'Mathematical biology, vol. 19 of biomathematics'.

Naceur, M. B., Akil, M., Saouli, R. and Kachouri, R. (2019), Deep convolutional neural networks for brain tumor segmentation: boosting performance using deep transfer learning: preliminary results, *in* 'International MICCAI Brainlesion Workshop', Springer, pp. 303–315.

Network, C. G. A. R. et al. (2008), 'Comprehensive genomic characterization defines human glioblastoma genes and core pathways', *Nature* **455**(7216), 1061.

Oktay, O., Nanavati, J., Schwaighofer, A., Carter, D., Bristow, M., Tanno, R., Jena, R., Barnett, G., Noble, D., Rimmer, Y. et al. (2020), 'Evaluation of deep learning to augment image-guided radiotherapy for head and neck and prostate cancers', *JAMA network open* **3**(11), e2027426–e2027426.

Oord, A. v. d., Dieleman, S., Zen, H., Simonyan, K., Vinyals, O., Graves, A., Kalchbrenner, N., Senior, A. and Kavukcuoglu, K. (2016), 'Wavenet: A generative model for raw audio', *arXiv preprint arXiv:1609.03499* .

Ostrom, Q. T., Gittleman, H., Truitt, G., Boscia, A., Kruchko, C. and Barnholtz-Sloan, J. S. (2018), 'Cbtrus statistical report: primary brain and other central nervous system tumors diagnosed in the united states in 2011–2015', *Neuro-oncology* **20**(suppl_4), iv1–iv86.

Pallud, J., Taillandier, L., Capelle, L., Fontaine, D., Peyre, M., Ducray, F., Duffau, H. and Mandonnet, E. (2012), 'Quantitative morphological magnetic resonance imaging follow-up of low-grade glioma: a plea for systematic measurement of growth rates', *Neurosurgery* **71**(3), 729–740.

Pedano, N., Flanders, A., Scarpace, L., Mikkelsen, T., Eschbacher, J., Hermes, B. and Ostrom, Q. (n.d.), 'Radiology data from the cancer genome atlas low grade glioma [tcga-lgg] collection,(2016)', *URL http://doi. org/10.7937 K* **9**.

Pereira, S., Pinto, A., Alves, V. and Silva, C. A. (2015), Deep convolutional neural networks for the segmentation of gliomas in multi-sequence mri, *in* 'BrainLes 2015', Springer, pp. 131–143.

Petersen, R. C., Aisen, P., Beckett, L. A., Donohue, M., Gamst, A., Harvey, D. J., Jack, C., Jagust, W., Shaw, L., Toga, A. et al. (2010), 'Alzheimer's disease neuroimaging initiative (adni): clinical characterization', *Neurology* **74**(3), 201–209.

Poldrack, R. A., Mumford, J. A. and Nichols, T. E. (2011), *Handbook of functional MRI data analysis*, Cambridge University Press.

Pollard, J. H. and Valkovics, E. J. (1992), 'The gompertz distribution and its applications', *Genus* pp. 15–28.

Powles, J. and Hodson, H. (2017), 'Google deepmind and healthcare in an age of algorithms', *Health and technology* **7**(4), 351–367.

Randall, E. C., Emdal, K. B., Laramy, J. K., Kim, M., Roos, A., Calligaris, D., Regan, M. S., Gupta, S. K., Mladek, A. C., Carlson, B. L. et al. (2018), 'Integrated mapping of pharmacokinetics and pharmacodynamics in a patient-derived xenograft model of glioblastoma', *Nature communications* **9**(1), 1–13.

Rehage, G., Ernst, O. and Fuhrmann, J. (1970), 'Fickian and non-fickian diffusion in high polymer systems', *Discussions of the Faraday Society* **49**, 208–221.

Romportl, J., Zackova, E. and Kelemen, J. (2016), *Beyond Artificial Intelligence*, Springer.

Sagheer, S. V. M. and George, S. N. (2020), 'A review on medical image denoising algorithms', *Biomedical signal processing and control* **61**, 102036.

Sallemi, L., Njeh, I. and Lehericy, S. (2015), 'Towards a computer aided prognosis for brain glioblastomas tumor growth estimation', *IEEE transactions on nanobioscience* **14**(7), 727–733.

Samuel, A. L. (1959), 'Some studies in machine learning using the game of checkers', *IBM Journal of research and development* **3**(3), 210–229.

Sanger, F., Nicklen, S. and Coulson, A. R. (1977), 'Dna sequencing with chain-terminating inhibitors', *Proceedings of the national academy of sciences* **74**(12), 5463–5467.

Schmainda, K. and Prah, M. (2018), 'Data from brain-tumor-progression', *The Cancer Imaging Archive* .

Sethian, J. A. (1996), 'A fast marching level set method for monotonically advancing fronts', *Proceedings of the National Academy of Sciences* **93**(4), 1591–1595.

Seyfioğlu, M. S., Özbayoğlu, A. M. and Gürbüz, S. Z. (2018), 'Deep convolutional autoencoder for radar-based classification of similar aided and unaided human activities', *IEEE Transactions on Aerospace and Electronic Systems* **54**(4), 1709–1723.

Shen, Y., Harris, N. C., Skirlo, S., Prabhu, M., Baehr-Jones, T., Hochberg, M., Sun, X., Zhao, S., Larochelle, H., Englund, D. et al. (2017), 'Deep learning with coherent nanophotonic circuits', *Nature Photonics* **11**(7), 441.

Shin, H.-C., Tenenholtz, N. A., Rogers, J. K., Schwarz, C. G., Senjem, M. L., Gunter, J. L., Andriole, K. P. and Michalski, M. (2018), Medical image synthesis for data augmentation and anonymization using generative adversarial networks, *in* 'International workshop on simulation and synthesis in medical imaging', Springer, pp. 1–11.

Smith, R. R. (1990), Brain stem tumors, *in* 'Seminars in roentgenology', Vol. 25, Elsevier, pp. 249–262.

Smith, S. M. (2002), 'Fast robust automated brain extraction', *Human brain mapping* **17**(3), 143–155.

Smoll, N. R., Schaller, K. and Gautschi, O. P. (2013), 'Long-term survival of patients with glioblastoma multiforme (gbm)', *Journal of Clinical Neuroscience* **20**(5), 670–675.

Suh, C. H., Kim, H. S., Jung, S. C., Choi, C. G. and Kim, S. J. (2019), 'Imaging prediction of isocitrate dehydrogenase (idh) mutation in patients with glioma: a systemic review and meta-analysis', *European radiology* **29**(2), 745–758.

Svensson, A. (2015), *Mesenchymal Stromal Cells in Malignant Glioma: Functions and Therapeutic Potential*, Citeseer.

Swanson, K. R., Alvord Jr, E. C. and Murray, J. (2000), 'A quantitative model for differential motility of gliomas in grey and white matter', *Cell proliferation* **33**(5), 317–329.

Swanson, K. R., Bridge, C., Murray, J. and Alvord Jr, E. C. (2003), 'Virtual and real brain tumors: using mathematical modeling to quantify glioma growth and invasion', *Journal of the neurological sciences* **216**(1), 1–10.

Swanson, K., Rostomily, R. and Alvord, E. (2008), 'A mathematical modelling tool for predicting survival of individual patients following resection of glioblastoma: a proof of principle', *British journal of cancer* **98**(1), 113–119.

Tamimi, A. F. and Juweid, M. (2017), 'Epidemiology and outcome of glioblastoma', *Exon Publications* pp. 143–153.

Tenenbaum, J. B., Kemp, C., Griffiths, T. L. and Goodman, N. D. (2011), 'How to grow a mind: Statistics, structure, and abstraction', *science* **331**(6022), 1279–1285.

Tracqui, P. (1995), 'From passive diffusion to active cellular migration in mathematical models of tumour invasion', *Acta biotheoretica* **43**(4), 443–464.

Tracqui, P., Cruywagen, G., Woodward, D., Bartoo, G., Murray, J. and Alvord Jr, E. (1995), 'A mathematical model of glioma growth: the effect of chemotherapy on spatio-temporal growth', *Cell proliferation* **28**(1), 17–31.

Vapnik, V. N. (1999), 'An overview of statistical learning theory', *IEEE transactions on neural networks* **10**(5), 988–999.

Villanueva-Meyer, J. E., Wood, M. D., Choi, B. S., Mabray, M. C., Butowski, N. A., Tihan, T. and Cha, S. (2018), 'Mri features and idh mutational status of grade ii diffuse gliomas: impact on diagnosis and prognosis', *American Journal of Roentgenology* **210**(3), 621–628.

Vuorinen, V., Hinkka, S., Färkkilä, M. and Jääskeläinen, J. (2003), 'Debulking or biopsy of malignant glioma in elderly people–a randomised study', *Acta neurochirurgica* **145**(1), 5–10.

Walker, M. D., Strike, T. A. and Sheline, G. E. (1979), 'An analysis of dose-effect relationship in the radiotherapy of malignant gliomas', *International Journal of Radiation Oncology* Biology* Physics* **5**(10), 1725–1731.

Wang, X. and Gupta, A. (2016), Generative image modeling using style and structure adversarial networks, *in* 'European conference on computer vision', Springer, pp. 318–335.

Weller, M., Wick, W., Aldape, K., Brada, M., Berger, M., Pfister, S. M., Nishikawa, R., Rosenthal, M., Wen, P. Y., Stupp, R. et al. (2015), 'Glioma', *Nature reviews Disease primers* **1**(1), 1–18.

Woodward, D. i. w., Cook, J., Tracqui, P., Cruywagen, G., Murray, J. and Alvord Jr, E. (1996), 'A mathematical model of glioma growth: the effect of extent of surgical resection', *Cell proliferation* **29**(6), 269–288.

Woolrich, M. W., Jbabdi, S., Patenaude, B., Chappell, M., Makni, S., Behrens, T., Beckmann, C., Jenkinson, M. and Smith, S. M. (2009), 'Bayesian analysis of neuroimaging data in fsl', *Neuroimage* **45**(1), S173–S186.

Xu, T., Zhang, P., Huang, Q., Zhang, H., Gan, Z., Huang, X. and He, X. (2018), Attngan: Fine-grained text to image generation with attentional generative adversarial networks, *in* 'Proceedings of the IEEE conference on computer vision and pattern recognition', pp. 1316–1324.

Yeghiazaryan, V. and Voiculescu, I. D. (2018), 'Family of boundary overlap metrics for the evaluation of medical image segmentation', *Journal of Medical Imaging* **5**(1), 015006.

Yi, X., Walia, E. and Babyn, P. (2019), 'Generative adversarial network in medical imaging: A review', *Medical image analysis* **58**, 101552.

Zhang, B., Chang, K., Ramkissoon, S., Tanguturi, S., Bi, W. L., Reardon, D. A., Ligon, K. L., Alexander, B. M., Wen, P. Y. and Huang, R. Y. (2017), 'Multimodal mri features predict isocitrate dehydrogenase genotype in high-grade gliomas', *Neuro-oncology* **19**(1), 109–117.

Zhou, H., Vallières, M., Bai, H. X., Su, C., Tang, H., Oldridge, D., Zhang, Z., Xiao, B., Liao, W., Tao, Y. et al. (2017), 'Mri features predict survival and molecular markers in diffuse lower-grade gliomas', *Neuro-oncology* **19**(6), 862–870.

Zhou, X., Qiu, S., Joshi, P. S., Xue, C., Killiany, R. J., Mian, A. Z., Chin, S. P., Au, R. and Kolachalama, V. B. (2021), 'Enhancing magnetic resonance imaging-driven alzheimer's disease classification performance using generative adversarial learning', *Alzheimer's research and therapy* **13**(1), 1–11.

LIST OF PUBLICATIONS

1. . Kamli, A., Saouli, R., Batatia, H., BenNaceur, M. and Youkana, I. (2020), 'Syntheticmedical image generator for data augmentation and anonymisation based on generativeadversarial network for glioblastoma tumors growth prediction',IET Image Processing14(16), 4248–4257
2. . Mathematical Modeling of Glioma Tumor Growth: a literature review" by A. Kamli; I. Youkana; R. Saouli; M. Bennaceur; L.Boublatta. Brain Tumor Meeting, Berlin, Germany 2019, .

Appendices